January 2021

Assessment Of GOES-16 Satellite And High-Resolution Rapid Refresh Model Data For Blowing Snow Impact-Based Decision Support Services

Elizabeth Sims

[How does access to this work benefit you? Let us know!](#)

Follow this and additional works at: https://commons.und.edu/theses

ASSESSMENT OF GOES-16 SATELLITE AND HIGH-RESOLUTION RAPID REFRESH
MODEL DATA FOR BLOWING SNOW IMPACT-BASED DECISION SUPPORT
SERVICES

by

Elizabeth Michelle Sims
Bachelor of Science, Birmingham-Southern College, 2019

A Thesis
Submitted to the Graduate Faculty

of the

University of North Dakota

in partial fulfillment of the requirements
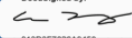
for the degree of
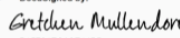Master of Science

Grand Forks, North Dakota

December
2021

Name: Elizabeth M. Sims

Degree: Master of Science

This document, submitted in partial fulfillment of the requirements for the degree from the University of North Dakota, has been read by the Faculty Advisory Committee under whom the work has been done and is hereby approved.

Aaron Kennedy

Gretchen Mullendore

Catherine Finley

This document is being submitted by the appointed advisory committee as having met all the requirements of the School of Graduate Studies at the University of North Dakota and is hereby approved.

Chris Nelson
Dean of the School of Graduate Studies

12/7/2021

Date

PERMISSION

Title   Assessment of GOES-16 Satellite and High-Resolution Rapid Refresh Model
                     Data for Blowing Snow Impact-Based Decision Support Services

Department   Atmospheric Sciences

Degree   Master of Science

In presenting this thesis in partial fulfillment of the requirements for a graduate degree from the University of North Dakota, I agree that the library of this University shall make it freely available for inspection. I further agree that permission for extensive copying for scholarly purposes may be granted by the professor who supervised my thesis work or, in his absence, by the Chairperson of the department or the dean of the School of Graduate Studies. It is understood that any copying or publication or other use of this thesis or part thereof for financial gain shall not be allowed without my written permission. It is also understood that due recognition shall be given to me and to the University of North Dakota in any scholarly use which may be made of any material in my thesis.

<div align="right">

Elizabeth Michelle Sims
9 December 2021

</div>

TABLE OF CONTENTS

LIST OF FIGURES

LIST OF TABLES

xvii

ACKNOWLEDGMENTS

ABSTRACT

Regions of the globe, including the Northern Great Plains, are subject to adverse conditions during the wintertime. Among these conditions is blowing snow, which can cause significant societal and economic impacts by reducing visibility. The lack of this process in numerical weather prediction models creates a forecasting challenge for the region. In recent years, however, forecasters have gained access to a variety of National Oceanic Atmospheric Administration (NOAA) modeling and satellite tools such as the High-Resolution Rapid Refresh (HRRR) model and Geostationary Operational Environmental Satellites (GOES) that may improve Impact-Based Decision Support Services (IDSS) goals for blowing snow. This project worked to identify how GOES-16 and HRRR data may improve IDSS during blowing snow events. This was done through a case study approach for events over the winters of 2018-2019 and 2019-2020. To understand the model biases and provide useful insight into the performance of the models, HRRR forecasts were compared to surface observations across the Fargo/Grand Forks NWS County Warning Area (CWA). Visibility for point locations were also subjectively compared to output from GOES-16 imagery. Results of this study demonstrated that GOES-16 is most useful during clear sky events such as Arctic fronts. Limitations due to cloud cover and overnight timing of events suggest a continued need for in situ observations to monitor blowing snow conditions. Error between the model and observations showed the model had difficulty in forecasting visibility. However, small errors in wind speed, temperature, and relative humidity suggests that HRRR model output may be useful for driving blowing snow models. This will provide future utility for real-time forecasting and guidance for blowing snow events.

CHAPTER 1

BACKGROUND AND INTRODUCTION

1.1 Overview of Blowing Snow

Blowing snow is a common wintertime phenomenon in the Northern Great Plains. By definition in the National Weather Service (NWS) glossary, blowing snow is caused by falling snow or by fallen snow lifted off the surface by strong winds (NWS 2009). This process is differentiated from drifting snow by height; blowing snow reaches heights of 2 m or more, reducing horizontal visibility to less than 11 km (American Meteorological Society 2012a).

The process of blowing snow happens when a strong enough wind dislodges particles from the surface snowpack. Threshold wind speeds to initiate the process are dependent on snowpack conditions such as temperature and age (Li and Pomeroy 1997a). Schmidt (1980) showed that aging and warmer snowpacks require a higher wind speed than fresh, cold snow to begin transport. Results from a study looking at observations over the prairies of western Canada (Li and Pomeroy 1997b) agreed with this finding; mean 10 m threshold wind speeds for fresh snow and aged snow were 7.5 m s^{-1} and 8.0 m s^{-1} respectively (Figure 1). Results concluded that for temperatures of -25 ºC to 0 ºC wind speed thresholds increase with increasing ambient air temperature. However, with temperatures below -25 ºC the threshold wind speed increases slightly with decreasing temperature due to the dominant effects of elastic and kinetic frictional forces on cohesion and resistance to movement (Li and Pomeroy 1997b, Figure 2).

The process of blowing snow can have a large impact on society as visibility is significantly reduced during these events. Visibility is defined by the American Meteorological Society (2012b) as the greatest distance at which it is possible to see a prominent dark object against the sky in the daytime, and a moderately intense light source at night. According to Pomeroy and Male (1988),

this reduction is dependent on the number density, particle size, and parameters of the snow particle size distribution, and is caused because snow particles scatter and absorb electromagnetic radiation. For blowing snow, the contrast between sources of luminance is reduced by scattering along with absorption, which limits the distance that objects can be seen (Pomeroy and Male 1988). The NWS uses visibility to determine levels of impacts during blizzard and other blowing snow events. During daylight, impacts are considered for visibility at 0 mi, ¼ mi, ½ mi, and ¾ to 1 mile (Grafenauer 2021). Rasmussen et al. (1999) determined that visibility is reduced to a lesser degree during the nighttime hours than the daytime hours, and this can impact how blizzard events are verified. During the nighttime, impacts are considered for visibility at 0 to ¼ mi, ½ to ¾ mi, 1 mi, and 1 ¼ of a mile (Grafenauer 2021). While impacts are considered for visibility of up to a mile during the day and 1 ¼ of a mile during the night, blizzards and associated blizzard warnings are often determined by visibilities of ¼ of a mile or less. These impacts related to visibility and how the NWS uses visibility to determine impact levels will be discussed further in section 1.4.1.

1.1.1 Climatology of Blizzards

Within the United States, the Northern Plains is home to what has been coined the "blizzard zone" (Schwartz and Schmidlin 2002). Investigation of the National Centers for Environmental Prediction (NCEP) Storm Events Database has revealed that this region is climatologically the most favorable for blizzards in the contiguous United States (CONUS) (Coleman and Schwartz 2017). This area encompasses all of North Dakota, South Dakota, and approximately 34 counties in western Minnesota (Figure 3). Schwartz and Schmidlin (2002) found that each county within this blizzard zone had an average of one or more blizzards per winter over a 41-year span. In an updated climatology study, counties along the Red River Valley (RRV) in North Dakota reported

over 100 blizzards over 55-years, with the maximum blizzard frequency in the entire CONUS being reported in this region (Coleman and Schwartz 2017). Further work by Kennedy et al. (2019) and the NWS in Grand Forks provided additional detail on blizzard events over the Fargo/Grand Forks (FGF) County Warning Area (CWA). An average of 2.6 blizzards occur annually, with the majority occurring between December and March (Kennedy et al. 2019).

Climatologically, this frequency in blizzards makes sense for the area due to location, topography, snow cover, and storm tracks (Kennedy et al. 2019). What was once a lakebed of Lake Agassiz is now the RRV. Forming the border between North Dakota and Minnesota, the slow-moving Red River of the North flows north until emptying into the Hudson Bay in Canada. With little tree cover, the agriculturally dominant RRV shows evidence of enhanced winds in the region. For example, Kennedy et al. (2019) noted blowing snow plumes are often seen only within the RRV (Figure 4). Further, the location is susceptible to multiple storm tracks that often bring different types of blizzard conditions.

1.1.2 Classification of Blizzard and Blowing Snow Events

The meteorological patterns associated with these blizzard events have been classified into four different blizzard patterns: Alberta Clippers, Arctic fronts, Colorado lows, and Hybrids (Figure 5; Kennedy et al. 2019). Alberta Clippers, as the name suggests, originate in Western Canada near the Alberta province. From here, these fast-moving low-pressure systems move southeast through southern Canada and into the Northern Plains and Great Lakes region in the CONUS. Typically, these systems produce light snow, strong winds capable of reaching blizzard criteria, and cold temperatures (Kennedy et al. 2019, NWS 2009). As implied, Colorado lows are a low-pressure system that form over southeastern Colorado and move northeastward over the US.

Lasting over several days, these systems are known to produce hazardous winter weather and well-known blizzard events that can impact large areas (NWS 2009). The National Weather Service also recognizes systems, coined 'Hybrids', that originate outside of these areas. These systems are defined by a low-pressure center but have characteristics of multiple patterns (Kennedy et al. 2019).

The FGF CWA often experiences events known as ground blizzards, which can happen under clear sky conditions (Figure 6, US Department of Commerce 2019). These events often occur behind Arctic (Cold) fronts, which are associated with frigid temperatures and strong winds well removed from precipitation (US Department of Commerce 2019a). These increased winds loft already fallen snow into the atmosphere, causing low visibilities and near whiteout conditions in some areas. While each of these events may originate in different areas, they each have the potential to bring different blizzard condition and in turn a wide range of significant impacts to the area.

1.2. Impacts and Hazards

Nationally, winter storms accounted for nearly $8.5 billion in insured losses from 1950 to 1997 (Changnon 2003). Coleman and Schwartz (2017) found that federal disaster declarations for blizzards have increased over the past half century, with more than 50% of the declarations occurring in the 21st century alone. Winter storms have numerous adverse impacts on agriculture, commerce, transportation, infrastructure, emergency services, daily activities, health, and more. An example of widespread significant impacts comes from a case study of a blizzard in southern Ontario (Burrows et al. 1979). Impacts in Toronto, Canada were assessed through responses to questionnaires as well as reviews of reports from the local newspapers. This event alone showed

cost estimates of over $41 million when including sales (Burrows et al. 1979). Of the economic impacts listed, the largest came from lost work hours and lost commodity sales with nearly $39 million in costs reported between them. From there the remaining costs came from impacts including categories for snow removal, structural damage, auto accidents, medical injuries, and miscellaneous. The storm also negatively affected transportation with only 7 of 125 flights able to take off that day (Burrows et al. 1979).

Within the FGF CWA, news stories dedicated to blizzards are common. These event are important enough that the local paper, the Grand Forks Herald, names these events (Grand Forks Herald 2017, 2019; Shirley 2020). Due to the frequency of these blizzard events in the area, the FGF CWA is susceptible to a wide range of impacts as a result of high wind speeds, snowfall, and resultant reductions in visibility and drifting associated with these events. Several examples of blizzards with varying impacts are discussed below.

The historic blizzard in March of 1966 was one of the most severe blizzards on record for the Northern Plains (US Department of Commerce 2021a). This Colorado Low weather system produced wind gusts exceeding 70 mph, snowfall totals of 38 inches, and snow drifts up to 40 feet high, brought significant impacts across the region. Blizzard conditions made it difficult for people to find their way out of the storm and work to remove the snow was strenuous. These dangerous conditions resulted in at least 9 reported human deaths and the death of thousands of livestock across North Dakota and Minnesota (US Department of Commerce 2021b). During a blizzard event 6-7 February 2019, a strong hybrid system developed and moved over eastern ND and northwest MN. While a band of heavy snow brought 8 to 12 inches of snow to the area, the main impacts occurred due to strong, gusty winds throughout the day on the 7th. The resulting blowing and drifting snow created hazardous travel conditions and snow drifts as tall as houses. Due to

these widespread reduced visibilities and dense snow drifts, portions of the interstate in eastern ND and western MN were temporarily closed. A strong clipper system on 27 January 2019 brought similar travel impacts, as 4-8 inches of snow fell, and gusty winds produced blizzard conditions across ND. As most of the FGF CWA was under a blizzard warning, blowing snow created significantly reduced visibility resulting in a "No Travel Advised" alert across most of the state. Contrary to these previous events, a ground blizzard on 24 January 2019 resulted from an Arctic Front with very little concurrent snowfall. However, snow that had fallen days prior, and winds gusting to nearly 56 miles per hour created dangerous driving conditions and wind chill temperatures. With significantly reduced visibility across the area, many drivers were stranded along the highway overnight as temperatures continued to drop.

As seen with each of these events, impacts can range significantly between different events and locations. It is important to note that because of this, impacts related to blizzards, specifically blowing snow, are often difficult to quantify for forecasters (Makowski and Grafenauer 2016). Further discussion on how the FGF NWS works to quantify these impacts is found in section 1.4.

1.3. Monitoring and Modeling of Blowing Snow

1.3.1. Satellite Observations of Blowing Snow

Previous literature has looked at active and passive remote sensing satellite studies of blowing snow. Active remote sensing of blowing snow by satellite has been a successful way at looking at properties such as frequency, layer height, and optical depth of blowing snow (Palm et al. 2018). However, many of these studies are confined to the Antarctic region. Scarchilli et al. (2010) used satellite images in true-color and infrared images from the Moderate Resolution Imaging Spectroradiometer (MODIS) aboard NASA's TERRA and AQUA satellites to observe

billows (blowing snow plumes) associated with katabatic winds in Antarctica. These features were tall enough to cast shadows. During these events, the height of the blowing snow layer was estimated to at least 200 meters high (Scarchilli et al. 2010). Work done by Palm et al. (2011) used MODIS data combined with Cloud-Aerosol Lidar and Infrared Pathfinder Satellite Observations (CALIPSO) data to identify blowing snow regions. Constructing false color imagery using the 2.1μm channel and 0.85 μm visible channel allowed for areas of blowing snow to be identified easily against background ice and snow. Using the visible satellite imagery, thick 'billows' such as those seen in Scarchilli et al. (2010) were evident.

Blowing snow plumes have been detected with satellite imagery over the CONUS, but formal documentation of these events is limited. Kennedy et al. (2019) used false color imagery from the Visible Infrared Imaging Radiometer Suite (VIIRS) onboard the Suomi satellite to identify blowing snow plumes along the RRV. Unfortunately, polar orbiting satellites do not allow for continuous coverage in space and time, and visible satellite observations are not available during the nighttime hours. Even when satellite observations are available, it can be hard to differentiate blowing snow from the icy/snow covered background (Burrows and Mooney 2021).

Since polar-orbiting satellites have limited overpasses over a given area, geostationary satellites have been identified by Kennedy and Jones (2020) as the better platform for observing blowing snow. The Advanced Baseline Imager on board the Geostationary Operational Environmental Satellite- 16 (GOES-16), has made the detection of blowing snow easier. This is due to the availability of the "Day Snow-Fog" product, which combines the 0.86-, 1.6-, 3.9-, and 10.3-μm bands. Of these bands, the utility of the 1.6- μm band has proved most useful as it discriminates between snow, ice, and liquid/ice phase clouds. These products have allowed FGF NWS office forecasters to use GOES-16 imagery for detection of ground blizzards and areal

coverage of blowing snow events (i.e., widespread or isolated). In some cases, it has even helped forecasters to refine blizzard warnings which in turn refined messaging (personal communication, Fargo/Grand Forks NWS). Utilizing GOES-16 imagery along with radar observations and automated reports has led to improved Impact-Based Decision Support Services (IDSS) provided by the Grand Forks NWS office (Kennedy and Jones 2020).

Although the use of GOES-16 in the detection of blowing snow has many benefits, a few limitations exist. It was found that cloud cover can obstruct the detection of blowing snow (Kennedy and Jones 2020). This means that GOES-16 will work best for ground blizzards and blowing snow under predominantly clear skies. It is also noted that detection of blowing snow is contingent on near-infrared reflectance. So, blowing snow cannot be seen in GOES-16 imagery overnight. Further, while there is evidence that GOES-16 data is useful in blowing snow applications, the climatology of how often GOES-16 imagery is useful still needs to be investigated.

1.3.2. Modeling of Blowing Snow

Current applications for predicting blowing snow conditions range from rules of thumb, to empirical guidance, to numerical blowing snow models (Burrows and Mooney 2021). In many areas, such as northern Canada and the Antarctic, observations are limited. As a result, modeling has become a useful tool, especially as studies have shown the importance of surface and blowing snow transport on the snow mass budget (Yang et al. 2010). Many physically based blowing snow models have been developed and can be used in a stand-alone mode to evaluate blowing snow sublimation over a certain area (Yang et al. 2010). Studies have also discussed the development of coupled blowing snow-atmospheric modeling systems which have allowed for the identification

of sensitivities of sublimation rate and highlighted the need for accurate observations of important variables (Xiao et al. 2000). Unfortunately, many operational models do not have blowing snow parameterizations and often underestimate atmospheric variables associated with blowing snow, resulting in biases and errors in the model.

Burrows and Mooney (2021) evaluated three forecast products to forecast blizzard conditions in the Canadian Arctic. These automated products are from output generated by Numerical Weather Prediction (NWP) models run by the Canadian Center for Meteorological and Environmental Prediction (CCMEP). The first product called the blizzard potential (BP) comes from rules created by forecasters that identify where blizzard conditions may occur. This product is mostly used as a "heads-up" guidance for areas that forecasters should center their attention on versus point forecasts. The next product is created from work done by Baggaley and Hanesiak (2005), allowing for probability forecasts of blowing snow at specific points. Since these two products are derived from predictors sourced from observations versus NWP output, forecast accuracy is subject to error. However, the final product is a "model output statistics (MOS)" product so it can account for NWP model error (Burrows and Mooney 2021). This product is built to predict the likelihood that blizzard or near blizzard conditions will occur through a random forest (RF) algorithm. After verification, it was found that all three product forecasts performed well and have received positive feedback from forecasters (Burrows and Mooney 2021). Although all three are used, RF forecasts see the most use among operation forecasters. However, it is important to note that there are limitations with these methods as there is no physical coupling to the model.

Many studies relating to blowing snow modeling focus on understanding the influence of blowing snow on the surface mass balance. For example, Déry and Yau (2001a) investigated a

9

ground blizzard in the Northwest Territories of Canada to explore the blowing snow process and its interaction with the atmospheric boundary layer. A coupled atmospheric-blowing snow model was created using the Mesoscale Compressible Community (MC2) model and the PIEKTUK-D blowing snow model. Yang et al. (2010) studied the influence surface sublimation and blowing snow transport have on the snow mass budget. This was done by including the triple-moment version of PIEKTUK into the mesoscale MC2 model. PIEKTUK-T comes as an extension of the double-moment PIEKTUK-D as it predicts three moments of size distribution and includes predictive equations that allow for feedback from blowing snow sublimation. Results from this study showed that the model was able to simulate fields such as surface winds, temperature, pressure, and relative humidity well. Simulations in the study also showed that surface and blowing snow sublimation contribute greatly to the mass budget. This and other studies demonstrate the importance of sublimation, although it is often not included in operational models, possibly introducing errors.

Most recently, a physically based blowing snow model has been implemented in the Weather Research and Forecasting model by Luo et al. (2021). Named, WRF-ice, this high-resolution atmospheric model is used to capture the snow-ice-air interaction over polar regions. For this study WRF-ice was coupled with the double-moment blowing snow model developed by Déry and Yau (2001) and used to model a cyclone in the Antarctic Peninsula. First, performance of WRF-ice in modeling near-surface conditions, including sea level pressure, 10-m wind speed, surface temperature, 2-m temperature, and 2-m dew point temperature, was evaluated using both in situ observations and MODIS satellite imagery. Then impacts of blowing snow on the surface energy and mass balance were determined through a comparison of control and sensitivity simulations. Verification of the model showed that WRF-ice did well in modeling the observed

surface conditions with strong correlation coefficients from 0.88-0.99 (p-value < 0.0001), 0.79-0.95 (p-value < 0.005), 0.68-0.94 (p-value < 0.005), and 0.78-0.89 (p-value < 0.005) for sea level pressure, 2-m temperature, 2-m dew point, and 10-m wind speed, respectively. However, there were still biases observed for 10-m wind speed, 2-m temperature, and 2-m dew point. Further, results from the sensitivity simulations showed that blowing snow enhances water vapor in the lower atmosphere and can enhance precipitation when moistening and upward lift are present. With these results, the authors concluded that the neglect of blowing snow in atmospheric models can cause biases in forecasts of near surface conditions and surface mass balances. While these results are useful, they are based on a single case and a lack of blowing snow observations creates a degree of uncertainty in the evaluation of the blowing snow impacts.

While physically coupled schemes have not been used in the CONUS, model output has been used to drive empirical models. In a recent study done to improve visibility forecasts, a physically based blowing snow model was driven by output from a reforecast WRF simulation for a blowing snow event on February 24, 2019 (Letcher et al. 2021). Evaluation showed that WRF did quite well at simulating the event even though it did overestimate wind speeds. The authors concluded that applying components of the physically based blowing snow model to NWP output can improve forecast of blowing snow and visibility (Letcher et al. 2021).

While these blowing snow models may provide inputs and blowing snow parameterizations for atmospheric models, many of these studies did not focus on the performance of the models themselves. These impacts on model performance are important to understand as output will be dependent on meteorological forcing provided by them. Today, NOAA runs a vast suite of operational models. Of these models, the High-Resolution Rapid Refresh (HRRR) model has become an important tool used among forecasters. Many efforts such as the NOAA Hazardous

Weather Testbed (HWT) Spring Forecasting Experiment (SFE) have demonstrated the utility of models such as the HRRR during convective events (Clark et al. 2012, 2018). Further, studies have looked at object-based verification to evaluate warm-season forecasts, how well the HRRR simulates near-surface meteorological fields, and the HRRRs ability to predict mesoscale convective systems (Duda and Turner 2021; Lee et al. 2019; Pinto et al. 2015).

While there has been substantial verification of HRRR model performance during warm season/convective events, there is still considerable uncertainty in how HRRR model data can be used for winter hazards. The 2017 Hydrometeorology Testbed at the Weather Prediction Center (HMT-WPC) addressed some of these winter weather forecasting challenges tied to precipitation (Bodner et al. 2017). Among other models, participants looked at HRRRv3 1-hour snowfall accumulations. Throughout the experiment it was noted that while the HRRRv3 generally showed where snowfall would occur, the magnitude was too light (Bodner et al. 2017). Despite this bias, forecasters found hourly snowfall accumulation fields from the HRRRv3 to be beneficial. Recommendations were then made to make these fields available for forecasters to use in operations (Bodner et al. 2017).

Additional research on HRRR verification has been performed out of formal testbeds. Radford et al. (2019) evaluated snowband predictability in the HRRR. Results showed that HRRR does not predict band timing and location well but may be important in identifying snowfall events that have potential for band development. Evaluations have also looked at the ability of HRRR to predict cold-season precipitation and timing/location of snow, rain, and mixed-phase precipitation (Ikeda et al. 2013). Validation of HRRR forecasts was done using observations from the Automated Surface Observing System (ASOS) stations during the 2010-2011 cold season. Results showed that while the HRRR was able to represent the location and extent of both rain and snow

well, performance was much lower for mixed-phase precipitation. This is partially dependent on the size and organization of the weather system. It was concluded that larger, synoptically forced systems are better predicted than smaller systems. Expanding upon this study, Ikeda et al. (2017) focused on surface precipitation phase in HRRR. The authors used upper-air soundings, ASOS, and Meteorological Phenomena Identification Near the Ground (mPING) observations to investigate forecasts of modeled temperature profiles. Results showed that when surface observations indicated mixed-phased precipitation the HRRR model accurately represented the temperature profile. In some cases, the HRRR predicted rain while observations showed mix-phase precipitation associated with a warm bias of less than 2ºC in the model surface temperatures (Ikeda et al. 2017). In areas where cold-air damming was identified, the temperature bias was closer to 4ºC resulting in identification of the wrong precipitation phase and duration (Ikeda et al. 2017). Among the different cases, only two events where the observations indicated mix-phase and the model forecasted snow were observed. Profiles showed good agreement except in vertical levels where a cold bias exists just above the near surface inversion (Ikeda et al. 2017).

Operationally, the NWS has highlighted events in which the HRRR supported accurate winter weather forecasts. On 3 January 2018, a winter storm hit northeast Florida and southeast Georgia. Since this is an uncommon event for the area, no known model accuracy or bias was available for helping to forecast the event (US Department of Commerce 2018). While other models had problems, the HRRR was able to forecast both the precipitation type and amount accurately. This allowed for accurate winter storm watches and warnings to be issued, keeping people off the roads and decreasing the number of accidents and injuries due to winter storm impacts (US Department of Commerce 2018).

While it is noted that the HRRR has been useful in some wintertime events, there is limited verification for areas that commonly face blizzard conditions such as the Northern Plains. Additionally, the HRRR does not include the process of blowing snow. Instead, forecasters at the FGF NWS office need to rely on pattern recognition such as those discussed in Kennedy et al. (2019), or empirical techniques to forecast this process. More specifically, the GFK office has spent time investigating the abilities of the Canadian Blowing Snow Model (CBSM, Baggaley and Hanesiak 2005) which will be discussed further in section 1.4. This empirical model was developed to help forecasters to determine the probability that blowing snow will occur based on snow age, air temperature, and wind speed.

1.4 Operational Forecasting and Monitoring of Blowing Snow

1.4.1 Blizzard Warning Decision Process

The blizzard warning decision process is often complicated and can vary from forecaster to forecaster. It is important that the process and messaging be consistent from event to event and forecaster to forecaster to keep the effectiveness of warnings and related products (Grafenauer 2021). By NWS definition, several criteria must be met to reach blizzard conditions. These include sustained winds or frequent gusts greater than or equal to 35 mph, concurrent falling and/or blowing snow, and reductions of visibility to < ¼ mi for three or more hours. The blizzard warning decision process is not simple because of the many factors such as temperature, wind speed, snowfall rate, and snow age that influence visibility due to blowing snow (Baggaley and Hanesiak 2005). The NWS in FGF has identified two primary factors that increase impacts due to low visibility blowing snow: duration and coverage (Grafenauer 2021).

Based on subjective analysis and feedback from customers, and considering duration and coverage of blizzard conditions, the NWS FGF determined four distinguishable impact levels (Grafenauer 2021, Table 1). As the combination of duration and impacts increase, so do the impacts due to the blizzard conditions. Increasing coverage of blizzard conditions increases the area affected and increases the area of dangerous travel. Likewise, increasing duration of blizzard conditions increases impacts by shutting down travel and commerce for longer periods of time (Grafenauer 2021).

The FGF NWS forecasting office (NWSFO) considers the anticipated combination of coverage and duration of blizzard (i.e., whiteout visibility due to blowing snow) conditions for messaging impacts and determining headline decisions. Forecasters must consider the fine line between each of these categories as a small increase in wind speed can quickly result in decreased visibility (Grafenauer 2021). As long as the expected duration of blizzard conditions is at least 3 hours, the main factor that influences the blizzard warning decision process, and overall impacts, is coverage. The blizzard warning is a flagship winter product of the NWS, and when issued, forecasters have the mentality that all travel and other activities will be halted. With that philosophy in mind, a blizzard warning should be issued when the coverage supports this philosophy, and thus related to the high and very high impact levels (Table 1). Lower impact messaging and headlines are considered at the lower impact levels. The moderate impact level typically will not 'shut down the world', but other factors such as drifting, destructive power from wind gusts, and duration may be enough to increase impacts to match the blizzard warning philosophy.

1.4.2 Blowing Snow Model Guidance

As mentioned in Section 1.3.2, the Grand Forks NWSFO uses guidance from the CBSM to determine impact levels. Using the 27 blowing snow events discussed earlier, Makowski and Grafenauer (2016) further evaluated the usefulness of the CBSM in helping forecast high impact blowing snow events. The CBSM itself is sensitive to wind speed and surface temperature. So given similar wind speeds, there is a higher likelihood for < ½ mile visibility to occur for lower temperatures (Grafenauer 2021; Baggaley and Hanesiak 2005). Likewise, stronger wind speeds will also result in a higher probability of visibilities < ½ mile (Grafenauer 2021; Baggaley and Hanesiak 2005). Makowski and Grafenauer (2016) used the model output, which is the probability that visibility will be less than a given threshold due to blowing snow, and compared it to the coverage from each of the blowing snow events. Results showed that as the probability of ≤ ½ mi visibility increased from the blowing snow model output, the coverage of the ½ mi visibility also increased. In order to see whether correlation improved if duration was included, a Blowing Snow Impact Level (BSIL) parameter was calculated (Makowski and Grafenauer 2016). When compared to the blowing snow model output the correlation increased from 0.62 to 0.78, concluding that the increasing probabilities of ½ mile visibility from the CBSM are associated with increasing impacts (Makowski and Grafenauer 2016).

Using this information, the CBSM output probabilities have been included in the guidance for impact levels discussed earlier (Table 2). This guidance is a useful way for forecasters to diagnose and message these potential impacts, as well as provide a consistent way for all forecasters to make similar product decisions (Grafenauer 2021).

1.4.4 Available Tools

To determine impacts in real-time, visibility observations from ASOS and AWOS stations can be used (Grafenauer 2021). These can be described in terms of the impact levels discussed above. For the daylight hours, if visibility is at 0 mi this is considered a high impact event where coverage may be widespread or constant. Visibility of a ¼ mi is considered high impact when coverage may be frequent or scattered. Visibility of a ½ mi is considered moderate impact when coverage is intermittent or isolated. Finally, visibility of ¾ mi to 1 mi is considered low impact when coverage is sporadic and brief. For nighttime, this shifts to visibility values of 0 - ¼ mi being considered very high impact. If visibility is at ½ - ¾ of a mi, impacts are classified as high. Finally, 1 - 1 ¼ mi visibilities are considered moderate and low, respectively.

There are also multiple tools available to forecasters to incorporate the CBSM. The Grand Forks office has a standalone tool in the Graphical Forecast Editor (GFE) that allows grid output such as snow age, blowable snow depth, and potential for blowing snow. This tool is useful as it can be run on the side to output temporary grids to see the raw model output (Grafenauer 2021). Guidance from the CBSM is also built into ForecastBuilder which uses the model to set descriptors for blowing snow including 'Patchy', 'Areas', 'Definite', and 'Blizzard' (Grafenauer 2021).

It is important to note that the CBSM is deterministic in nature, meaning it provides only one possible solution. While temperature forecasts are often accurate, wind speed is more sensitive as an increase in wind speed can quickly decrease visibility. So, only using one wind speed and temperature for input is not always the best approach. In this case forecasters can use the Sensitivity Webpage found at: https://www.weather.gov/abr/BLSN-Model. This page allows for a probabilistic approach where forecasters can identify different potential outcomes (Grafenauer 2021). This site allows for real-time sensitivity testing as it takes into account the temperature,

snowfall rate, and wind speed. This allows forecasters to see the probability that a certain visibility threshold will be met, as a wide range of possibilities are given depending on different wind speeds and temperatures given.

While the CBSM is used regionally, the Winter Storm Severity Index (WSSI) is used nationally. The purpose of the WSSI is to assist forecasters in being aware of the possible significance of weather-related impacts, and to enhance communication to partners and the public of the expected severity of impacts due to winter weather (NOAA 2020). The WSSI uses gridded forecasts from the National Digital Forecast Database (NDFD). It then combines this data with non-meteorological dataset such as land use maps and snow analyses from centers such as the National Operational Hydrologic Remote Sensing Center (NOHRSC). WSSI hazards include snow load, snow amount, ice accumulation, blowing snow, flash freeze, and ground blizzard. Each of the hazards are associated with a 0 to 5 ("none" to "extreme") index where the final WSSI value is the maximum from all individual WSSI components for each grid point (NOAA 2020).

Within the WSSI, blowing snow indicates the potential disruption due to blowing and drifting snow, while ground blizzards indicate the potential impacts of strong winds interacting with pre-existing snow cover. The numerical index for WSSI blowing snow is calculated by multiplying the wind gust category, 6-hour snow ratio, 6-hour snow amount, and a land use factor. The index for WSSI ground blizzards is found by multiplying factors for snow age, snowpack temperature, wind speeds, and land use. These indices are then converted to a scale of 'None' where no impacts are expected to 'Extreme' where widespread damage and disruptions to daily life are expected (NOAA 2020). Minimal verification has been performed to assess WSSI performance for blizzards.

The empirical tools listed above are used at the FGF NWS office but are reliant on accurate input data. The development of these tools from downstream grids (e.g., the NDFD) obscures the utility from high resolution models. Ideally, blowing snow products should be based on raw model output, thus, it is necessary to understand how accurate variables (e.g., wind speed) are in models such as the HRRR.

1.5 Objectives

As discussed previously, forecasters have a variety of tools at their disposal, but rely on rules of thumb and empirical techniques to forecasting blowing snow. These techniques are often dependent on observations, accurate forecast of winds, knowing the condition of the snowpack, and being cognizant of land-cover. Due to the harsh temperatures and strong winds that usually accompany these events, the collection of observations is often difficult (Kennedy et al. 2021). Observations of snowpack are also usually not available to forecasters in real time, and a lack of understanding in the breaking of the snowpack crust also poses a difficult challenge to forecasters. Although uncertainty remains regarding the utility of high-resolution modeling systems for wintertime hazards such as blowing snow, high-resolution fields such as temperature, humidity, and wind could be used to determine blowing snow risk via empirical models such as the Canadian Blowing Snow Model or be used to drive physical blowing snow models. Prior to doing so, the performance of high-resolution models such as the HRRR needs to be understood.

Once blowing snow commences, the latest generation of GOES satellites has shown utility in identifying areas of the hazard. This has proven useful operationally at local weather forecasting offices. When used with other resources, GOES-16 has helped to improve situational awareness and Impact-Based Decision Support Services (IDSS) during blowing snow events (Kennedy and

Jones 2020). While it has proven beneficial, it is unknown how often and how long this imagery is useful during blowing snow events.

Given these uncertainties, this project will identify how GOES-16 and HRRR data may improve IDSS during blowing snow events. This will be done through a case study approach for events over the winters of 2018-2019 and 2019-2020. The NWS in Grand Forks has provided a list of 22 cases that are classified under blizzard, blowing snow that did not reach blizzard criteria, and null events. To understand the model biases and provide useful insight into the performance of the models, HRRR forecasts will be compared to surface observations across the FGF CWA. Surface meteorological variables will be subjectively and objectively analyzed, and visibility for point locations will be subjectively compared to output from GOES-16 imagery. Further, the utility of GOES-16 satellite imagery and HRRR model output will be determined for each event in the case study. In summary, results will allow for improved understanding of these tools, paving the way for future guidance to be incorporated into real-time IDSS displays.
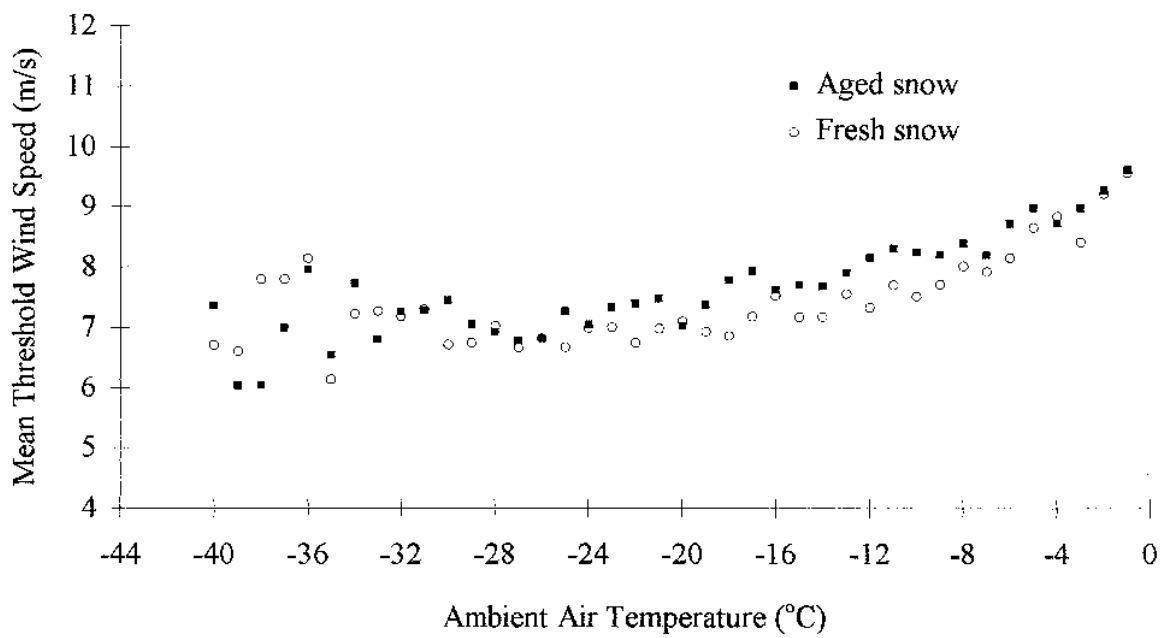
Figure 1.Transport threshold wind speeds for fresh- and aged snow as a function of ambient temperature. Adapted from Li and Pomeroy (1997b).
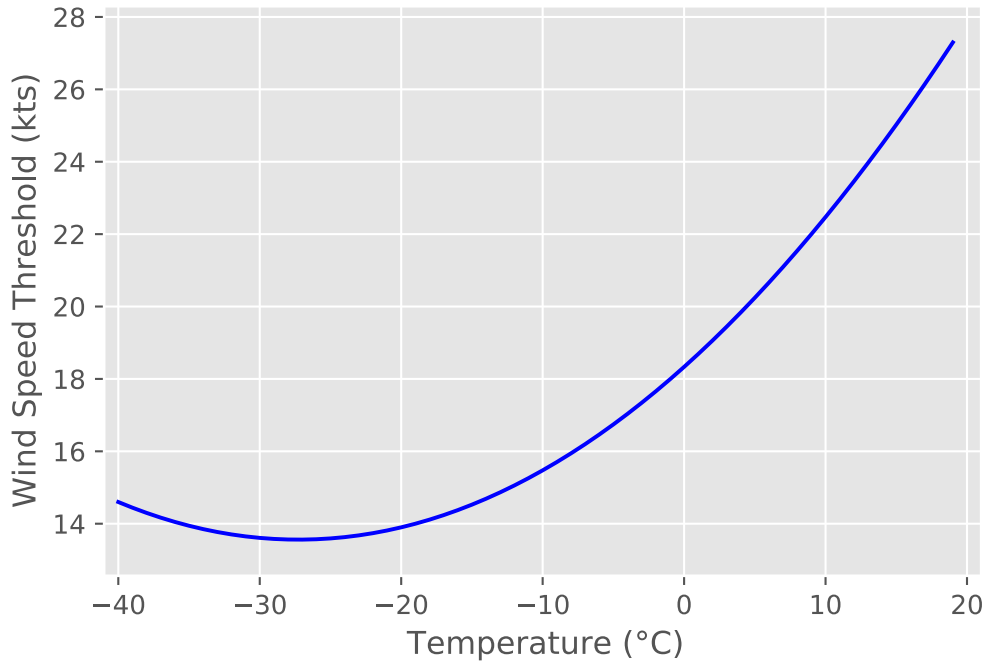
Figure 2. Wind speed threshold (kts) as a function of Temperature (ºC). Courtesy of Aaron Scott.
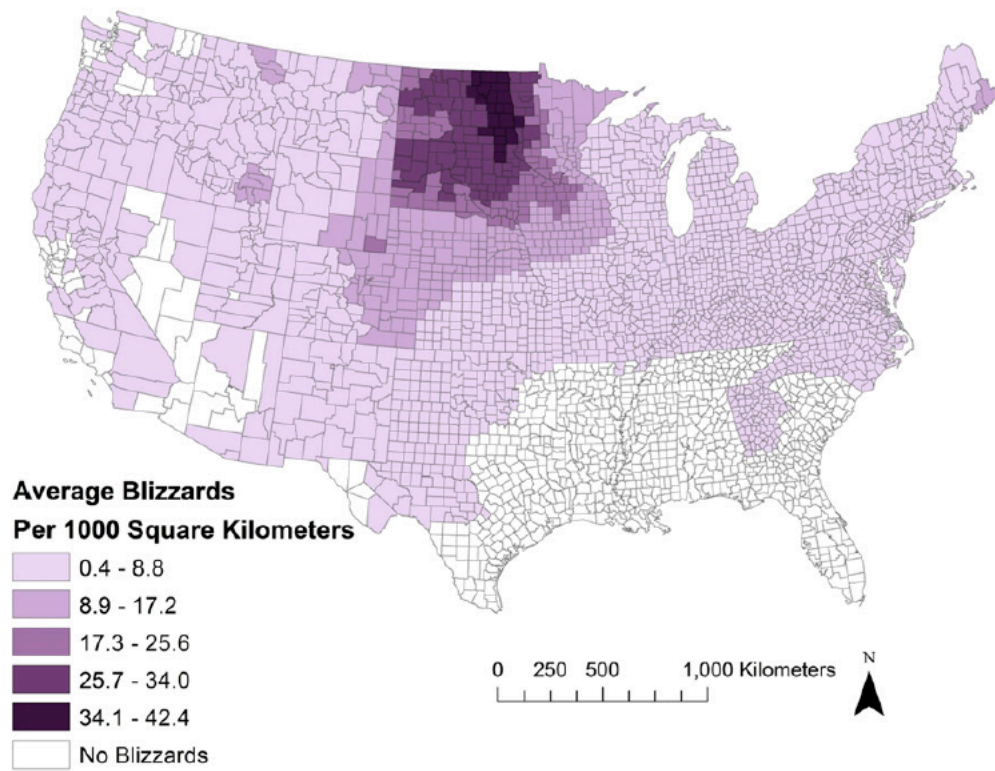
Figure 3. Average number of blizzards per 1000 km^2 for the winters of 1959/60 through 2013/2014. Adapted from Coleman and Schwartz (2017).
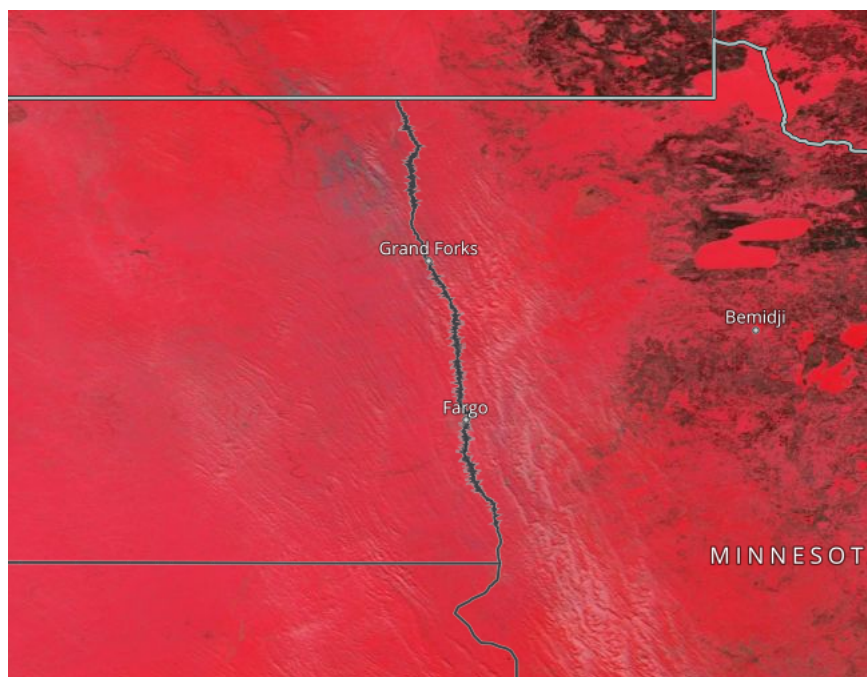
Figure 4. False color imagery from VIIRS on 24 January 2019. Snow cover (blowing snow) is depicted by red (white) colors, respectively. Darker areas in Minnesota are regions of forest.
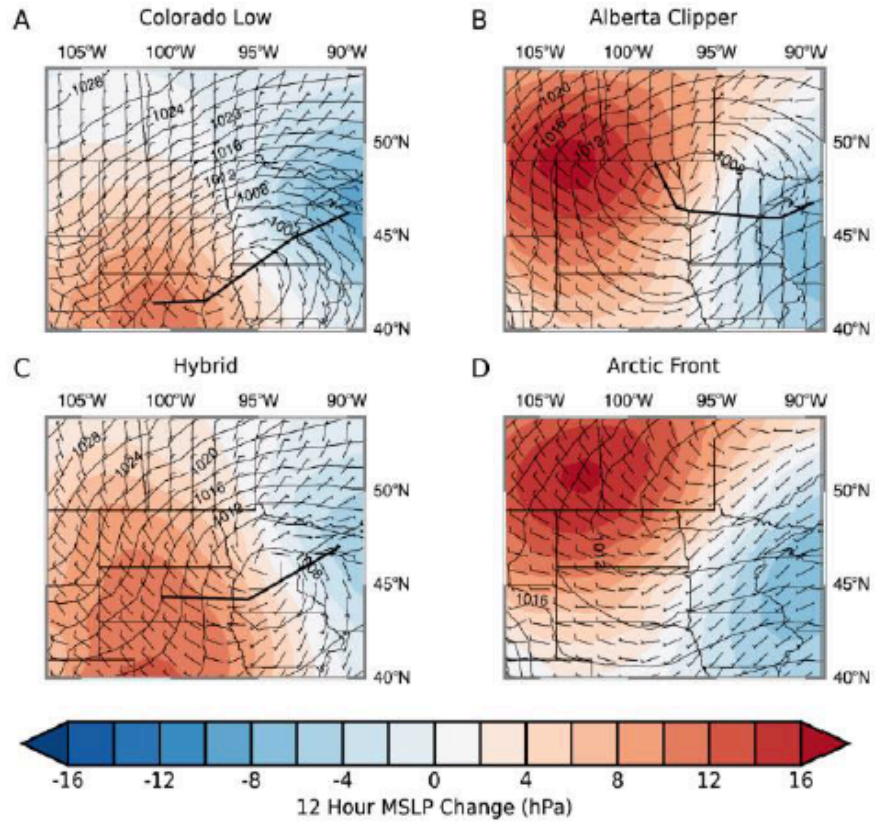
Figure 5. Composite meteorological patterns associated with blizzards in the FGF NWSFO CWA. MSLP 12 hours prior to the event is contoured. Thick black lines represent the mean storm track during (a) Colorado Low, (b) Alberta Clipper, (c) Hybrid, (d) Arctic Front blizzards. Adapted from Kennedy et al. (2019).

Figure 6. Picture taken by the UND Skycam showing blowing snow occurring under clear skies on 24 February 2019.

Table 1. Terminology for impact levels describing whiteout conditions (visibility ≤ ¼ mile). Adapted from Grafenauer (2021).

Impact Level	If a person is Stationary	If a person is Moving	GFE Terminology
Very High	Constant	Widespread	Definite
High	Frequent	Scattered to Widespread	Definite
Moderate	Occasional, Periods of, Intermittent	Isolated to Scattered	Areas of
Low	Sporadic, Brief	Isolated	Patchy

Table 2. Canadian Blowing Snow Model (CBSM) terminology for output and impact level. Adapted from Grafenauer (2021).

Probability	Impact	Description
0-14%	**Minimal**	Little if any impact
15-59%	**Low**	Advisory or isolated blizzard conditions (OK in town, bad in more prone rural areas)
60-79%	**Moderate**	Isolated to scattered blizzard conditions (OK in town, periodically bad in rural areas)
80-89%	**High**	Scattered to widespread blizzard conditions (bad in rural areas, periodically bad in town)
90-100%	**Very High**	Widespread blizzard conditions (bad in rural areas and town)

CHAPTER 2

DATA SOURCES

2.1 Surface Observations

2.1.1 Iowa Environmental Mesonet (IEM)

ASOS sites (Figure 7) are the primary source for providing sub-hourly surface weather observations for the NWS, Federal Aviation Administration (FAA), and the Department of Defense (DOD). While the automation eliminates direct human involvement in collecting data, the ASOS still requires Quality Control (QC). This is done in three different levels where level 1 is performed on-site, level 2 is performed at Weather Forecasting Offices (WFO), and level 3 is performed nationally at the ASOS Operations and Monitoring Center (AOMC). With routine maintenance and quality control, ASOS has been considered a reliable resource for surface weather observations. AWOS stations are similar to ASOS stations but are often operated by non-federal entities. Of the AWOS stations in the FGF CWA, most are either AWOS III or AWOS III P/T. AWOS III measures altimeter, wind data, temperature, dew point, density altitude, visibility, precipitation accumulation, and cloud height (US Department of Transportation 2017). AWOS III P/T sites have the same measurements as in AWOS III but includes optional sensors such as present weather and thunderstorm/lightning (US Department of Transportation 2017).

The automation of weather elements is broken into objective and subjective weather elements. Objective elements are directly measured and are easier to automate and include ambient temperature, dew point temperature, wind, pressure, and precipitation accumulation (ASOS Users Guide 1998). Subjective elements are more complex to automate as the system must sample

29

conditions in a small volume and average the data over a set time period (ASOS Users Guide 1988). These subjective elements include sky condition, visibility, and present weather.

Of the different elements discussed, visibility, temperature, and wind observations are important when monitoring blowing snow events. Due to the importance of temperature measurements, ASOS provides a 5-minute average air temperature every minute. This is measured through the hygrothermometer which uses a Resistive Temperature Device (RTD) to measure ambient temperature (ASOS Users Guide 1988). Overall, ambient temperature observations show many strengths, especially with improvements made to location of the sensor and the continuous monitoring and application of quality control (ASOS Users Guide 1988). Wind is measured using an ultrasonic ("sonic") wind sensor (Tuomaala 2005). This comes as an upgrade from the original cup and vane method used previously. These modernized sensors are now ice free and do not contain any moving parts, so the amount of maintenance needed has decreased and reliability has increased (Tuomaala 2005). Unlike the old system, the ultrasonic sensor also measures a change in direction as well as the standard 3-second average gust in real time (Tuomaala 2005). The ASOS visibility sensor (Figure 8) relies on the principle of forward scattering. There are many advantages of the visibility sensor including its location, consistency of observations such that variations introduced by human observers is eliminated, and the use of a wider 0-45 degree scattering angle range to get measurements more indicative of current conditions (ASOS Users Guide 1988). However, a major disadvantage of the sensor is the smaller sampling volume. So, if certain conditions are present in one area and the sensor is not in that location those observations may be missed.

Surface observations from ~29 sites across the CWA (Fig. 9) were used from ASOS and AWOS data downloaded from Iowa State University's Iowa Environmental Mesonet (IEM)

website. Note that ASOS and AWOS are used interchangeably on the site (Herzmann 2021). IEM maintains an archive of automated airport weather observation in the US and around the world from 1928 to the present. The data is sourced from many places including: Unidata IDD, NCEI ISD, and MADIS One Minute ASOS and is transmitted in a format called Meteorological Aerodrome Report or METAR. The IEM is simple to use and allows the user to select a network from a list by clicking on the location. The user then selects and downloads the available data of interest. This includes five-minute air temperature (ºF/ºC), dew point (ºF/ºC), relative humidity (%), heat index/wind chill (ºF), wind direction, wind speed (kts/ mph), altimeter (in), sea level pressure (mb), 1 hour precipitation (mm/in), visibility (miles), wind gust (kts/mph), cloud coverage level (1-3), cloud height level (1-3), present weather code(s), and 1- and 3-hour ice accretion. However, as some ASOS data does not come in exactly on the hour, a time frame was set so that data would be collected 10 minutes before and 15 minutes after the hour. This allowed for data from all of the sites to be collected, and any duplicates or missing data to be filtered out.

In order to fill in the gaps in visibility data between ASOS stations for this study, data from North Dakota, Minnesota, South Dakota, and Manitoba were interpolated using the 'nearest neighbor' method. This method determines the nearest neighboring pixel and takes that value, making it one of the simplest approaches to interpolation. The advantage of using this method is that the input values in the grid are preserved, such that the output is not different than the nearest input or outside of the range of input values.

2.2 Satellite Observations

2.2.1 Satellite Data

Imagery from the Suomi National Polar-Orbiting Partnership (Suomi NPP) and NASA Terra satellites were downloaded from the Worldview tool from the National Aeronautics and Space Administration's (NASA) Earth Observing System Data and Information System (EOSDIS). This application allows for users to browse and download over 900 global, full resolution satellite imagery layers (NASA 2021). With layers updated daily, a 'full globe' view and imagery available within three hours of observation, users can look at the Earth as it is 'right now' (NASA, 2021).

Satellite imagery from the GOES-16 satellite was downloaded from the University of Utah site found at: https://home.chpc.utah.edu/~u0553130/Brian_Blaylock/cgibin/goes16_download-.cgi. This site is provided as a way to download GOES datasets from Amazon Web Services (AWS). Users can select the source, satellite, domain, product, date, and hour needed on the website, or can use scripted downloads to retrieve data. Final downloaded files are received in NetCDF format.

2.2.2 Overview of Polar Orbiting Satellites

The Suomi NPP, previously known as the National Polar-orbiting Operational Environmental Satellite System (NPOESS) Preparatory Project, is a NOAA satellite that was launched in 2011 (Christopherson et al. 2019). This satellite serves as a bridge between the NOAA Polar Operational Environmental Satellites (POES), NASA's Earth Observing System (EOS) missions, and the NOAA Joint Polar Satellite System (JPSS) (Christopherson et al. 2019). Suomi

NPP carries five instruments including the Visible Infrared Imaging Radiometer Suite (VIIRS). Providing global coverage twice a day, the VIIRS instrument gathers infrared and visible imagery of clouds, land, atmosphere, ice, and oceans across twenty-two spectral bands and develops products for operational use (King et al. 2006). Of the twenty-two spectral bands, five are high-resolution image bands and sixteen are moderate resolution bands, some of which are sensitive to blowing snow events and allow for the detection of blowing snow for cloud free scenes. These bands include the combination of the visible M3 (0.49-μm) band and the near-infrared I3 (1.61-μm) and M11 (2.25-μm) bands.

The Terra satellite is a moderate-resolution multispectral satellite that provides quantitative measurements of the atmosphere, land, and oceans (King et al. 2006; Christopherson et al. 2019). Formally called EOS AM-1, Terra is the first EOS satellite, and is considered the flagship of NASA's Earth Science Missions (Christopherson et al. 2019). Terra also carries five instruments including the Moderate Resolution Imaging Spectroradiometer (MODIS). This instrument is designed to get observations of biological and physical processes in the atmosphere and on land and ocean surfaces across thirty-six discrete bands (King et al. 2006). Similar to VIIRS, MODIS also has bands that are sensitive to blowing snow such as the combination of visible Band 1 (0.645-μm), near-infrared Band 2 (0.859-μm), and near-infrared Band 7 (2.13-μm). Due to its large viewing swath, MODIS provides imaging of most of globe in one day, and the whole globe in two (King et al. 2006).

2.2.4 Overview of GOES-16

NOAA's third generation of Geostationary Operational Environmental Satellites (GOES), known as the GOES-R series, is the most recent and advanced set of geostationary weather

satellites developed to improve observations of the environment. This series consists of four satellites including GOES-16 which orbits at 75.2ºW longitude. Often referred to as GOES East, coverage is provided over North and South America and the Atlantic Ocean. Six instruments are aboard GOES-16 including the Advanced Baseline Imager (ABI). With 16 spectral bands (2 visible, four near-infrared, and ten infrared), four times the spatial resolution, and five times faster imaging cycles than previous GOES imagers, the ABI is the primary instrument aboard GOES-16 for imaging the Earth's environment. Currently, forecasters at the Fargo/Grand Forks NWSFO utilize the ABI to detect blowing snow plumes, which can be seen by combining the 0.86-, 1.6-, 3.9-, and 10.3-µm bands to help distinguish snow and clear ground from clouds (Kennedy and Jones 2020). The 0.86 µm and 1.6 µm bands are used for the red and green colors of the composite, while the difference between the 3.9 µm and 10.3 µm band make up the blue color and provide a proxy for the reflected solar radiance (Kennedy and Jones 2020). Unfortunately, use of the 0.86-µm and 1.6-µm bands limit the product to the daytime hours when reflective solar radiation reaches the sensor (Kennedy and Jones 2020). Of the three channels, the 1.6 µm is the most useful due to varying reflectance between ground cover and blowing snow plumes. For this study, the 1.6 µm band was sufficient for detection of blowing snow plumes and allowed for less data manipulation.

2.3 High-Resolution Rapid Refresh Model

2.3.1 Model Download Source and Overview

The HRRR is a 3-km resolution, convection-allowing atmospheric model run hourly at NCEP. The HRRR is initialized from the Rapid Refresh (RAP) and radar reflectivity observations are assimilated every 15 min. Although the current operational model is the HRRRv4, the HRRRv3 was operational during the timeframe of this project. Implemented in 2018, HRRRv3

ran every hour and provides hourly forecasts out to 36 hours for the 00, 06, 12, and 18 runs and to 18 hours for all times. Improvements to the HRRRv3 included updates to the Thompson microphysics (Thompson and Eidhammer 2014), improvements in the Mellor-Yamada-Nakanishi-Niino (MYNN) Planetary Boundary Layer (PBL) scheme (Nakanishi and Niino 2009), updates to the RUC land surface model, and a refined roughness length over different land-use types (Bodner et al. 2017).

HRRR data was obtained from the University of Utah MesoWest HRRR archive, which is made up of output from the National Centers for Environmental Prediction (NCEP) (Blaylock et al. 2017; Horel and Blaylock 2015). The archive contains output files in Gridded Binary Version 2 (GRIB2) format including the Experimental HRRR, Operational HRRR, and HRRR-Alaska. These files were downloaded from NOAA Earth System Research Laboratories and the NOAA Operational Model Archive and Distribution System.

Figure 7. Example of an Automated Surface Observing Station (ASOS Users Guide 1988).
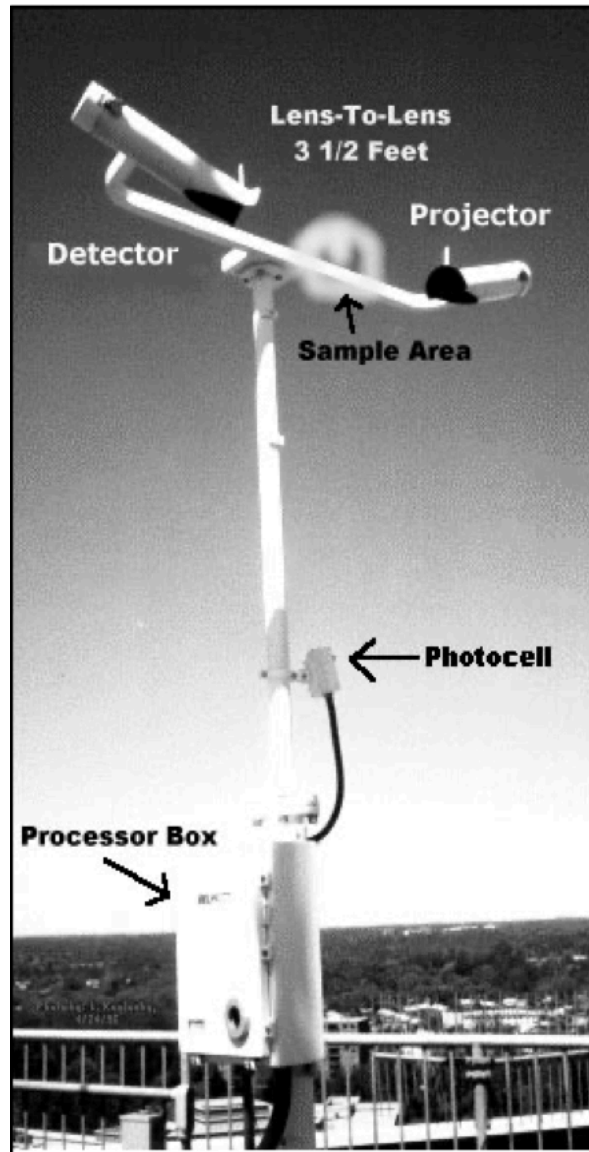
Figure 8. Example of a forward scattering visibility sensor (ASOS Users Guide 1998).
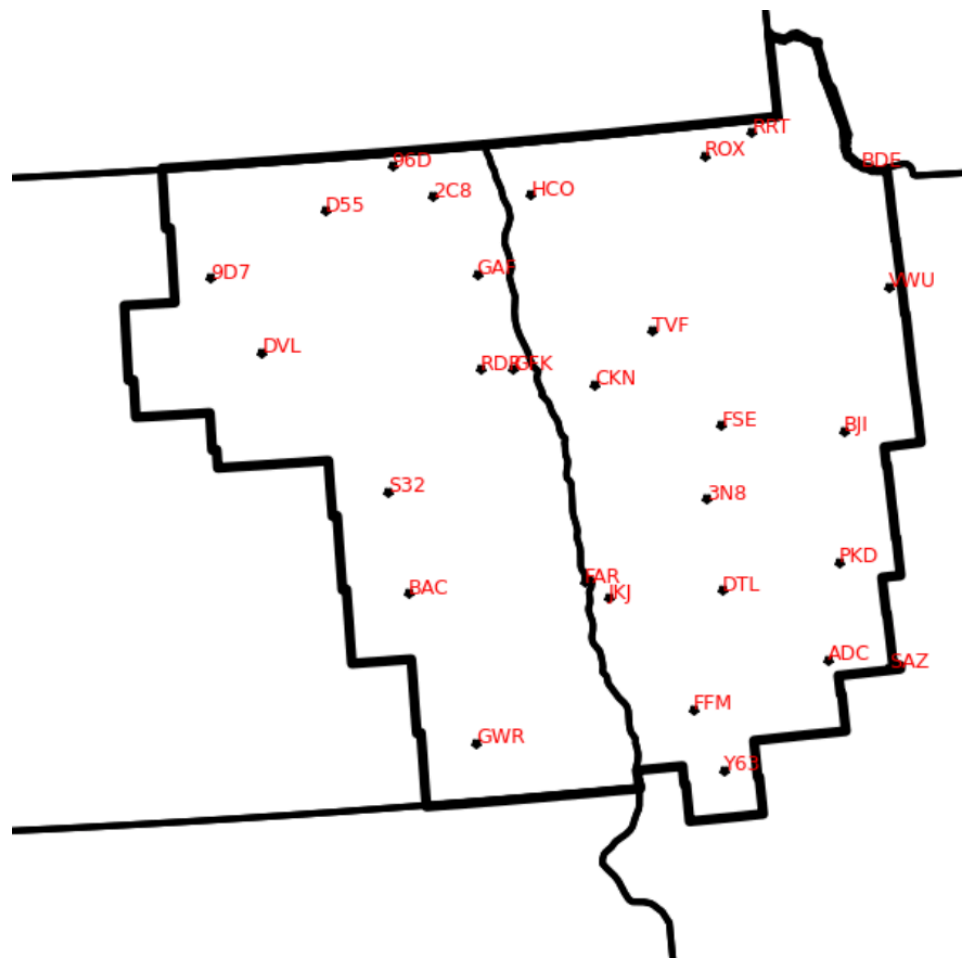
Figure 9. ASOS and AWOS stations across the FGF CWA.

CHAPTER 3

METHODOLOGY

3.1 Case Selection

A case study approach was used to investigate blowing snow events for the winters of 2018- 2019 and 2019- 2020. The Grand Forks NWS office provided a list of 22 cases (Table 3) that included blizzard events, blowing snow events that did not reach blizzard criteria, and null events. The start time, midpoint, and end time were determined for each of the events, as well as the classification (e.g., Arctic front) When appropriate, data was collected for the days before and after to account for circumstances in which an event spanned multiple days.

Surface data was obtained from ASOS and AWOS stations across North Dakota, Minnesota, South Dakota, and Manitoba for duration of each case. Of the many variables available, those most relevant to blowing snow frequency including temperature (°C), dewpoint (°C), wind direction (°), wind speed (kts), sea level pressure (mb), visibility (miles), wind gust (kts), present weather code(s), and peak wind gust (kts) were selected. Missing and trace reports were included but were represented as 'M' and 'T', respectively in the data.

Surface field (2D) data from the Operational HRRRv3 was downloaded for each individual case during the 2018-2019 and 2019-2020 winter seasons. For qualitative and quantitative assessment and verification of HRRR fields, data from the first model forecast hour ('f01') was downloaded for each model run hour (00-23z). The first forecast hour (F01) is used as it provides all model outputs such as visibility and precipitation, whereas the initial forecast hour does not. This time is used as a gridded analysis during the event and represents the 'best guess' forcing that could be used to drive blowing snow IDSS products.

In order to evaluate forecasts, model run hours 6 and 12 hours (6HR and 12HR) in advance of the start time for each event were identified. This allows for spin-up periods to be neglected yet provide short-term guidance useful to forecasters. Once model run hours were determined for each event, the model forecast hours, 'f00-f18' or 'f00-f36' depending on data availability for that event, were then obtained.

ABI (L1b Radiances) data was downloaded for GOES-16/East. Data was downloaded for each hour for each of the events. Since CONUS scans are available every 5 minutes, the first minute was chosen for each hour requested. ABI Band 5 (1.6 µm) was chosen as this is the near-infrared or snow/ice band, which allows for daytime snow, ice, and cloud discrimination. Satellite imagery from Suomi NPP and Terra were also collected. The VIIRS corrected reflectance (Bands M3-I3-M11) and MODIS corrected reflectance (Bands 3, 6, 7,) were selected. Both of these combinations are used to show snow and ice, which are reflective in the visible part of the spectrum and absorbent in the short-wave infrared (NASA, 2021). Since the visible light is assigned to red, snow and ice appear in different shades of red, and small ice crystals in clouds appear pink. In MODIS however, thicker snow and ice, and ice crystals can appear in a red-orange color as well.

3.2 Assessment of Data

In order to evaluate the performance of the HRRR during blowing snow events, verification was done by comparing HRRR forecasts to surface observations across the FGF CWA. As Turner et al. (2020) noted, this evaluation is done subjectively through "eyeball comparison" and objectively to understand actual model biases. Through both of these approaches, conditions where the model performs well and where the model needs improvement can be identified. This study

has taken a similar approach by qualitatively and quantitatively analyzing ASOS/AWOS surface observations, satellite data from GOES-16, and HRRR model data.

3.2.1 Qualitative Analysis

To begin this analysis, HRRR and surface observations were first inspected. HRRR visibility, surface wind gusts, and precipitation were downloaded and plotted for each individual event. Note that HRRR visibility is in meters, winds are in m/s, and precipitation rate is in kg m^{-2} s^{-1} so values were converted to miles for visibility, knots for winds, and millimeters per hour for precipitation rate. This allowed for an analysis and comparison among the HRRR surface conditions to subjectively see whether there was any relationship between these three conditions. A time series for the event was also created for three locations (Devils Lake, Grand Forks, and Fargo) in the CWA using surface observations of sustained wind, wind gusts, and visibility. This allowed for a visual of when visibility (mi) dropped in those locations, the sustained wind (kts) throughout the event, and timing of highest wind gusts throughout the event. The time series and HRRR plots were then compared to see how well the HRRR did with timing and magnitude of the various variables.

Next, GOES-16 data for each event was plotted and evaluated for times in which there was cloud cover or blowing snow plumes that could be seen. Suomi NPP and Terra imagery were then used to supplement the imagery collected from GOES-16. Imagery from Suomi NPP and Terra were looked at for a couple days before the event, during the event, and after the event to see areas in which there was snow on the ground, whether there were clouds, and whether blowing snow plumes could be seen. Identification of snow cover before the event was specifically helpful in

seeing whether there was snow on the ground that could produce blowing snow/ground blizzard conditions on the day being studied.

To compare this data, HRRR visibility and surface wind gusts, a time series of visibility from surface observations, and GOES-16 satellite overlaid with station plots showing wind barbs and visibility values layered over the interpolated visibility contours were plotted in a four panel display for each hour of each event. The same three locations were chosen from the FGF CWA, and visibility was plotted from 00 UTC on the day of the event to 00 UTC of the next day. As mentioned in section 2.2, GOES-16 satellite data for the 1.6 μm band is limited to daytime hours. So, for each month satellite images were observed to find the start time and end time in which satellite data was available. For times in which satellite was not available imagery was not plotted in order for a better view of the overlaid surface visibility and wind speed observations.

Using this data, a table for each case was created (see Appendix A). For every hour a qualitative assessment was done and the HRRR visibility, HRRR winds, and ASOS visibility and winds were recorded. A fourth column provided a notes section in which timing and location of visibility reductions, comparison of HRRR and observations of winds, and comparison of HRRR and observations of visibility were recorded. Final notes also included evaluation of Suomi NPP and Terra satellite imagery to assess snow coverage before, during, and after each event.

Next, supplemental tables were created to visualize values for each event (see Appendix B). All ASOS stations in the FGF CWA were identified and visibility and wind gust data were collected using the same process as previously discussed. Maximum visibility, minimum visibility, average visibility, and maximum wind gust were determined for each hour and recorded within the table. Coverage of reduced visibility was determined and classified in one of four categories: "Isolated", "Scattered", Widespread", and "Everywhere". Each of these were determined

subjectively by setting a visibility threshold and determining what percentage of stations report visibilities at or below that threshold. If less than or equal to 25% of stations report visibility less than the threshold then it is considered "Isolated", if greater than 25% and less than 50% of the stations report visibility less than the threshold then it is reported as "Scattered", if more than 50% and less than or equal to 75% of stations report visibility less than the threshold it is reported as "Widespread", and finally any reports greater than 75% are considered "Everywhere".

Finally, supplemental tables were created highlighting when warnings and advisories were issued and when blizzard criteria was met for each event (see Appendix B). Valid time event code (VTEC) products issued from the Grand Forks NWS office for winter storm warnings, watches, and advisories, and blizzard warnings were collected from the IEM site. Then for each of the warnings, watches, and advisories the time the product was issued and the time the product expired was noted. As discussed earlier, for an event to meet blizzard criteria, there must be sustained winds or frequent gust greater than or equal to 35 mph AND concurrent falling and/or blowing snow that reduces visibility to less than ¼ mile for three or more hours. To determine whether blizzard criteria was met for each event, information for visibility and winds were evaluated from the first table above.

3.2.2 Quantitative Analysis

For this case study, the surface observation data was compared to the nearest model grid point within the FGF CWA. For each of the ~29 sites selected, a 'nearest neighbor' method was used to find matching HRRR data. Select HRRR meteorological fields (e.g., 2m temperature, 10m wind, 2m humidity, pressure, and visibility) were extracted from the model grid point closest to each station. For each event a dataset was created containing observations and nearest neighbor

model fields from each of the three model runs. This data was then used to find model error at each forecast hour by subtracting the observation data from the model data.

Box plots showing the error at each event hour were created for the 12HR, 6HR, and F01 forecasts for each variable. The box represents the bounds of the interquartile range of the data. The whiskers represent 1.5 times the interquartile range and the empty circles represent outliers that fall outside of this range. Biases were then calculated for each blizzard type by taking the average and standard deviation of the mean and median values.

Table 3. List of events received from the Grand Forks NWS. The list includes blizzards, blowing snow events that did not meet blizzard criteria, and null events.

Event Date	Classification Type
31 Dec. 2018	Arctic Front
28 Dec. 2018	Colorado Low
24 Jan. 2019	Arctic Front
27 Jan. 2019	Alberta Clipper
29 Jan. 2019	Arctic Front
8 Jan. 2019	Arctic Front
3-4 Feb. 2019	Hybrid
7 Feb. 2019	Hybrid
14 Feb. 2019	Hybrid
24 Feb. 2019	Arctic Front
4 Mar. 2019	Unclassified
14 Mar. 2019	Colorado Low
11 Apr. 2019	Colorado Low
11 Oct. 2019	Colorado Low
30 Nov. 2019	Colorado Low
8 Dec. 2019	Alberta Clipper
14 Dec. 2019	Hybrid
29 Dec. 2019	Colorado Low
18 Jan.2020	Hybrid
21 Jan. 2020	Unclassified
12 Feb. 2020	Arctic Front
19 Mar. 2020	Arctic Front

CHAPTER 4

CASE STUDIES

This chapter provides examples of the methodology for three different blizzard events: an Alberta Clipper on 27 January 2019, an Arctic front on 12 February 2020, and a Colorado low on 14 March 2019. These events were chosen based on impacts, representativeness of common blizzard events, and the availability of data and event reviews done by the FGF NWSFO. An overview of the environment leading up to and during the event, the resulting impacts, and a qualitative and statistical analysis is presented for each of these cases. The qualitative analyses were made to compare operationally important variables relevant to blowing snow forecasting including visibility, winds, relative humidity, and temperature. This allowed for conceptual understanding of the cases and allowed the author to note similarities across other events. Further, this type of analysis is more similar to the event summaries created in operational environments immediately following events where quantitative assessment is rarer.

4.1 27 January 2019 – Alberta Clipper

On 27 January 2019, a strong Alberta clipper system moved southeastward across Canada and North Dakota. This system had snow accumulation up to 8 inches in depth and gusty winds over 30 mph (~26 kts), creating blizzard conditions throughout the afternoon and evening time (NWS 2019a).

4.1.1 Environment

This system was forced by a shortwave trough that moved through Canada and across the Northern Plains (Figure 10). This created a deep, 998 mb surface low pressure associated with a

strong pressure gradient that allowed for gusty winds ahead of the surface low (NWS 2019a). In the lower levels, strong thermal gradients surrounded the clipper. Frontogenetical support from the tightening of these gradients helped to increase precipitation near the fronts. Just ahead of the warm front, snow rates of >1 inch per hour and gusty winds created blizzard conditions (NWS 2019a).

4.1.2 Impacts

Significantly reduced visibility due to blowing snow was seen across most of eastern North Dakota (Figure 11). This caused most of the state to be under a "No Travel Advised" alert during the late afternoon on 27 Jan 2019 (NWS 2019a). Across the region, most counties within the FGF CWA were in a blizzard warning. Four of the counties in the far eastern part of the CWA were in a winter weather advisory, while a couple remained in a wind chill advisory (Figure 12).

4.1.3 Qualitative Analysis

Meteograms for GFK, DVL, and FAR provide an overview of the event timing as visibilities (winds) decreased (increased) during the afternoon of the 27th and ending in the morning hours on the 28th (Figure 13). For this event, the start time, midpoint, and end time were identified as approximately 15Z on the 27th, 21Z on the 27th, and 04Z on the 28th, respectively. Analysis of observations show that as wind speeds began to increase above 20 kts (~23 mph), visibilities decreased to < 1 mile starting around 15Z in DVL, 18Z-21Z in GFK, and 19Z in FAR. Note that wind gusts began around or just before each of these start times, with gusts > 20 kts (~23 mph) reported in all three locations. By 21Z, visibilities decreased to nearly 0.25- 0.75 mi in all three locations, with winds gusting to over 30 kts in FAR. By 04Z, visibilities improved to > 5 mi in all three locations as winds decreased and wind gusts were no longer reported.

Figure 14 provides a broader overview of observations over the FGF CWA. At the start of the event, thick clouds covered the entire area as the surface low moved south towards ND. Visibility remained at 9 to 10 mi across most of the area as visibility at stations on the western edge of the CWA decreased significantly as snow began to make its way into the area. At 21Z, thicker cloud cover still remained over the CWA as heavy bands of snow east of the warm front moved over areas around and just east of GFK. This snowfall with the addition of increased wind speeds due to the tight pressure gradient created blizzard conditions. This is reflected in the observations as visibility was greatly reduced to ~0.25 mi along the RRV.

Since the early portion of the event had clouds, and later portions were during darkness, GOES-16 near-infrared satellite imagery was unavailable. However, observations reported visibilities back to nearly 10 mi with calmer winds as the system moved out of the area. Regardless of time of day, blowing snow could not be identified by GOES-16 due to the amount of cloud cover (Figure 15).

Next, model data is analyzed for the start, midpoint, and end of the event. At the start of the event (Figure 16), the HRRR forecasted an area of widespread low visibility across central ND and into the western portion of the CWA. HRRR surface wind gusts and relative humidity increased in the areas coinciding with these low visibilities where the system had forecast snowfall (not shown). Forecasted temperatures were similar to observations with a west-to-east gradient which corresponded well with the movement of the warm front south-eastward across the region. At 21Z (Figure 17), the widespread area of low HRRR visibility moved further east and coincided with increased surface wind gusts and relative humidity. Temperatures still varied across ND as the warm front continued to move through the state. At 04Z (Figure 18), the visibility reductions forecast by HRRR continued to move eastward. Although many areas in the CWA had improved

visibility, areas of low visibility remained across GFK and FAR. Surface wind gusts decreased through most of the CWA with higher wind gusts located both east and west of the CWA. Forecasted relative humidity was more uniform across the CWA, with values around 80%.

Overall, the HRRR F01 forecasts adequately captured the evolution of the event. As expected, low visibilities and high relative humidity from snowfall, increased wind gusts from pressure gradients, and large temperature gradients were all captured. Observed and F01 visibilities had good agreement throughout the event. Other than the model having observed visibilities that were reduced 1-2 hours before the observations, performance was good with bias within 1-2 mi throughout the event (Figure 19).

Similar patterns between relative humidity and temperatures are shown in Figure 20-21. Before the event, F01 forecasted relative humidity and temperatures were lower and colder than observed. The largest difference in observations and the model was approximately 20% and 5.5 ºC (42 ºF) for humidity and temperature, respectively. After the start of the event both relative humidity and temperature show better agreement between the model and observations, with the largest humidity and temperature errors being below 10% and 2 ºC, respectively.

4.1.4 Quantitative Analysis

Box plots are used to provide a statistical summary of the error between the model and observations for the variables discussed above. Several notable features are found for visibility forecasts (Figure 22). As expected, visibilities were better prior to the event with 10+ mi visibilities forecasted and observed at most stations in the CWA. Overall, there was good agreement between the HRRR and observations for the F01 and 6HR forecasts (Table 4). While the medians were approximately 0-mi through the duration of the 12HR forecast, there was a slight negative bias for

49

forecasted visibility. During the event, there was a -1.8 to -0.2 mile bias for all three forecasts, with greater spread in the data (Table 4). There were many outliers suggesting greater spatial variability. This could be due to the HRRR forecasting a greater coverage precipitation or having slightly different timing as noted earlier in the meteograms. Overall, visibility forecasts improved as timing approached the event (e.g., 12HR to 6HR forecasts).

It is important to note that during peak blizzard conditions between 21Z and 23Z (Figure 22), the F01 runs had some visibility observations higher than what were reported in observations; such biases between the model and observations could be caused by the HRRR not parameterizing blowing snow. However, towards the end of the event, the model forecasted visibilities were primarily lower than the observations, which is reflected in the negative mean median bias value of -0.2 (Table 4). Provided that blowing snow is not parameterized, this supports wider precipitation coverage than observed.

HRRR performance for wind gusts and sustained winds are shown in Figures 23- 24. Prior to the event, there were minimal wind gusts and analysis is limited to the event itself. All three forecasts had a positive bias of 7- 7.6 kts in (Table 5). While there are a few outliers, the spread among the data is large, with the largest errors > 15 kts. Despite this bias, there is better agreement for sustained wind speeds (Table 6). Overall, all three forecasts have a small positive bias of 0.8- 1.7 kts prior and 0.5-0.6 kts during the event.

Temporal variability in performance is found for HRRR forecasts of relative humidity and temperature (Figure 25- 26). The HRRR forecast had a substantial dry bias regardless of run (11.2- 12.1%) leading up to the event (Table 7). During the event this switched to a moist bias (2.1- 6.2%) for the 6HR and 12HR forecasts. Better performance is found for the F01 forecast (-1.5%) with some subtle variability during the event (slightly moist during peak blizzard conditions similar to

12HR and 6HR forecasts). Similar patterns are seen for temperature (Figure 26). While the error is much less than that seen with relative humidity, a negative bias of -1.2 to -1.9 is observed for all forecasts before the start of the event (Table 8). Before (during) the event the HRRR forecasted temperatures lower (higher) than what was observed. With magnitudes within ±2.3 ºC. There are also quite a few outliers, especially in the 6HR and 12 HR forecasts. Overall, this suggests that humidity biases were in part due to changes in specific humidity during the event.

Using this analysis, a few observations are made for this clipper event. Overall, the F01 and 6HR runs did well in forecasting visibilities across the CWA. While there was large spatial variability, this was likely due to greater coverage in precipitation or the timing of the system moving over each station. The HRRR consistently over forecasted wind gusts, but overall wind speeds were forecast well, with much less variability in the data. Forecasts for relative humidity and temperature showed a moist, warm bias during the event, with more spread in data seen for relative humidity than temperature. This suggests that specific humidity changes during the event could be the cause for the humidity bias observed and this could be tied to model microphysics and simulations of snowfall.
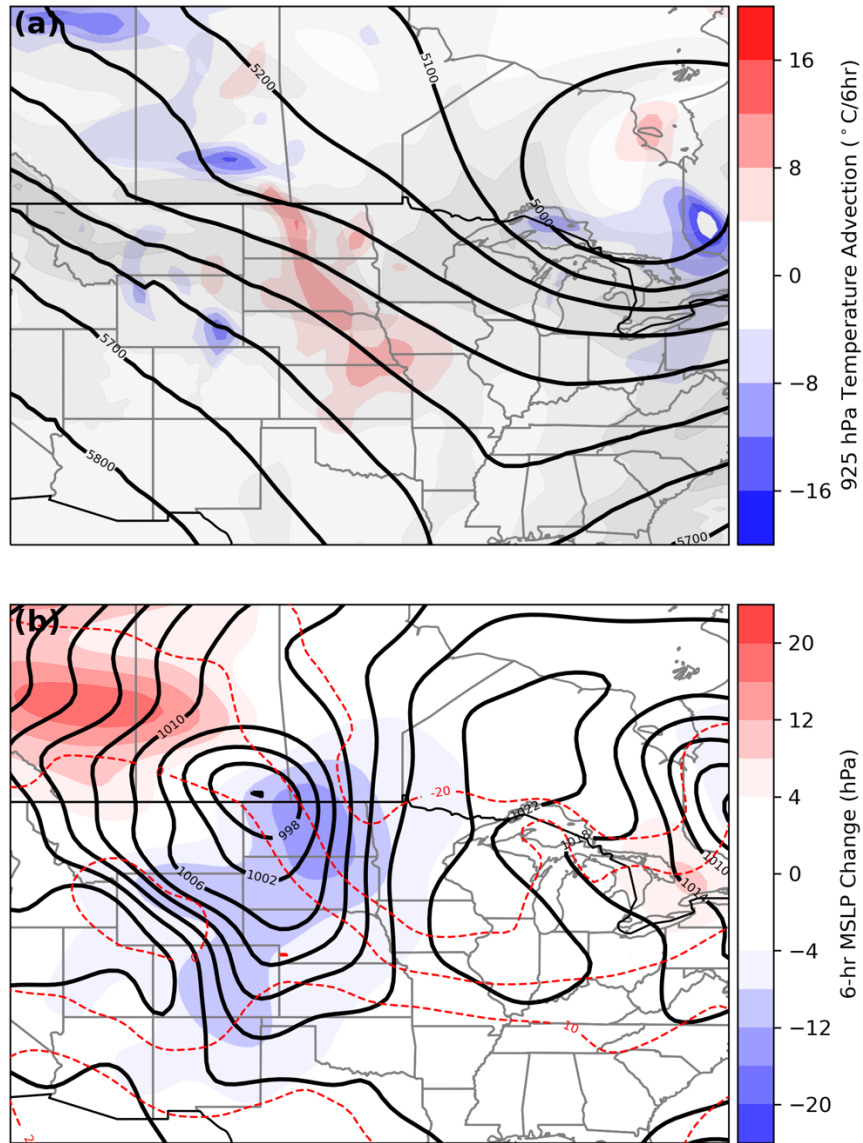
Figure 10. Meteorological fields from the GFS analysis valid at 1200 UTC 27 Jan 2019. (a) 500-hPa geopotential height (black contours), 500-hPa wind magnitude (semitransparent gray contours), and 925-hPa temperature advection (filled contours). (b) Mean sea level pressure (MSLP, black contours) and 6-h MSLP change (filled contours).
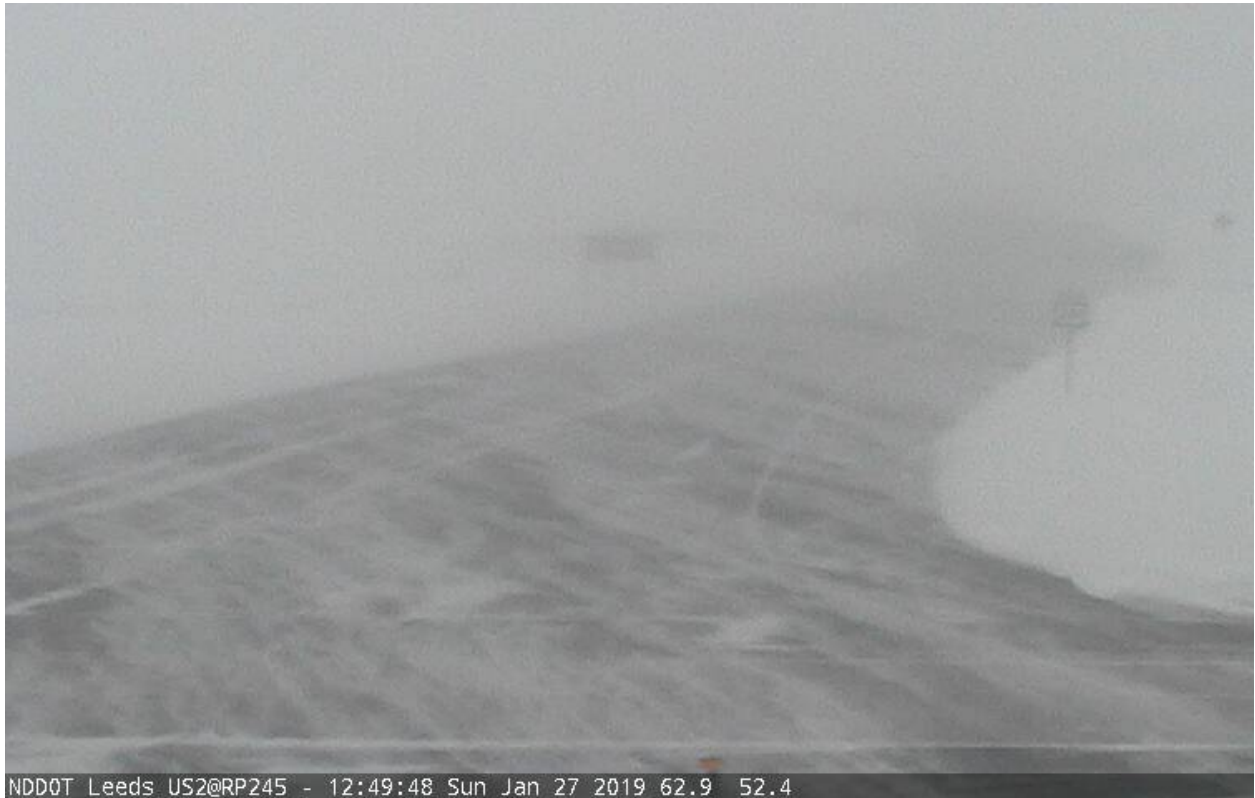
Figure 11. North Dakota Department of Transportation (DOT) road camera image from Leeds, ND taken at 1249 UTC (749 AM CST) 27 January 2019. Image provided by the Fargo/Grand Forks NWSFO (US Department of Commerce 2021c).
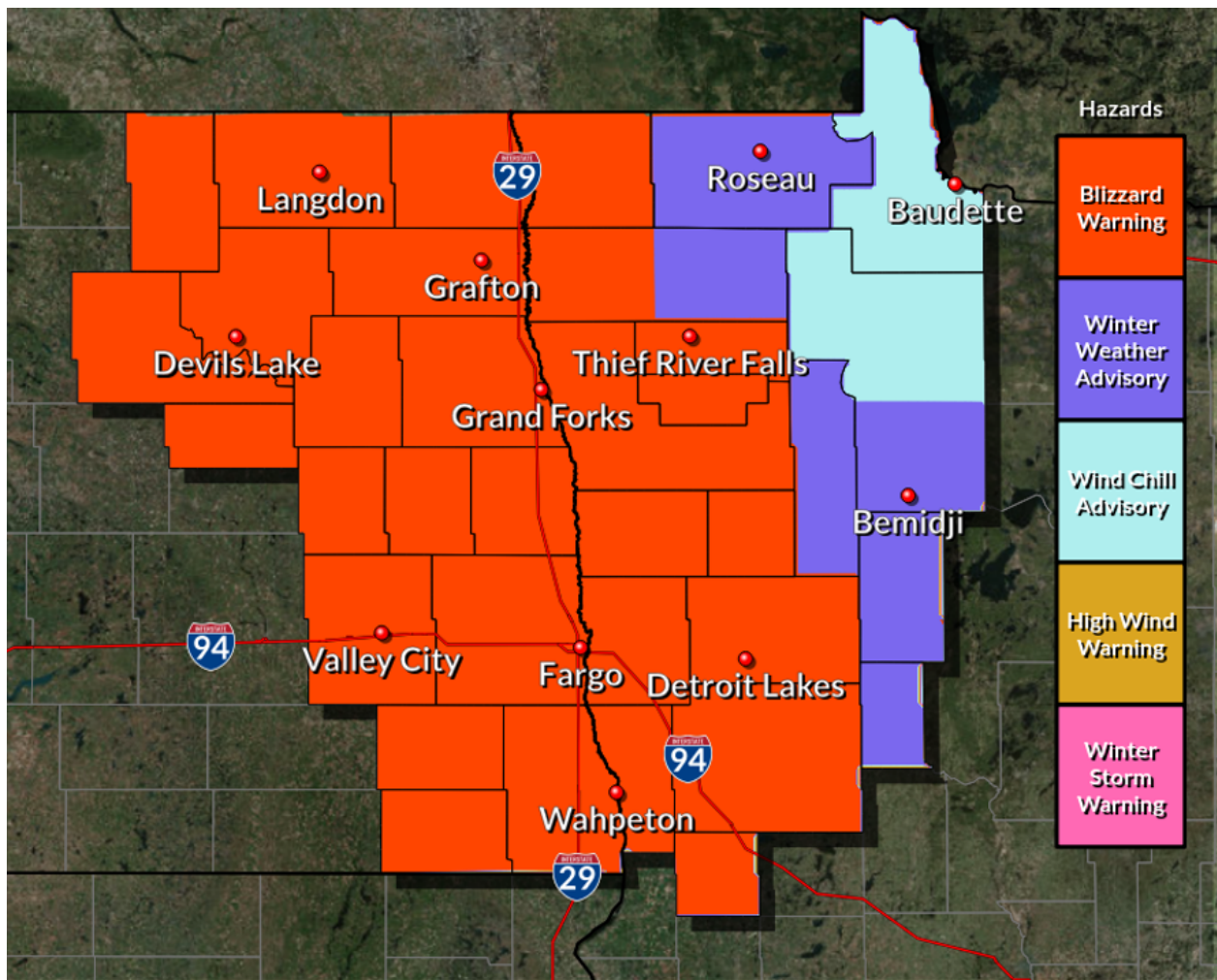
Figure 12. Map of hazards across the FGF CWA valid at 21 UTC (3pm CST) 27 January 2019. Source: US Department of Commerce 2021c
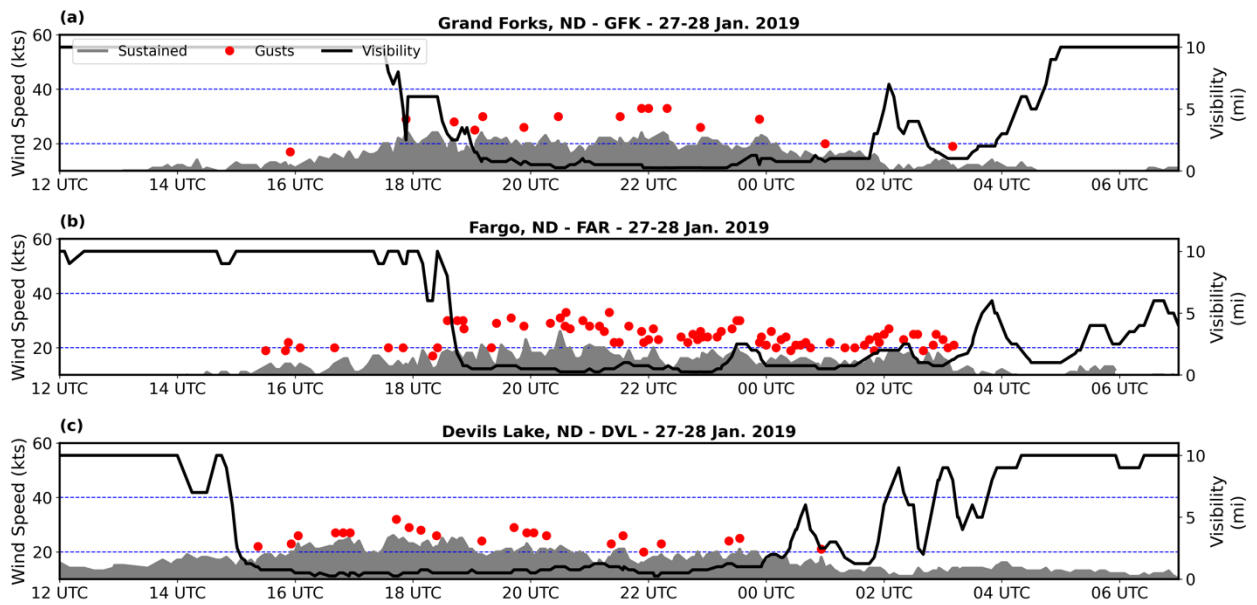
Figure 13. Meteograms of sustained winds (shaded grey), wind gusts (red dots), and visibility (black lines) for (a) GFK (Grand Forks, ND), (b) DVL (Devils Lake, ND), and (c) FAR (Fargo, ND) on 27 January 2019.
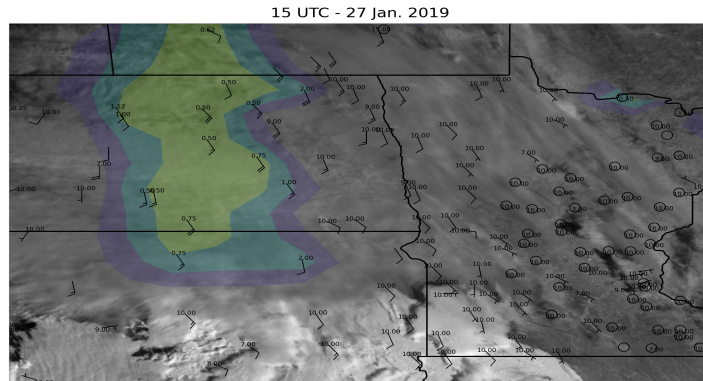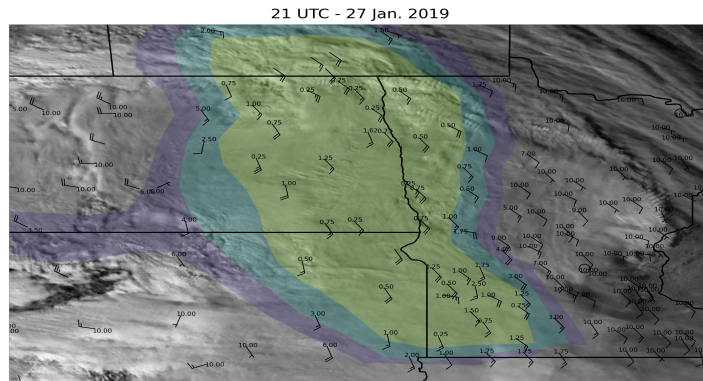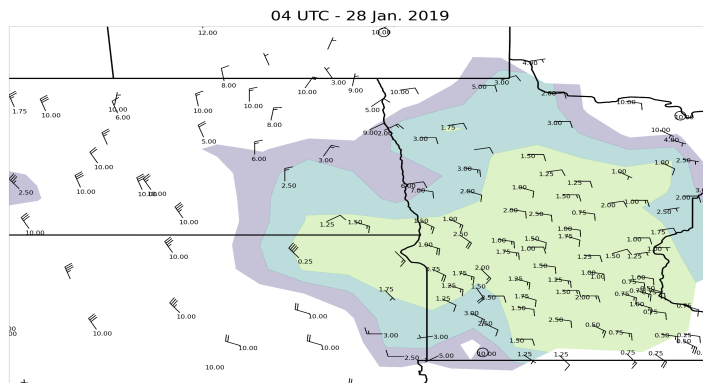
(a)

15 UTC - 27 Jan. 2019

(b)

21 UTC - 27 Jan. 2019

(c)

04 UTC - 28 Jan. 2019

Figure 14. 1.6 μm GOES-16 reflectance overlaid with observations of visibility and wind speeds valid at (a) 15 UTC 27 January 2019, (b) 21 UTC 27 January 2019, and (c) 04 UTC January 2019. Note that reflectance data is not available during the overnight hour in panel c. Shaded areas represent regions of reduced visibility with warmer colors representing poorer conditions.
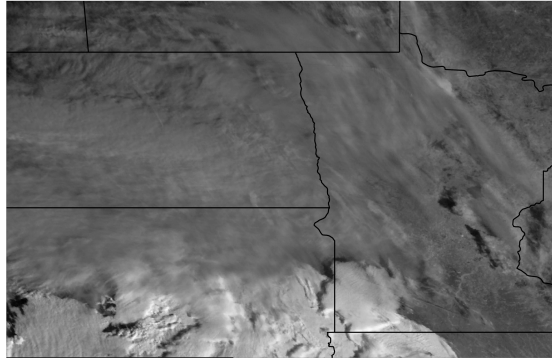
15 UTC - 27 Jan. 2019
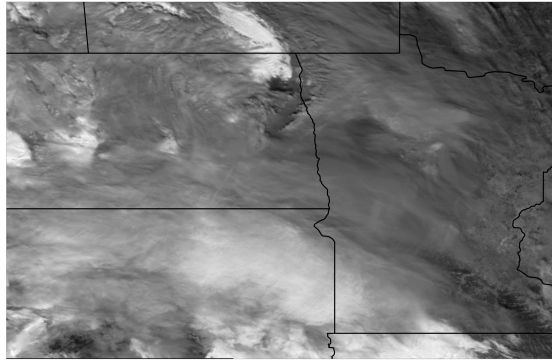
18 UTC - 27 Jan. 2019
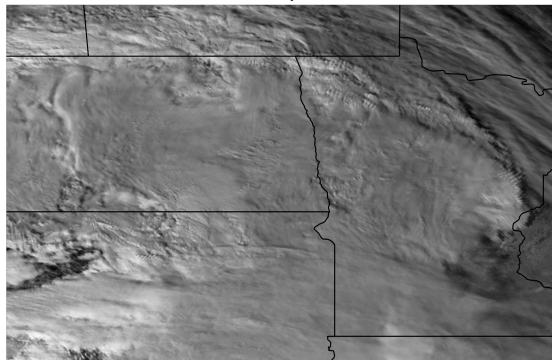
21 UTC - 27 Jan. 2019

Figure 15. GOES-16 Imagery valid for (a) 15 UTC, (b) 18 UTC, and (c) 21 UTC on 27 January 2019.
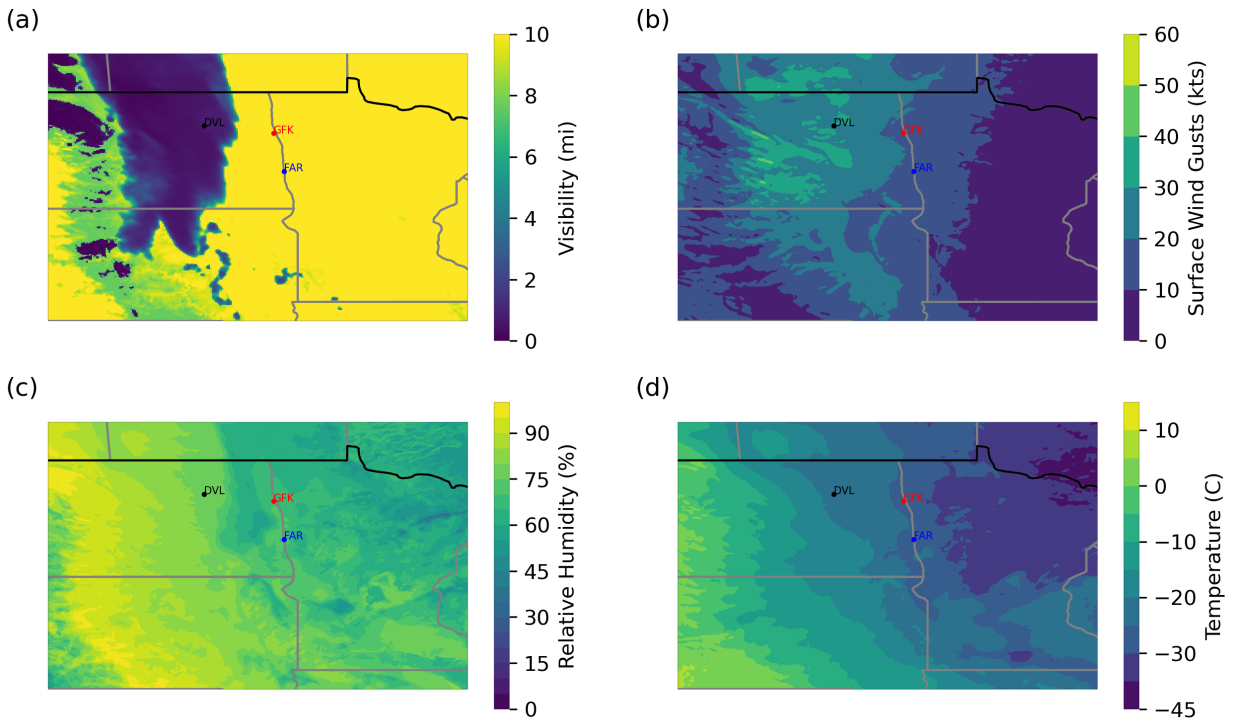
Figure 16. HRRR 27 January 2019 14 UTC F01 forecasts valid at 15 UTC 27 January 2019 for (a) visibility (mi), (b) wind gusts (kts), (c) relative humidity (%), and (d) temperature (ºC).

HRRR-F01-Valid 01272019 21 UTC
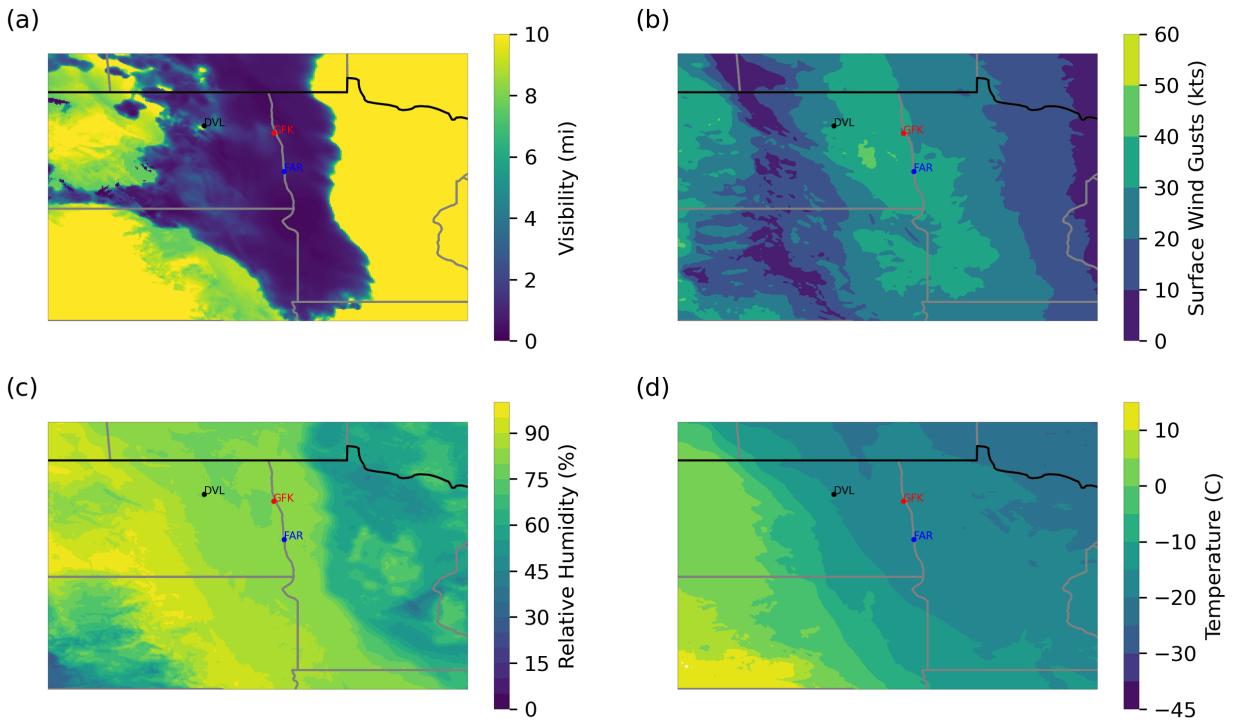
Figure 17. HRRR 27 January 2019 20 UTC F01 forecasts valid at 21 UTC 27 January 2019 for (a) visibility (mi), (b) wind gusts (kts), (c) relative humidity (%), and (d) temperature (ºC).
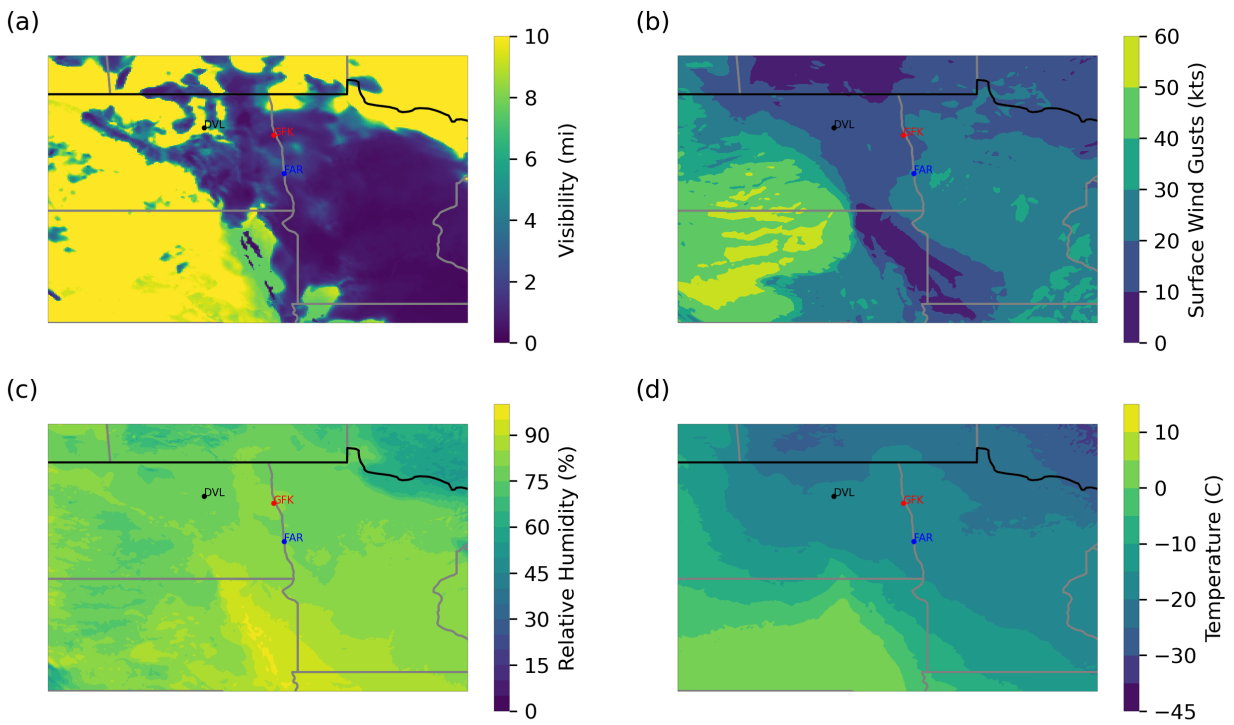
Figure 18. HRRR 28 January 2019 03 UTC F01 forecasts valid at 04 UTC 28 January 2019 for (a) visibility (mi), (b) wind gusts (kts), (c) relative humidity (%), and (d) temperature (ºC).
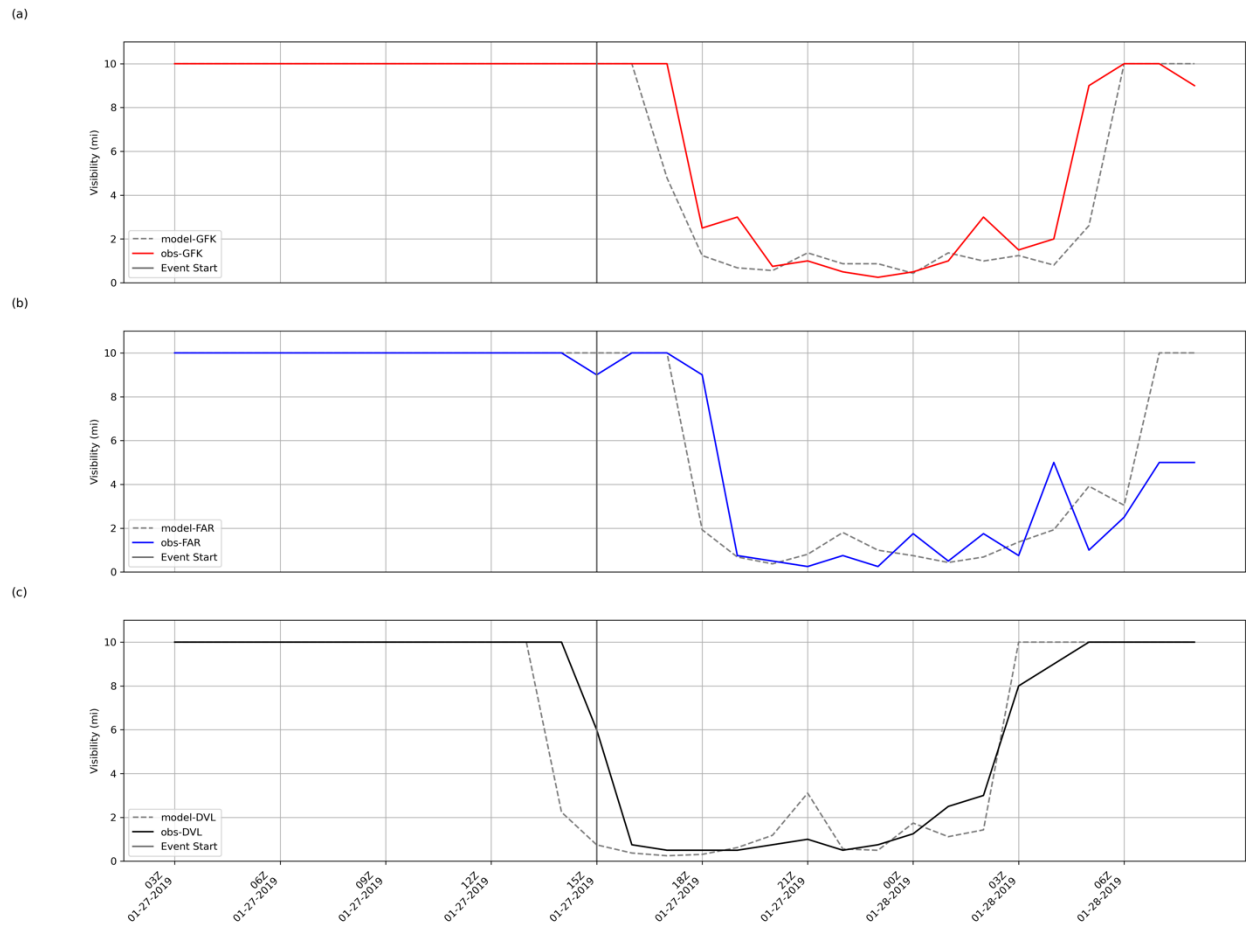
Figure 19. Time series of observed and HRRR 20190127 F01 forecasted visibility for (a) GFK, (b) DVL, and (c) FAR valid from 03Z 20190127 to 04Z 20190128.
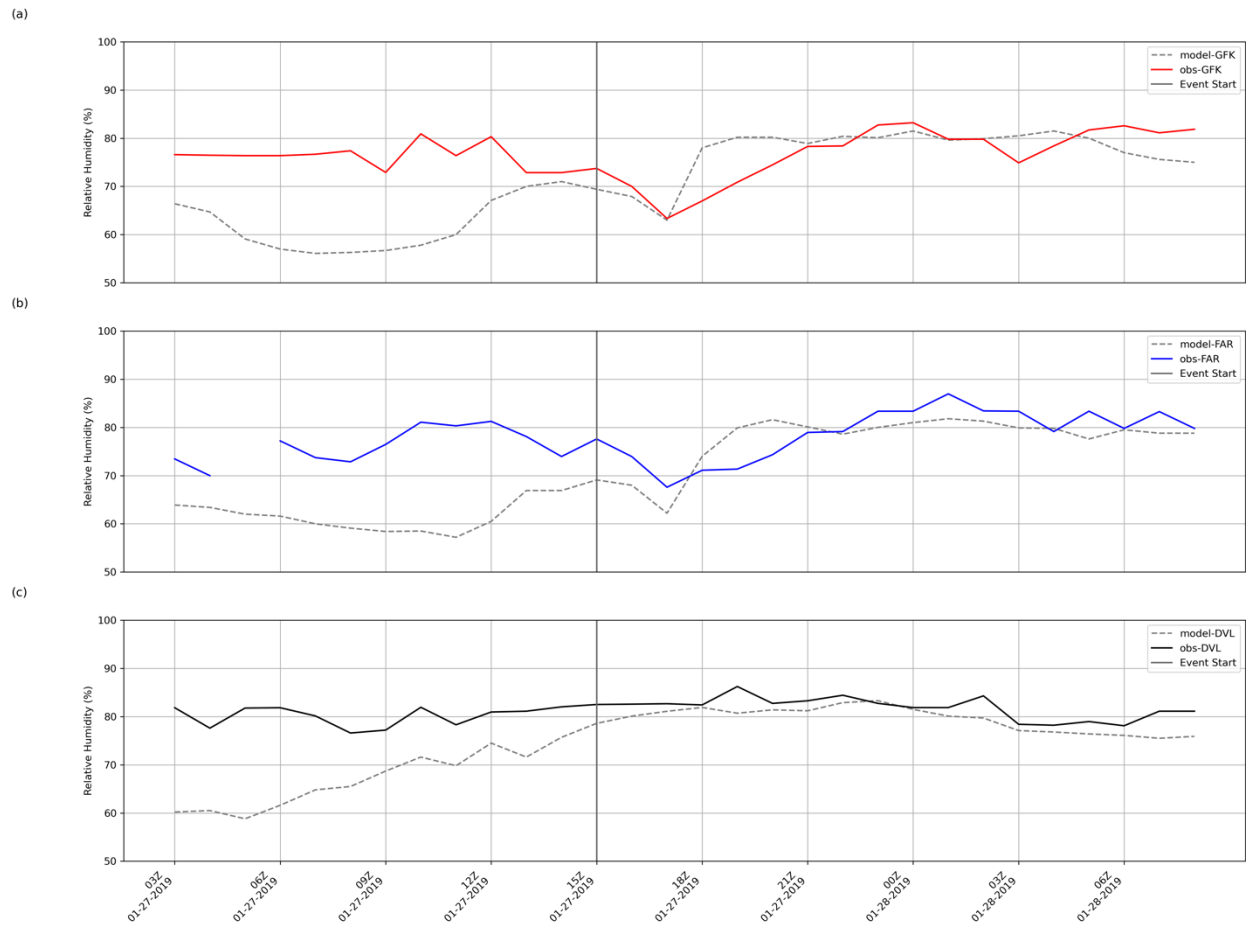
Figure 20. Time series of observed and HRRR 20190127 F01 forecasted relative humidity for (a) GFK, (b) DVL, and (c) FAR valid from 03Z 20190127 to 04Z 20190128
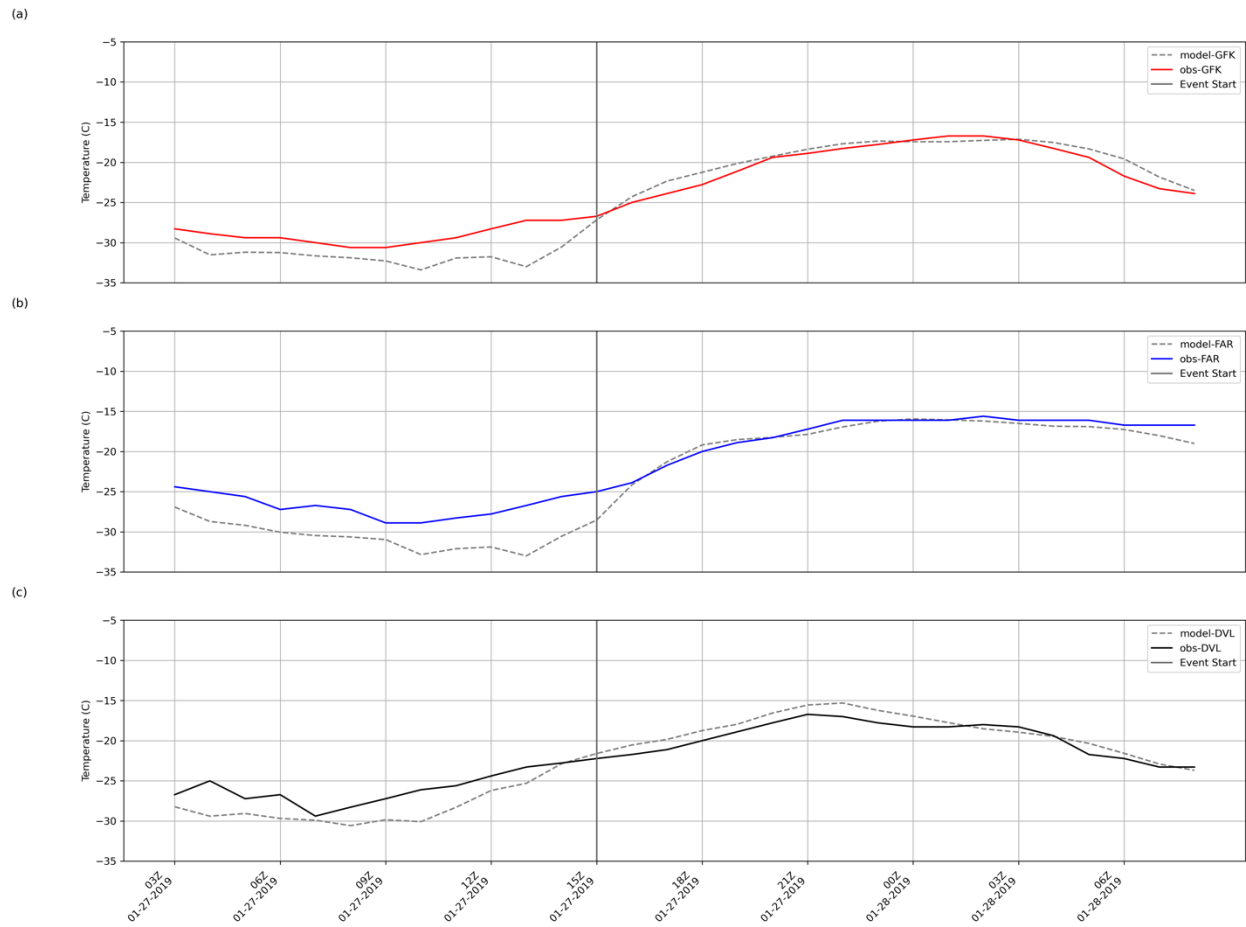
Figure 21. Time series of observed and HRRR 20190127 F01 forecasted temperature for (a) GFK, (b) DVL, and (c) FAR valid from 03Z 20190127 to 04Z 2019.

Visibility Error (Model-Obs)
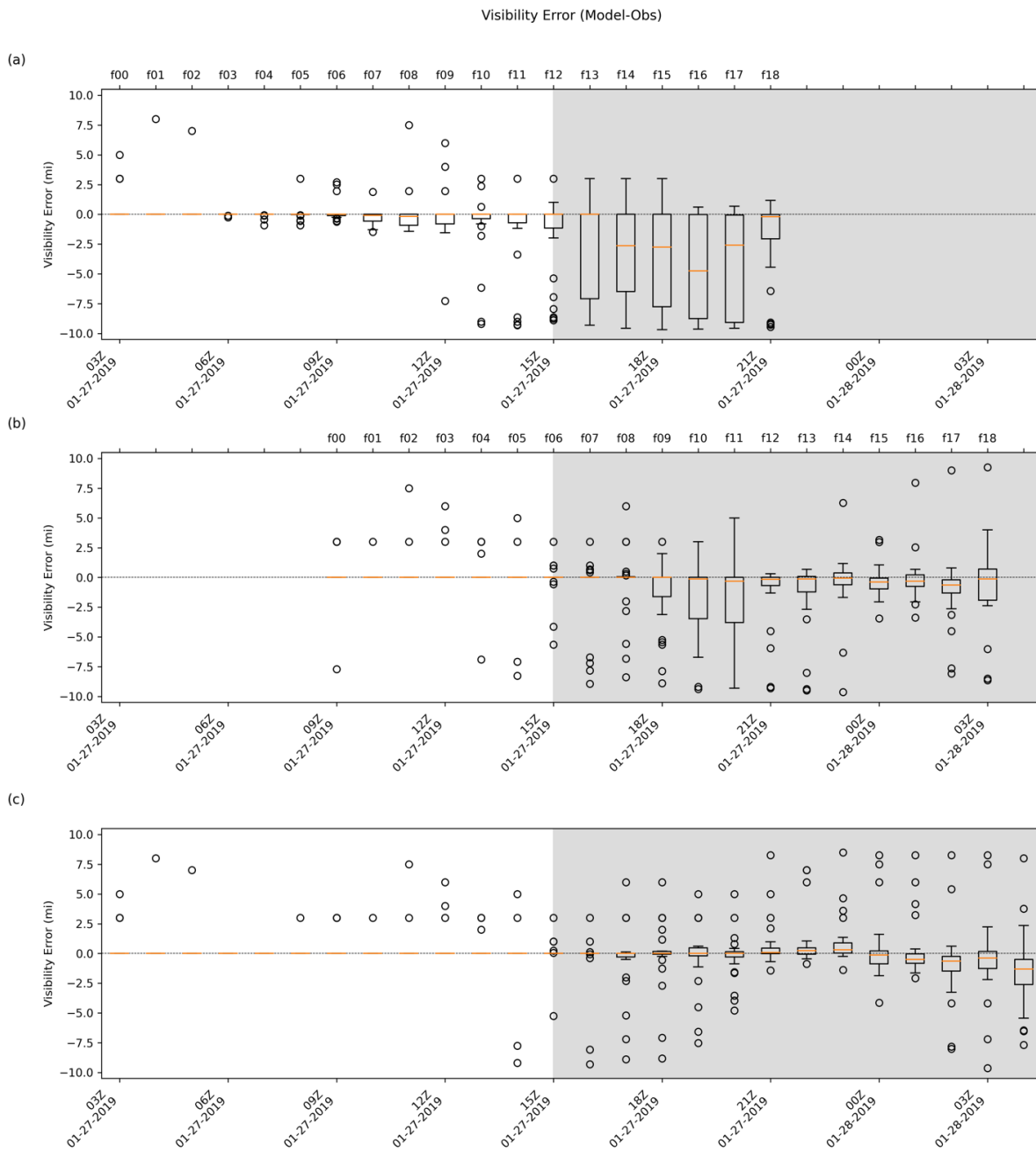
Figure 22. Box plots of HRRR visibility error (mi) for (a) 12HR, (b) 6HR, and (c) F01 forecasts for the 27 January 2019 event. The orange line represents the median of the distribution. The empty circles represent outliers that fall outside 1.5 times the interquartile range. Gray shading represents the duration of the event.

64

Table 4. Mean and standard deviation of the medians for visibility (mi) bias.

Mean and Standard Deviation

of Visibility Bias (mi)

Forecast	Before	During	All
12HR	0 ± 0.05	-1.8 ± 1.68	-0.7 ± 1.35
6HR	0 ± 0	-0.2 ± 0.18	-0.1 ± 0.17
F01	0 ± 0	-0.2 ± 0.41	-0.1 ± 0.31
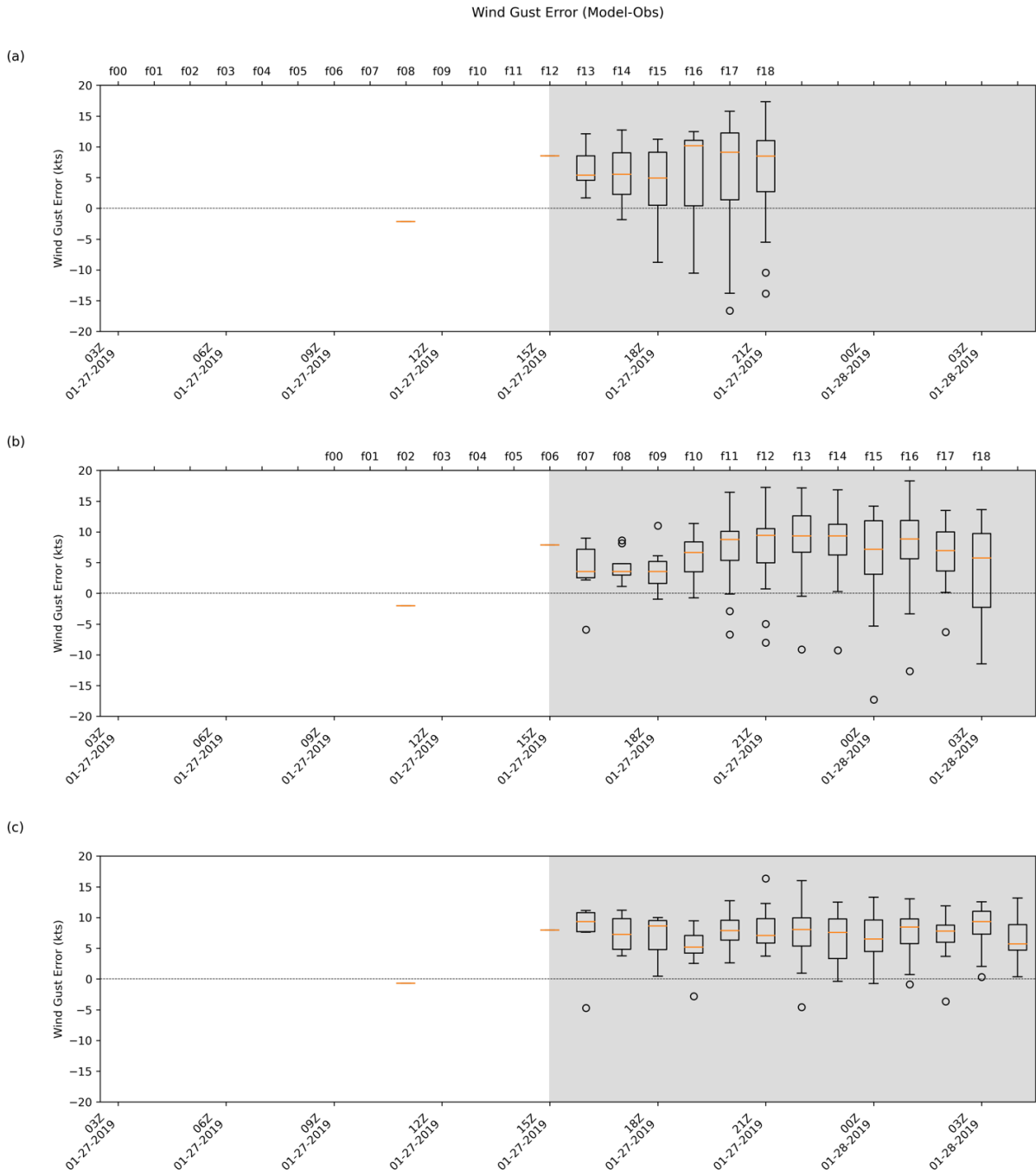
Figure 23. Box plots of HRRR wind gust error (kts) for (a) 12HR, (b) 6HR, and (c) F01 forecasts for the 27 January 2019 event.

Table 5. Mean and standard deviation of the medians for wind gust (kts) bias.

Mean and Standard Deviation

of Wind Gust Bias (kts)

Forecast	Before	During	All
12HR		7.5 ± 2	
6HR		7 ± 2.2	
F01		7.6 ± 1.2	
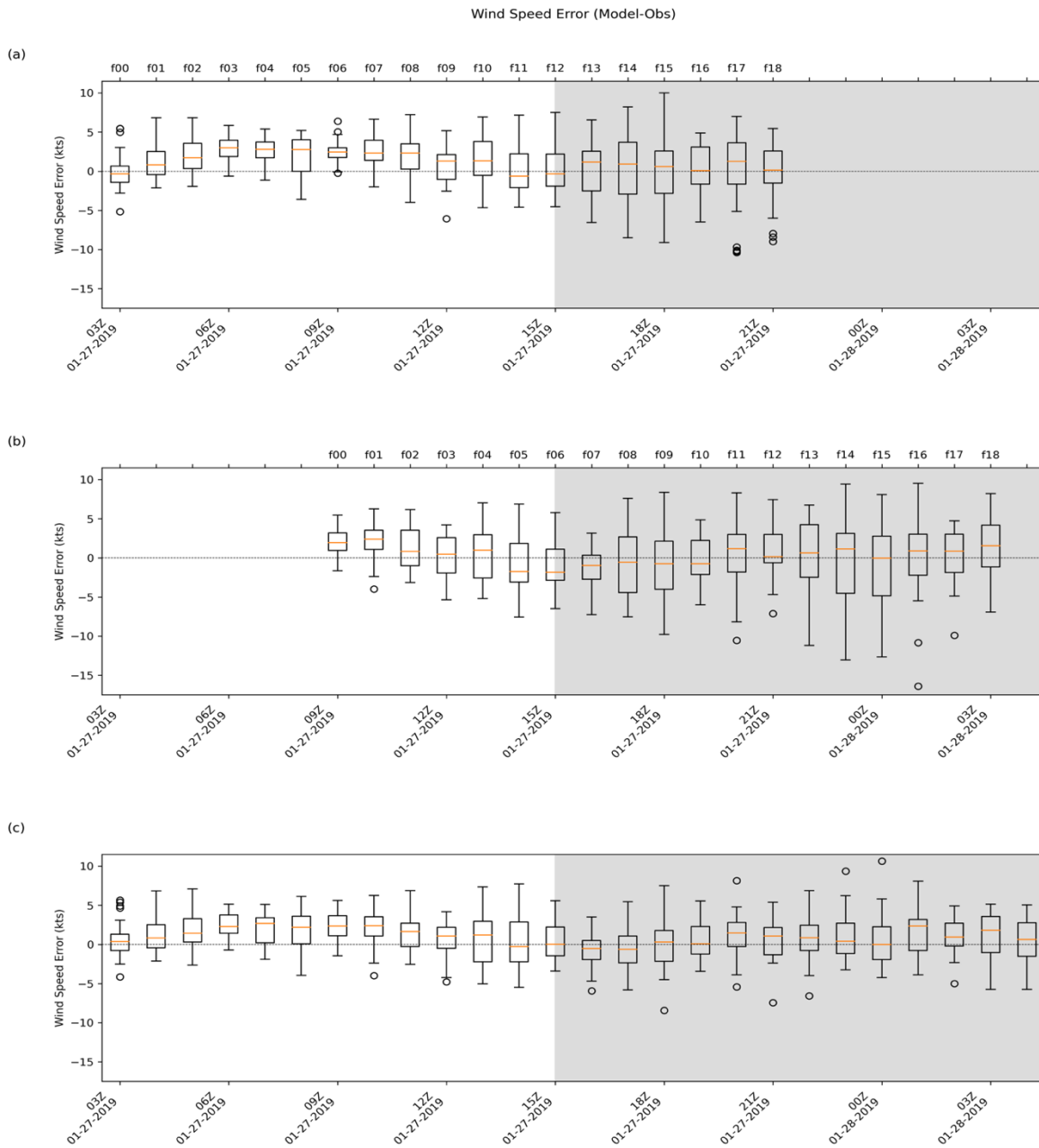
Figure 24. Box plots of HRRR wind speed error (kts) for (a) 12HR, (b) 6HR, and (c) F01 forecasts for the 27 January 2019 event.

Table 6. Mean and standard deviation of the medians for wind speed (kts) bias.

Mean and Standard Deviation

of Wind Speed Bias (kts)

Forecast	Before	During	All
12HR	1.7 ± 1.1	0.5 ± 0.6	1.3 ± 1.1
6HR	0.8 ± 1.3	0.1 ± 1	0.3 ± 1.1
F01	1.5 ± 0.9	0.6 ± 0.8	1 ± 1
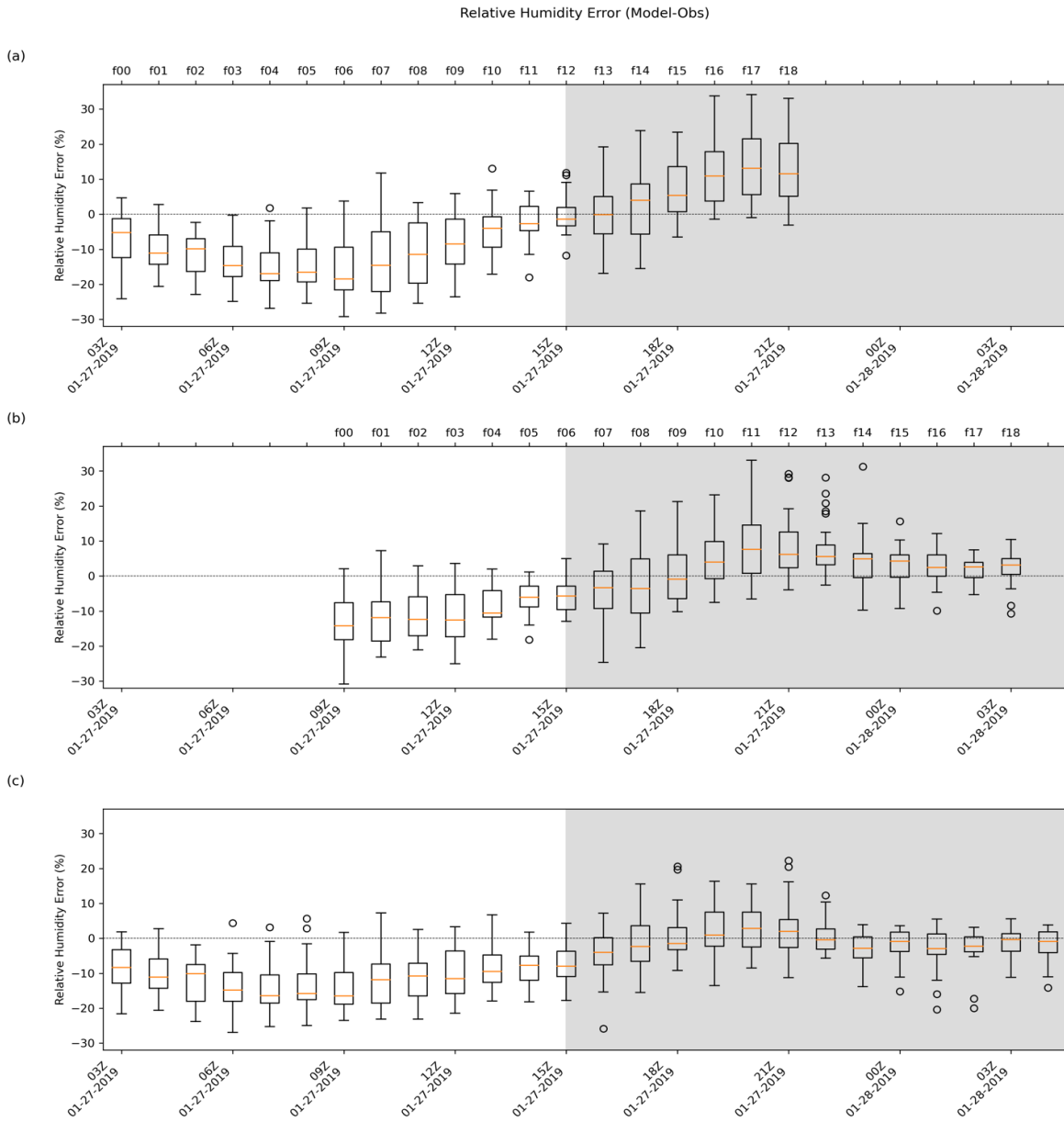
Figure 25. Box plots of HRRR relative humidity (%) for (a) 12HR, (b) 6HR, and (c) F01 forecasts for the 27 January 2019 event.

Table 7. Mean and standard deviation of the medians for relative humidity (%) bias.

Mean and Standard Deviation

of Relative Humidity Bias (%)

Forecast	Before	During	All
12HR	-11.2 ± 5.1	6.2 ± 5.4	-4.8 ± 9.9
6HR	-11.3 ± 2.6	2.1 ± 4	-2.1 ± 7.2
F01	-12.1 ± 3	-1.5 ± 2.6	-6.4 ± 6.1
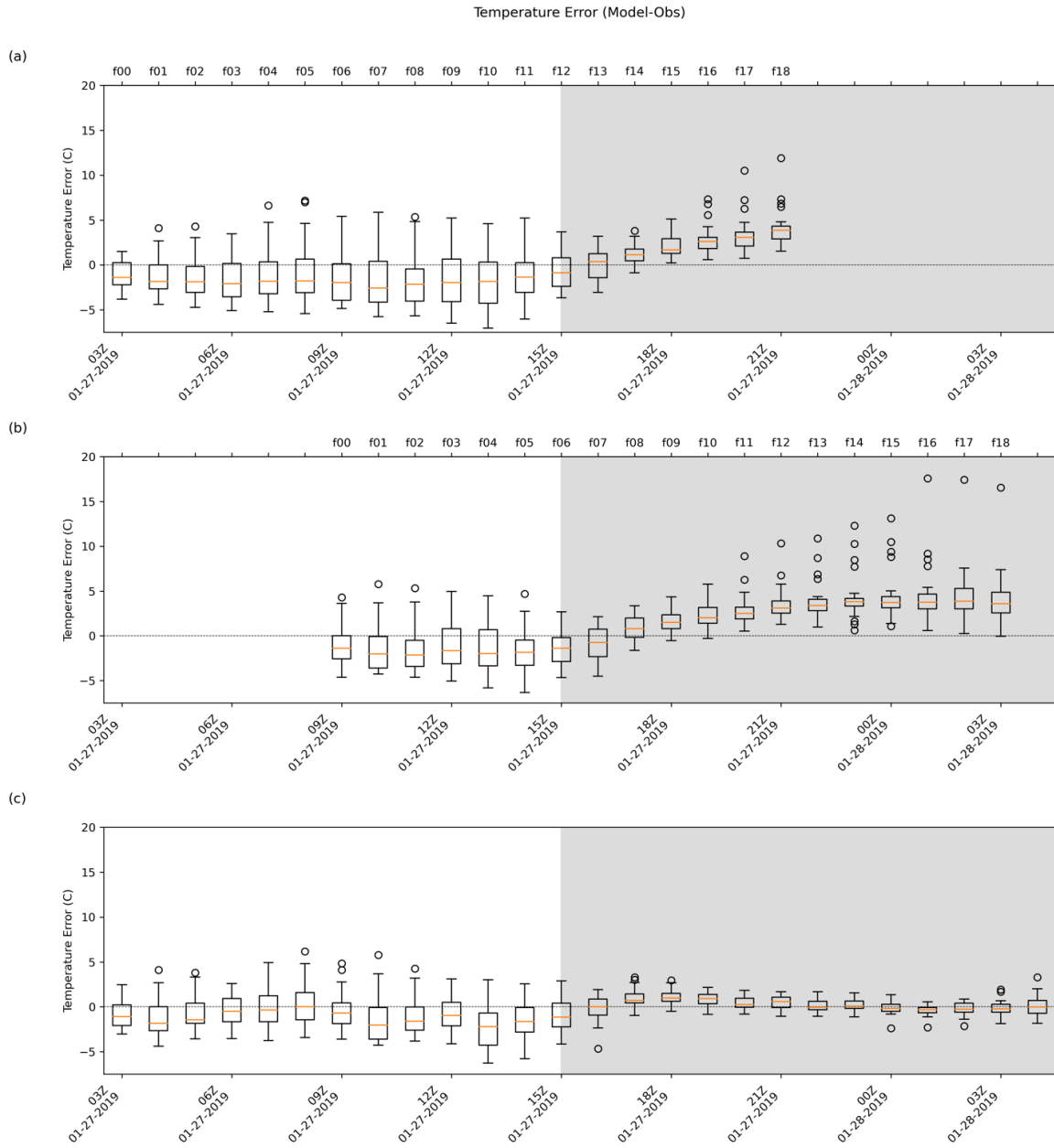
Figure 26. Box plots of HRRR temperature (ºC) for (a) 12HR, (b) 6HR, and (c) F01 forecasts for the 27 January 2019 event.

Table 8. Mean and standard deviation of the medians for temperature (ºC) bias.

Mean and Standard Deviation

of Temperature Bias (ºC)

Forecast	Before	During	All
12HR	-1.9 ± 0.3	1.7 ± 1.5	-0.6 ± 2
6HR	-1.8 ± 0.3	2.3 ± 1.7	1 ± 2.4
F01	-1.2 ± 0.7	0.1 ± 0.5	-0.5 ± 0.9

4.2 12 February 2020 - Arctic Front

In the early morning hours of 12 February 2020, a strong Arctic cold front moved through the area bringing dangerous wind chills, light snow, and gusty winds. Ground blizzard conditions resulted in the RRV that lasted into the early afternoon.

4.2.1 Environment

Prior to the passage of the Arctic cold front, a weak mid-level wave moved across the region (Figure 27). While frontogenetically forced snow along and just ahead of the front resulted in 0.5 to 1.5 inches of accumulation, the most notable part of the event were the strong winds (NWS 2020). With strong cold air advection, low level lapse rates steepened to nearly 8 ºC/km, allowing strong winds to mix down to the surface (NWS 2020). Strong pressure rises behind the front also forced strong isallobaric winds (NWS 2020). These along with other topographic factors allowed for wind gusts up to 50-60 mph (~43-52 kts) within the RRV causing widespread ground blizzard conditions.

4.2.2 Impacts

Blizzard conditions began early in the morning and lasted into the early afternoon hours. Extremely low visibility caused major impacts to those traveling along the I-29 corridor for their morning commute (NWS 2020). Many wrecks were reported across the area, especially multiple semi accidents along highways in MN and ND (NWS 2020). With low visibility and a high demand for tow trucks, many drivers were left stranded until the daylight hours (Figure 28). Sub-zero temperatures and frigid wind chills were observed across the area creating dangerous conditions for those that were stranded.

4.2.3 Qualitative Analysis

Meteograms for GFK, DVL, and FAR provide an overview of the event timing (Figure 29). Visibilities decreased and winds increased significantly starting during the early morning hours and continuing through the afternoon on the 12th. For this event, the start time and end time were identified as approximately 07Z and 21Z. Although not the exact midpoint time, 15Z will be used in this case as GOES-16 data was available at this hour.

Observations reported by ASOS/AWOS in Figure 29 show sustained wind speeds > 30 kts for most of the event in GFK and around 30 kts (35 mph) in FAR and DVL. Wind gusts were reported throughout the event, with gusts reaching over 40 kts (46 mph) in GFK and from 30-40 kts (35-46 mph) in FAR and DVL. Visibilities in all three locations decreased significantly. However, as blowing snow conditions were mostly confined to the RRV, lower visibilities were shorter lived in DVL compared to GFK and FAR. With reported visibilities of 0.25 mi and sustained wind speeds > 30 kts (35 mph), blizzard conditions persisted from the early morning hours into the afternoon on the 12th. By 22Z, all stations reported visibilities back to 10 mi as wind speeds slowly decreased through the rest of the evening. Figure 30 provides a broader overview of observations for each station over the entire CWA. Unfortunately, since the event began in the pre-dawn hours, GOES-16 imagery was unavailable for the start of the event.

As the cold front continued to move through the CWA, visibilities decreased significantly along the northern portion of the CWA. Corresponding with these low visibilities, a large increase in wind speeds to nearly 30 kts (35 mph) behind the front were observed. Although clouds moved out of the area by 15Z, blowing snow plumes can be seen in the satellite imagery (Figure 31) as visibilities and wind speeds remained at blizzard criteria. By 21Z, satellite imagery showed clear skies around the RRV and visibilities above blizzard criteria.

Model data demonstrate significant differences compared to the earlier clipper case (Figure 32). At the start of the event, a band of low visibility associated with frontal snow was forecast across northwest MN and northeast ND. The surface wind gusts and relative humidity increased along this area, where the system was expected to bring snowfall. A strong temperature gradient associated with the cold front was just across northern ND. At 15Z (Figure 33), visibility across the CWA was ≥10 mi, with only a few small patches of low visibility in various areas. Widespread surface wind gusts remained, as relative humidity decreased across the CWA. A large temperature gradient associated with the cold front was seen across the CWA ranging from -30 to -15 ºC (-22 to 5 ºF). By 21Z (Figure 34), visibility was still ≥10 mi across the entire area, with wind gusts remaining near 20 to 40 kts (23 to 46 mph). The relative humidity was more varied but continued to decrease as temperatures also decreased across the CWA.

Overall, the HRRR forecasted the general environment expected from the Arctic cold front passing through the area. However, there were a few discrepancies between the model and observations as ground blizzard conditions occurred after the passage of the front. This is especially seen in Figures 35-36, as visibility and relative humidity between the model and observations in GFK, FAR, and DVL were significantly different. After the cold front moved south out of the CWA, observed visibilities across GFK and FAR were at blizzard criteria and < 2 mi in DVL, while the HRRR forecasted visibilities of ≥10 mi. Relative humidity was shown to be under forecast at all three locations by as much as 10% during the event. These visibility and relative humidity differences are expected because the HRRR does not parameterize the process of blowing snow. This leads to an overestimation of visibility in regions of pure blowing snow, and an underestimation of relative humidity because the HRRR does not account for sublimation of blowing snow. After the start of the event, good agreement is shown between the model and

observations for wind speeds in FAR and DVL. However, the model under forecasted winds by as much as 12 kts in GFK (Figure 37). Temperatures also showed good agreement between the model and observations with a difference < 2 ºC at most times (Figure 38).

4.2.4 Operational use of GOES-16 Imagery

For this specific event, a GOES-16 mesoscale sector allowed for one minute imagery over the FGF NWSFO CWA. Analysis of this GOES-16 imagery proved useful during operations throughout the day. Forecasters were able to successfully track the progression of the event from the identification of the front to the resulting blowing snow conditions. This in turn directly impacted operations as forecasters used this information to refine warnings and advisories, messaging, and IDSS support (Jones 2020).

While forecasters expected little snowfall during this event, the question remained whether or not the existing snowpack would be susceptible to being lofted and blown around (Jones 2020). Forecasters at FGF were able to examine the snowpack using the 1.6 μm Snow/Ice band on GOES-R ABI discussed in Kennedy and Jones (2020). In this case, new snow had fallen across eastern South Dakota, southern MN, northern Iowa, and into Wisconsin and Michigan and was indicated by lighter shading in the imagery. This lighter shading allowed forecasters to more confidently identify areas of newer snow that may be more likely to be picked up and blown around.

As the cold front moved closer to the CWA, forecasters examined the GOES-16 Nighttime Microphysics RGB. This allowed them to see the exact location of the cold front by identifying an area of low stratus clouds moving south into the area (Jones 2020). By overlaying METAR observations, forecasters were able to closely look over the imagery to pick out synoptic and mesoscale features, such as the front. With the high temporal resolution of GOES-16, they were

also able to pinpoint important details such as the timing of impacts, which in this case were right after frontal passage (Jones 2020).

Although the FGF CWA was located in an area of darker shaded snowpack (older snow), observations, webcams, and reports suggested that blowing snow was occurring. With gusty winds forecasters assumed that it was possible the crust was broken, allowing for blowing snow conditions in the RRV (Jones 2020). Horizontal convective rolls associated with blowing snow, similar to those shown in Kennedy and Jones (2020), were seen in the 1.6 μm channel along with other composite products. Overlaying METARS also allowed for observed low visibilities to be matched with the blowing snow plumes. With a cloudless sky, these blowing snow plumes could be tracked with GOES-16 imagery throughout the day, allowing for improved IDSS.

4.2.5 Quantitative Analysis

Unlike the clipper case, box plots show significant issues during the ground blizzard (Figure 39). In the hours leading up to the event, ≥10 mi visibility was forecasted and observed at most stations. While there was good agreement between the HRRR and observations, the spread in data increased as the event began. This is likely due to timing of the front and the snowfall ahead of the front as it was passing through the CWA. During the event there was a large positive bias of 0.9-3.1 mi for all three forecasts (Table 9). Many stations had essentially no reductions in visibilities when in fact blizzard conditions were reported. This persisted throughout the event until the early afternoon hours.

Varying results were found for wind gusts and sustained winds (Figure 40-41). A positive bias from 0.9 to 4.1 kts (Table 10) was observed in all three forecasts, and the spread in the data was inconsistent from hour to hour. In the 12HR forecast for example, there is some evidence of

diurnal variability with a larger positive bias during the afternoon hours. During the event, all three forecasts had a positive bias of 1.9-3.5 kts. Spread in the data remained large with the greatest error near ~15 kts. Like the previous case, there was better agreement between the HRRR and observations for sustained wind speeds (Figure 41). Despite a slight positive bias during the event for all forecasts (0.7-1.5 kts, Table 11), there was a negative bias of -0.5 - -1.6 kts for the 12HR and 6HR forecasts. F01 forecasts had the best agreement with a slight positive bias of 0.3 kts. Overall, more uncertainty existed for earlier forecasts, and the negative bias suggested less mixing occurred than was actually observed and accounted for in the F01 forecast.

Biases in relative humidity (Figure 42) and temperature (Figure 43) suggest the HRRR struggled with several aspects of the event. There was variability in RH performance before the event; while the 12HR forecast had an overall positive bias of 1.1%, 6HR and F01 forecasts were drier than forecast with a bias of -2.2 - -2.4% (Table 12). As the event began, all forecasts showed a larger negative bias than observed with a range of -0.3 to -4.5% for all three forecasts. Although there is an overall negative bias in both the F01 and 6HR forecasts, an increase in the medians and greater spread amongst the data towards the end of the event was observed.

Analysis of temperatures (Figure 43) shows that before and during the event the HRRR under forecasted temperatures with biases of -0.2 to -3.1 °C shown (Table 13). However, the F01 forecast shows better agreement between the model and observations as the medians remain closer to 0 °C error and there is less spread in the data compared to the 6HR and 12HR forecasts.

Using this analysis a few observations are made for this event. As expected, the HRRR overestimated the visibility and underestimated the relative humidity during time periods of significant blowing snow. As discussed before, this is most likely because the HRRR does not parameterize the process of blowing snow, and the lack of sublimation is consistent with the

humidity bias. While the HRRR consistently over-forecasted the wind gusts, forecasted wind speeds were in better agreement with the observations and showed much less spread in the data. Although the 6HR and 12HR forecasts underestimated temperatures during the event, the F01 forecast showed much better agreement between the HRRR and observations. Earlier forecasts may be indicative of errors being caused more by temperature advection vs. cooling from blowing snow. In fact, it may be possible the lack of blowing snow sublimation improved temperature forecasts in this case. Finally, the utility of GOES-16 imagery was demonstrated as the forecasters at the FGF office were able to use imagery to locate areas affected by blowing snow. The caveat is this was limited to periods after 15Z when there was adequate sunlight to observe 1.6μm reflectance data.
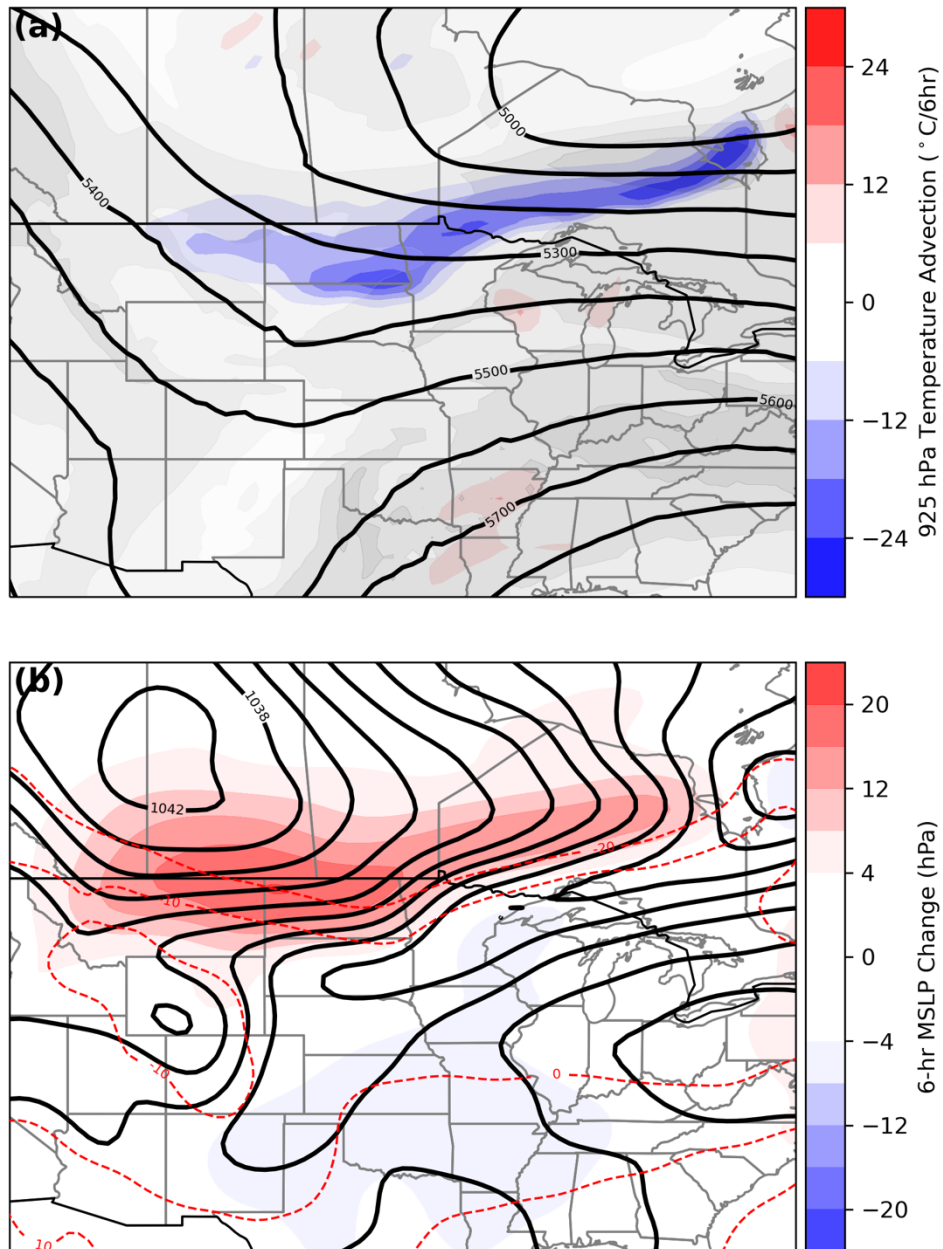
Figure 27. Meteorological fields from the GFS analysis valid at 0600 UTC 12 Feb 2020. (a) 500-hPa geopotential height (black contours), 500-hPa wind magnitude (semitransparent gray contours), and 925-hPa temperature advection (filled contours). (b) Mean sea level pressure (MSLP, black contours) and 6-h MSLP change (filled contours).

Figure 28. Low visibilities caused by a ground blizzard 15 mi east of Grand Forks at approximately 1500 UTC on 12 February 2020. Image provided by Aaron Kennedy.
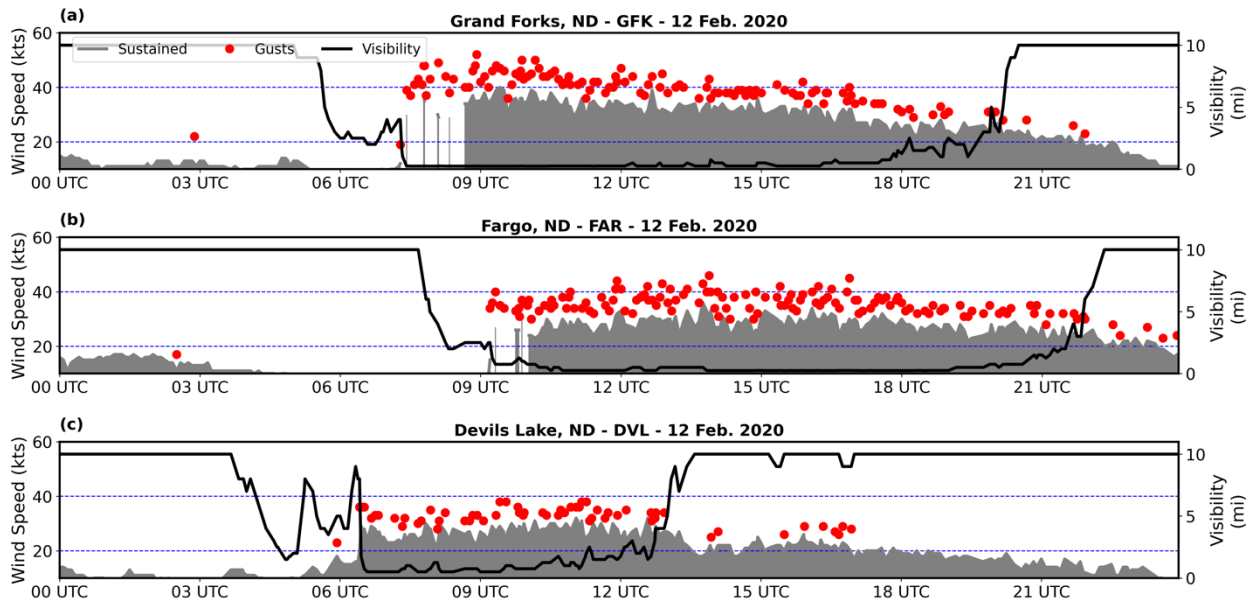
Figure 29. Meteograms of sustained winds (shaded grey), wind gusts (red dots), and visibility (black lines) for (a) GFK (Grand Forks, ND), (b) DVL (Devils Lake, ND), and (c) FAR (Fargo, ND) on 12 February 2020.
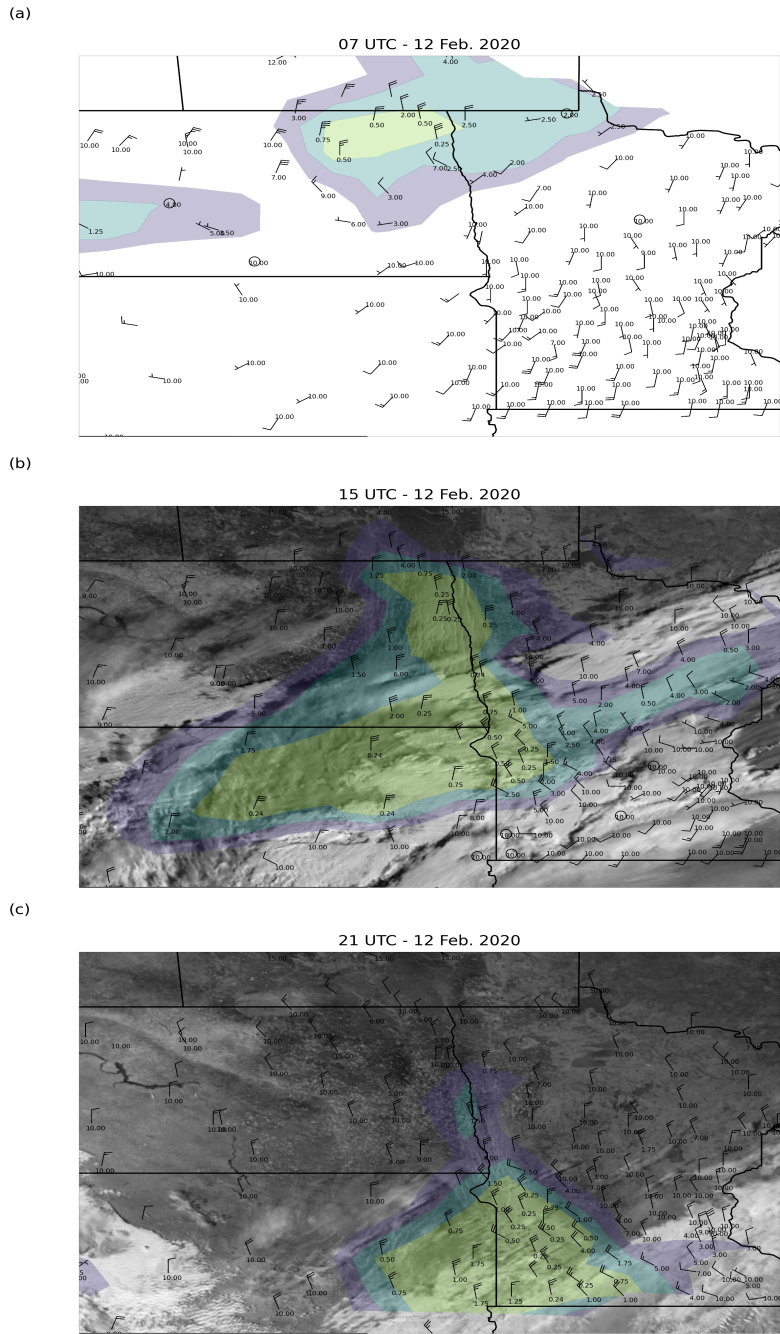
Figure 30. 1.6 μm GOES-16 reflectance overlaid with observations of visibility and wind speeds valid at (a) 07 UTC 12 February 2020, (b) 15 UTC 12 February 2020, and (c) 21 UTC 12 February 2020. Note that reflectance data is not available during the overnight hour in panel (a). Shaded areas represent regions of reduced visibility with warmer colors representing poorer conditions.
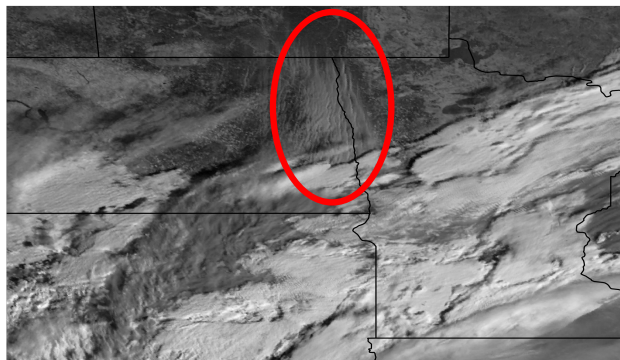
15 UTC - 12 Feb. 2020
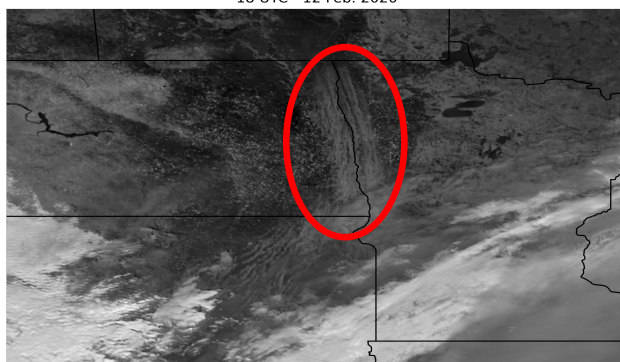
18 UTC - 12 Feb. 2020
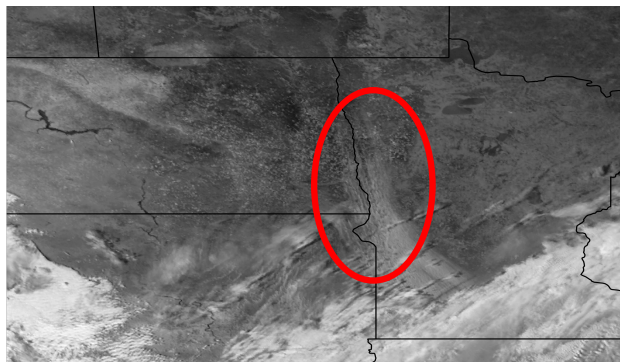
21 UTC - 12 Feb. 2020

Figure 31. GOES-16 satellite imagery of blowing snow plumes over the RRV valid for (a) 15 UTC, (b) 18 UTC, (c) 21 UTC on 12 February 2020.
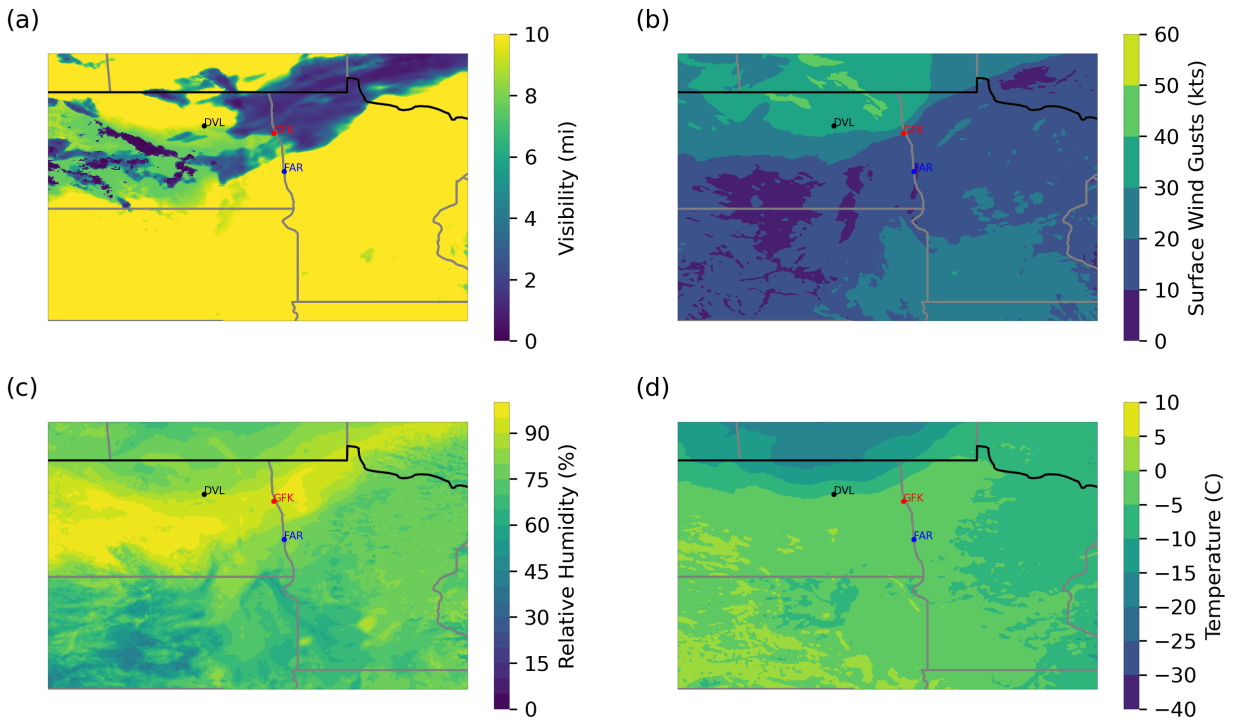
Figure 32. HRRR 12 February 2020 06 UTC F01 forecasts valid at 07 UTC 12 February 2020 for (a) visibility (mi), (b) wind gusts (kts), (c) relative humidity (%), and (d) temperature (ºC).

Figure 33. HRRR 12 February 2020 14 UTC F01 forecasts valid at 15 UTC 12 February 2020 for (a) visibility (mi), (b) wind gusts (kts), (c) relative humidity (%), and (d) temperature (ºC).

HRRR-F01-Valid 02122020 21 UTC
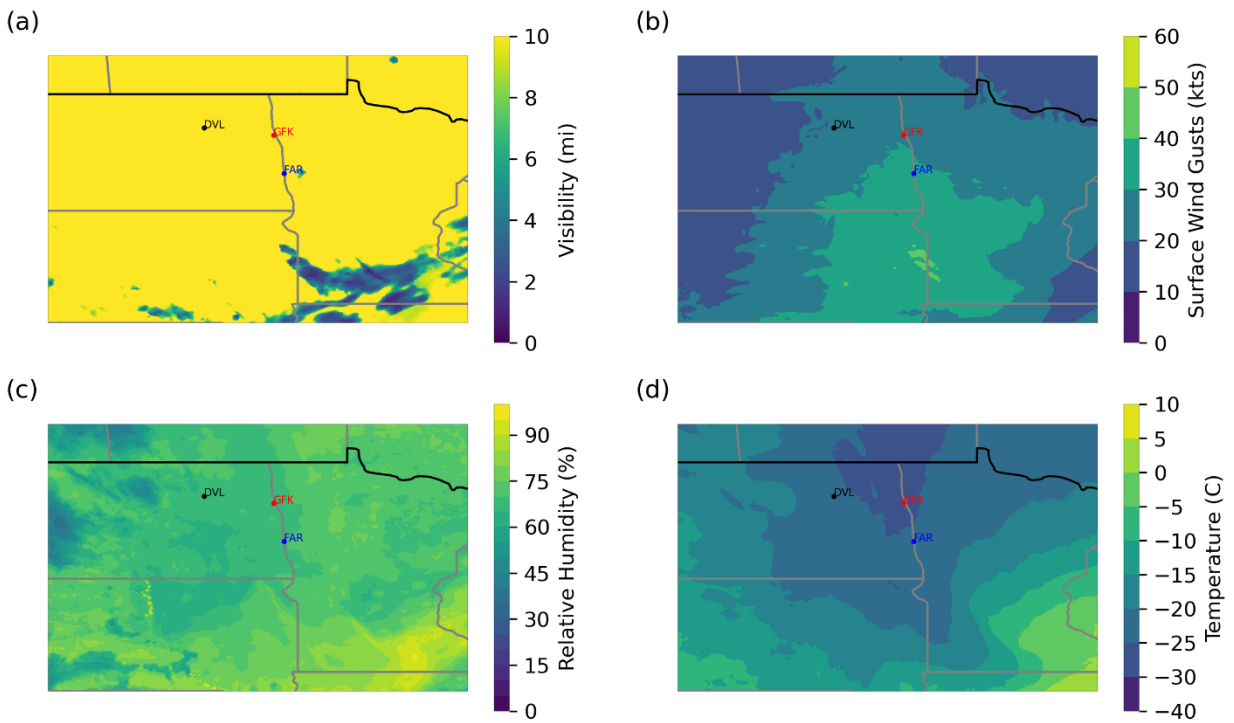
Figure 34. HRRR 12 February 2020 20 UTC F01 forecasts valid at 21 UTC 12 February 2020 for (a) visibility (mi), (b) wind gusts (kts), (c) relative humidity (%), and (d) temperature (ºC).
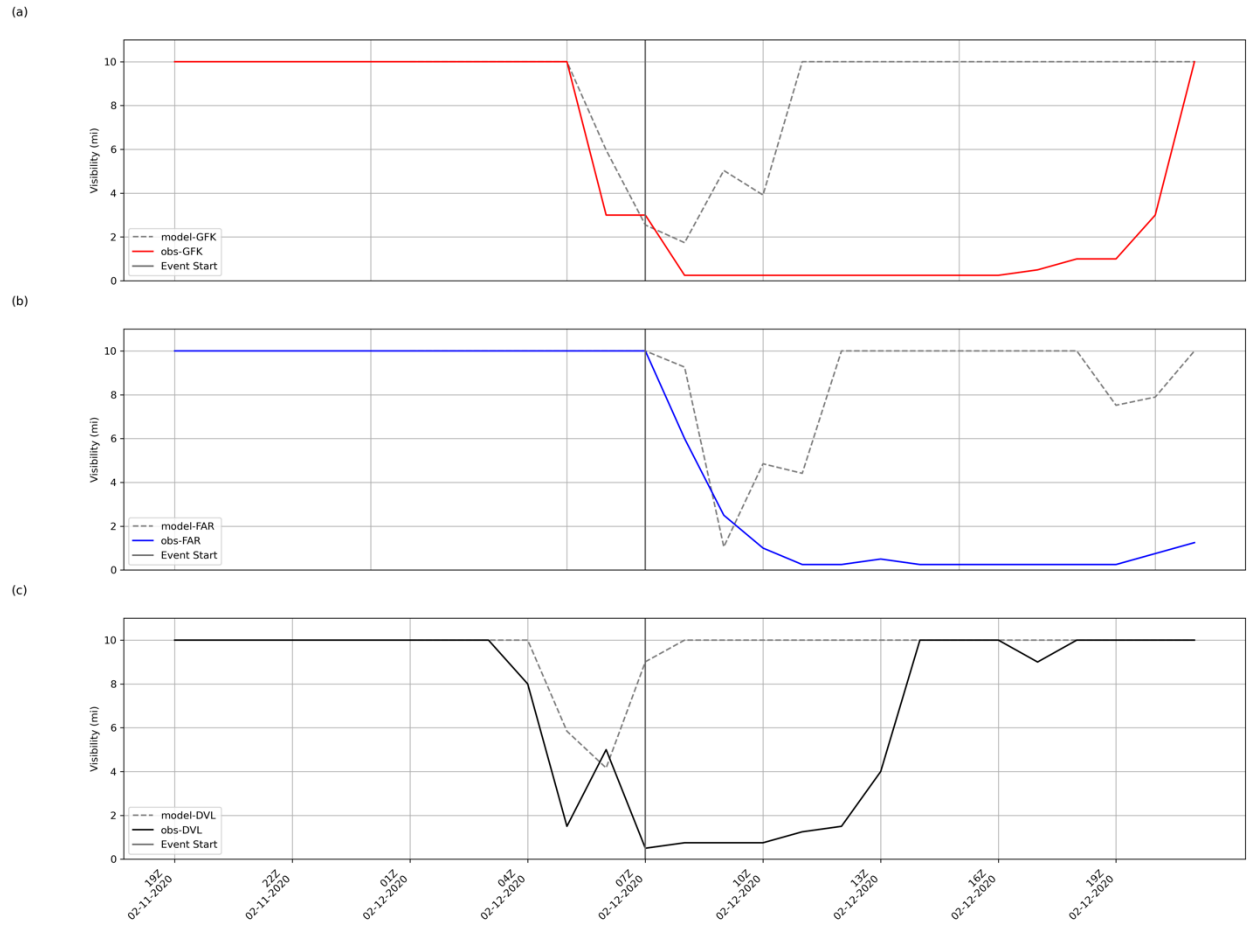
Figure 35. Time series of observed and HRRR 20200212 F01 forecasted visibility for (a) GFK, (b) DVL, and (c) FAR valid from 19Z 20200211 to 21Z 20200212.
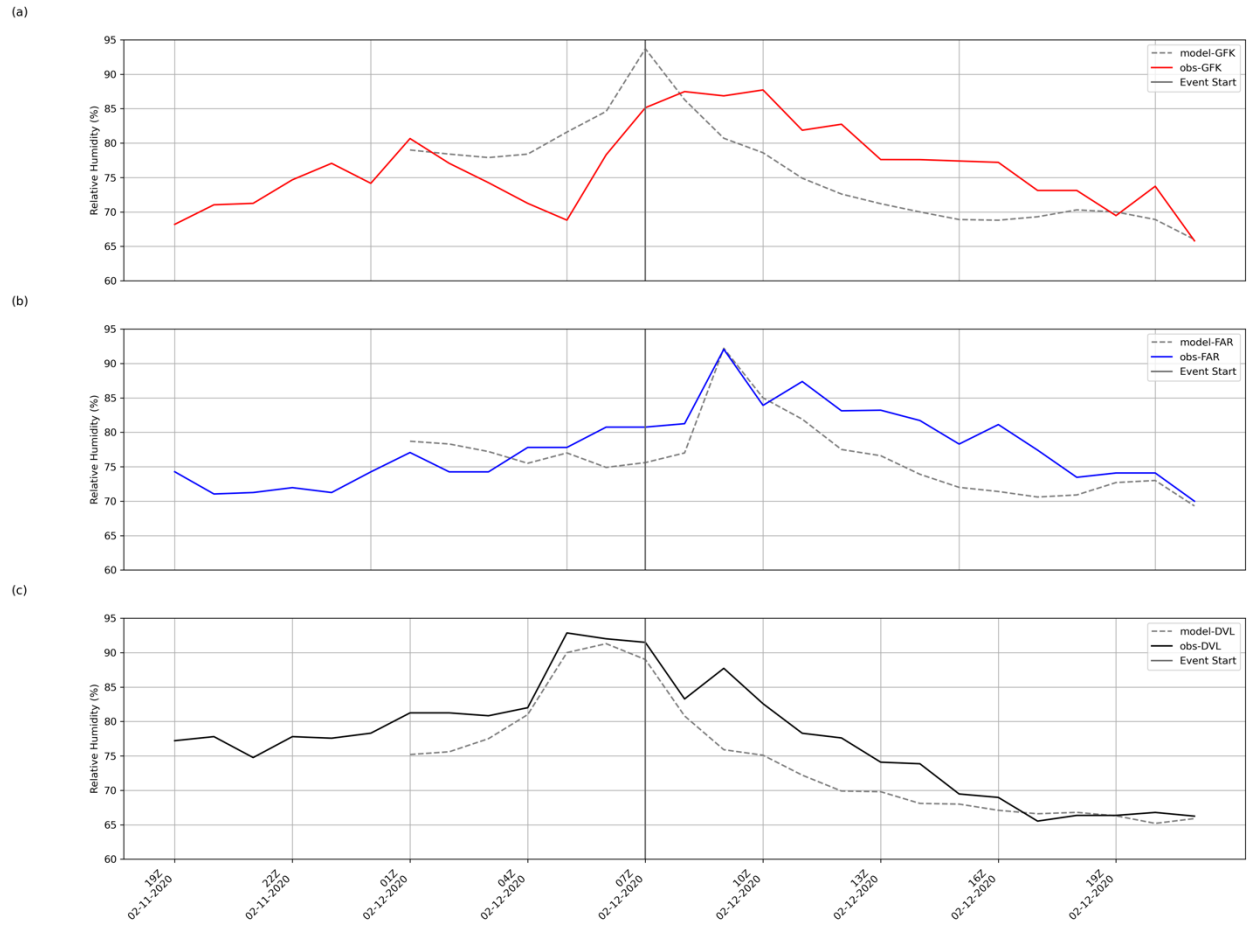
Figure 36. Time series of observed and HRRR 20200212 F01 forecasted relative humidity for (a) GFK, (b) DVL, and (c) FAR valid from 19Z 20200211 to 21Z 20200212.
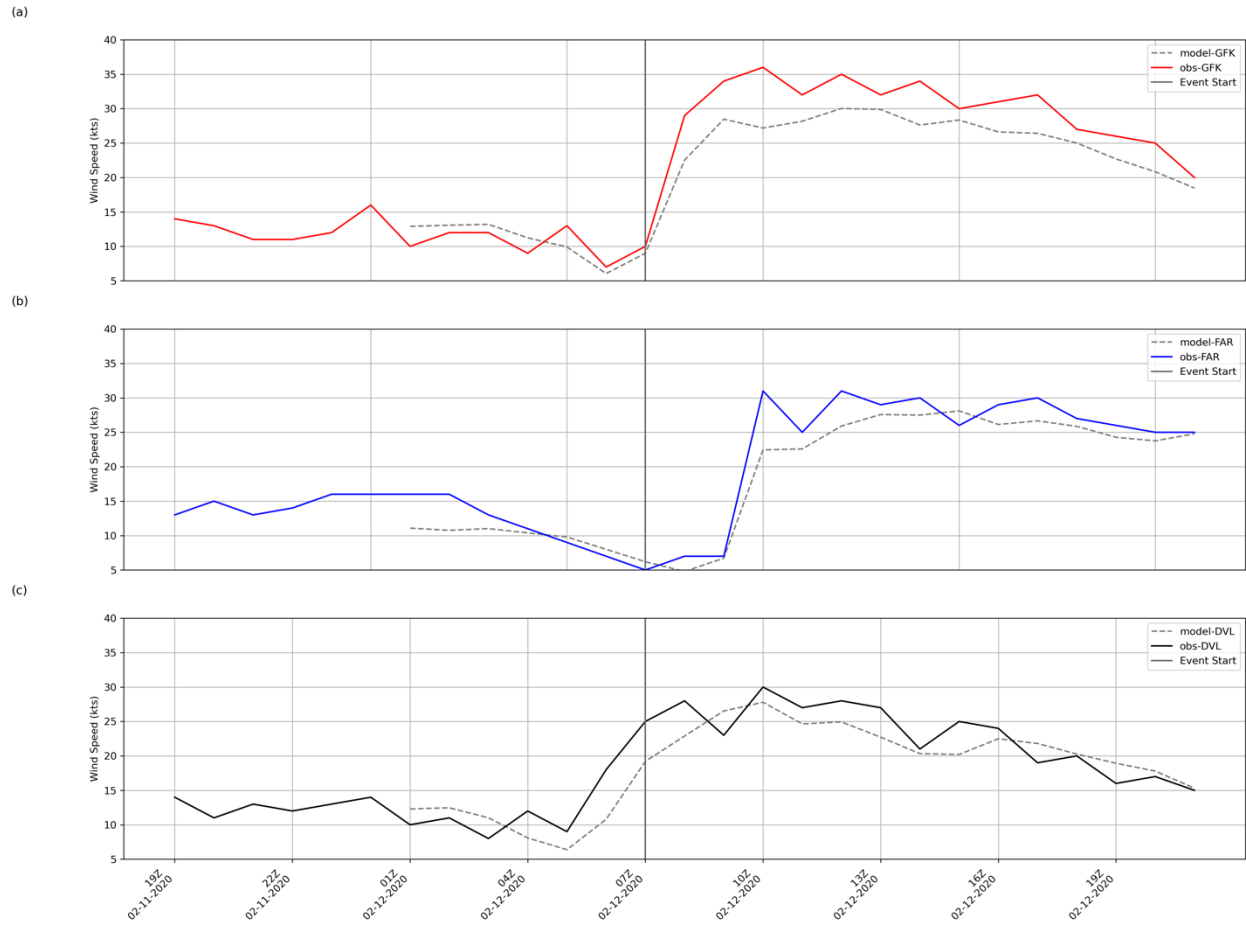
Figure 37. Time series of observed and HRRR 20200212 F01 forecasted wind speeds for (a) GFK, (b) DVL, and (c) FAR valid from 19Z 20200211 to 21Z 20200212.
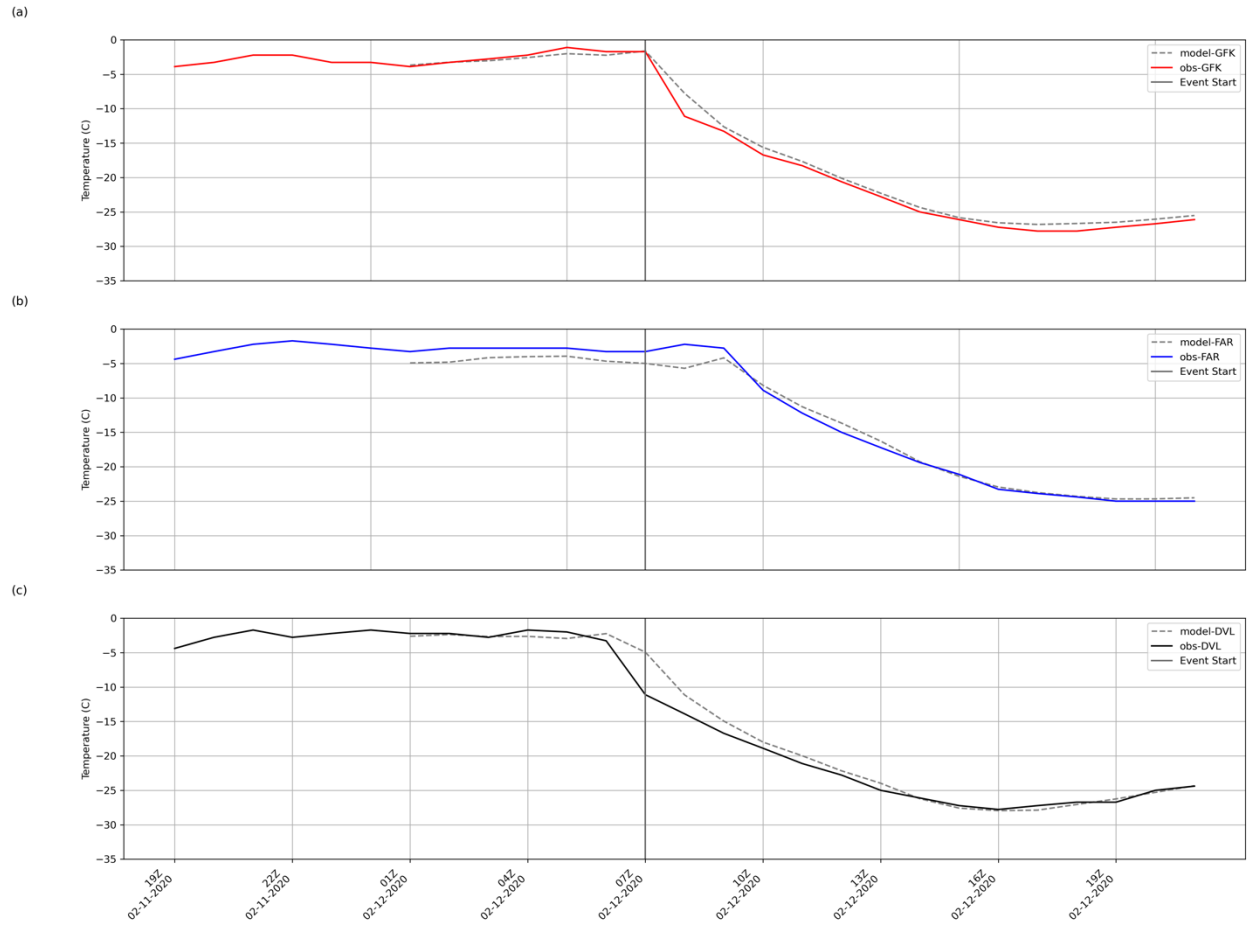
Figure 38. Time series of observed and HRRR 20200212 F01 forecasted temperature for (a) GFK, (b) DVL, and (c) FAR valid from 19Z 20200211 to 21Z 20200212.
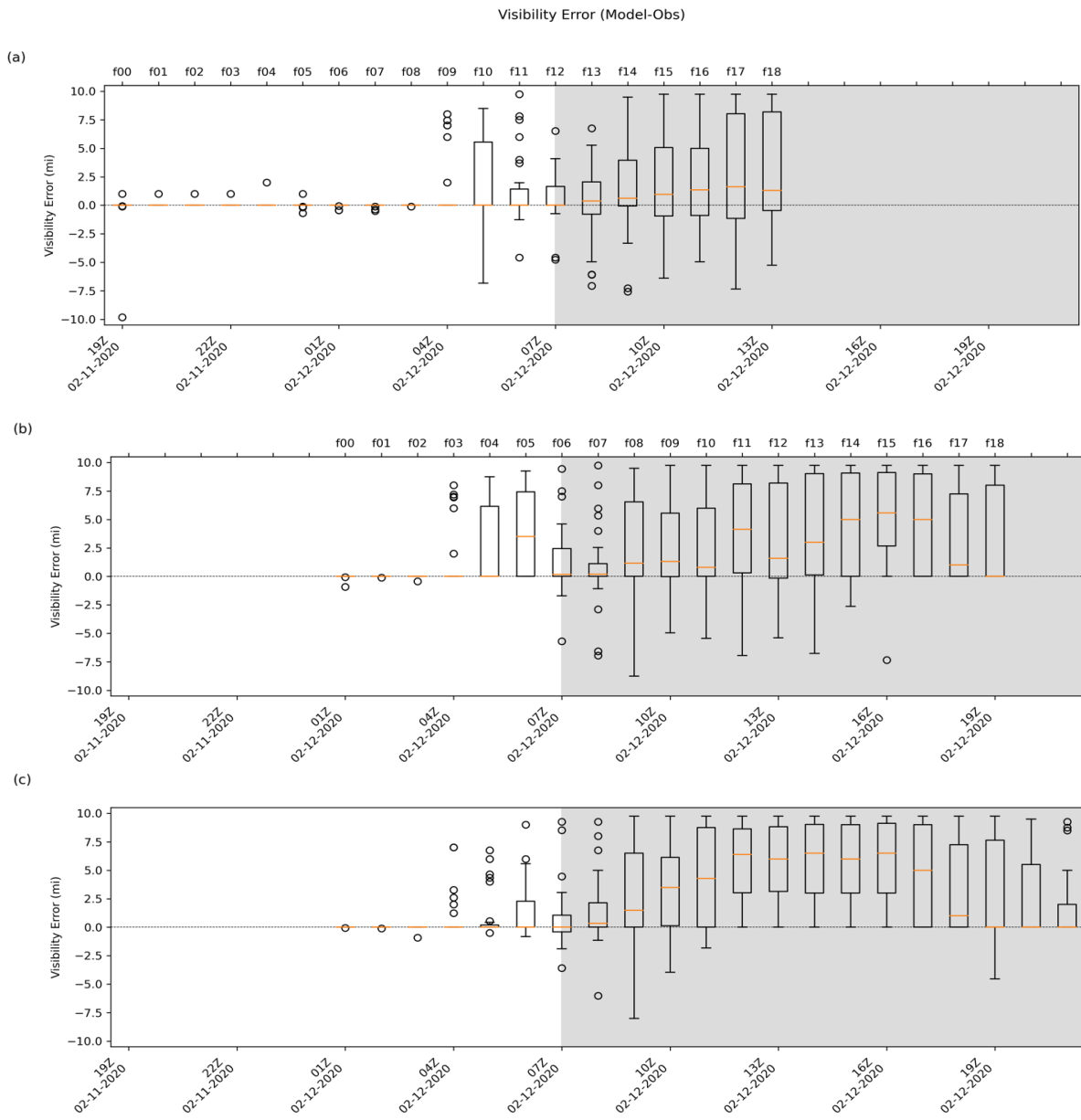
Figure 39. Box plots of HRRR visibility (mi) for (a) 12HR, (b) 6HR, and (c) F01 forecasts for the 12 February 2020 event.

Table 9. Mean and standard deviation of the medians for visibility (mi) bias.

Mean and Standard Deviation

of Visibility Bias (mi)

Forecast	Before	During	All
12hr	0 ± 0	0.9 ± 0.5	0.3 ± 0.5
6hr	0.6 ± 1.3	2.2 ± 2	1.7 ± 1.9
F01	0 ± 0	3.1 ± 2.7	2.2 ± 2.7
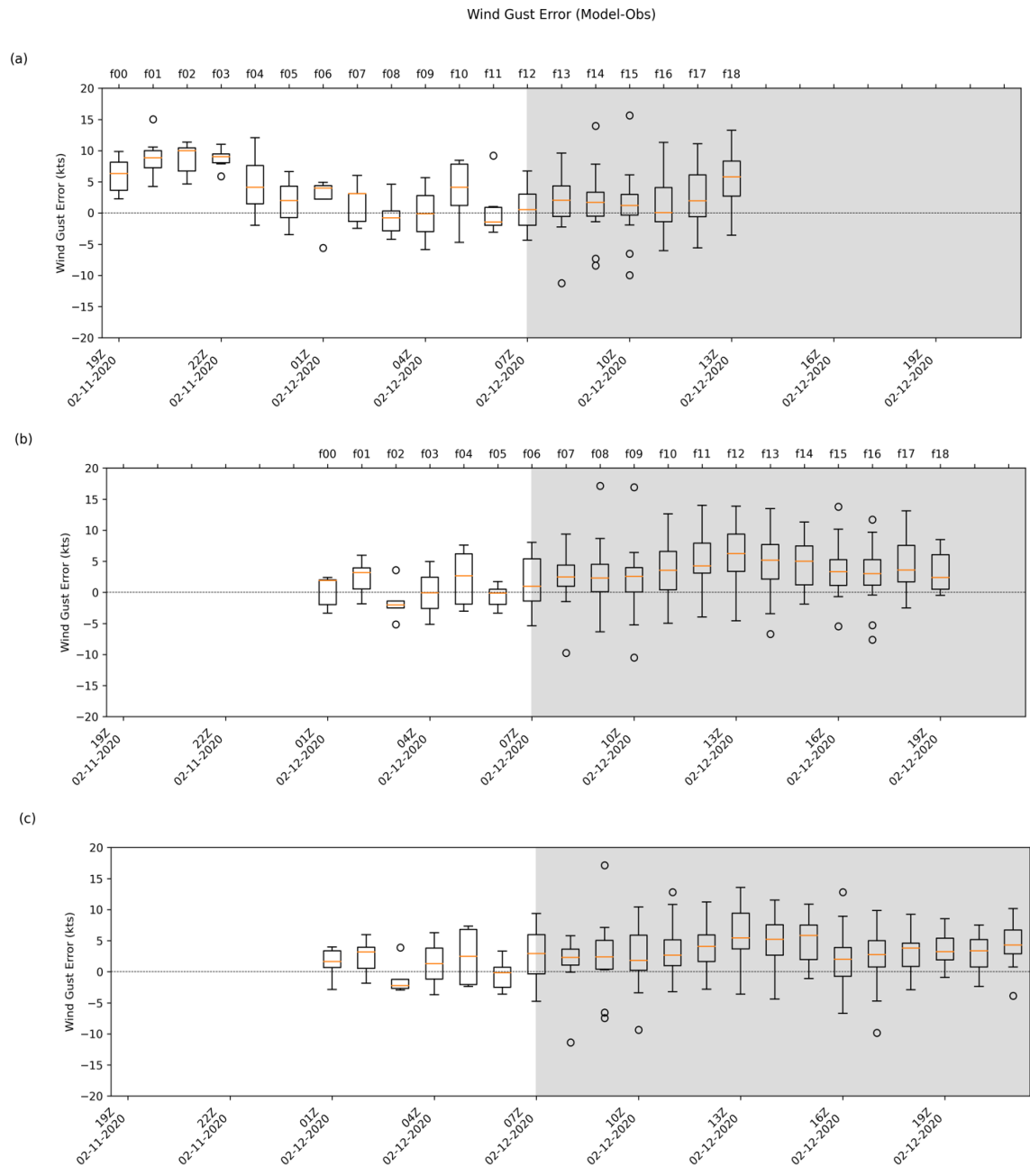
Figure 40. Box plots of HRRR wind gust (kts) for (a) 12HR, (b) 6HR, and (c) F01 forecasts for the 12 February 2020 event.

Table 10. Mean and standard deviation of the medians for wind gust (kts) bias.

Mean and Standard Deviation

of Wind Gust Bias (kts)

Forecast	Before	During	All
12hr	4.1 ± 3.7	1.9 ± 1.7	3.3 ± 3.3
6hr	0.9 ± 1.8	3.5 ± 1.4	2.7 ± 1.9
F01	1 ± 1.8	3.5 ± 1.2	2.8 ± 1.8
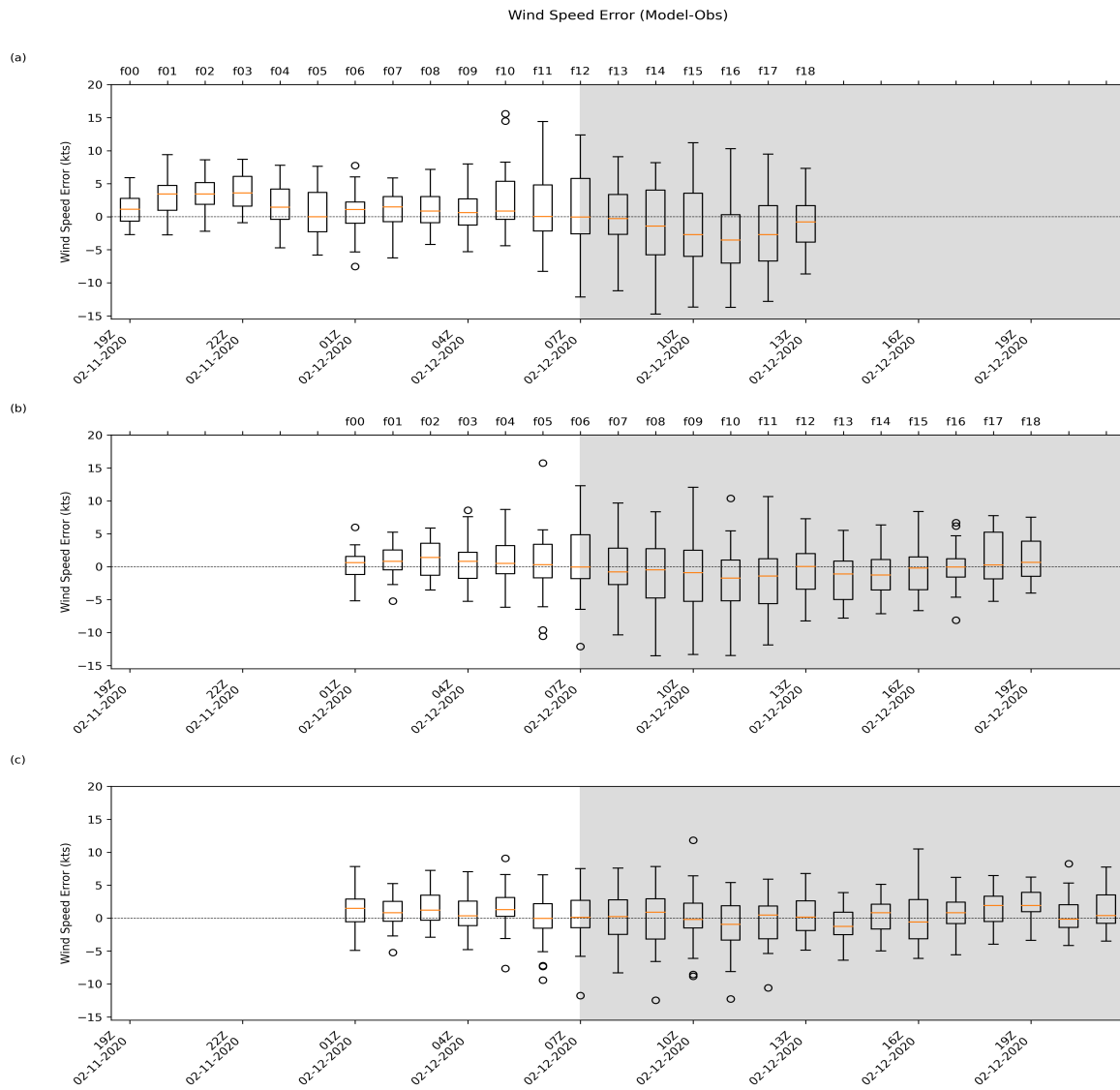
Figure 41. Box plots of HRRR wind speed (kts) for (a) 12HR, (b) 6HR, and (c) F01 forecasts for the 12 February 2020 event.

Table 11. Mean and standard deviation of the medians for wind speed (kts) bias.

Mean and Standard Deviation

of Wind Speed Bias (kts)

Forecast	Before	During	All
12hr	1.5 ± 1.2	-1.6 ± 1.3	0.3 ± 2
6hr	0.7 ± 0.3	-0.5 ± 0.7	-0.1 ± 0.9
F01	0.8 ± 0.5	0.3 ± 0.9	0.5 ± 0.8
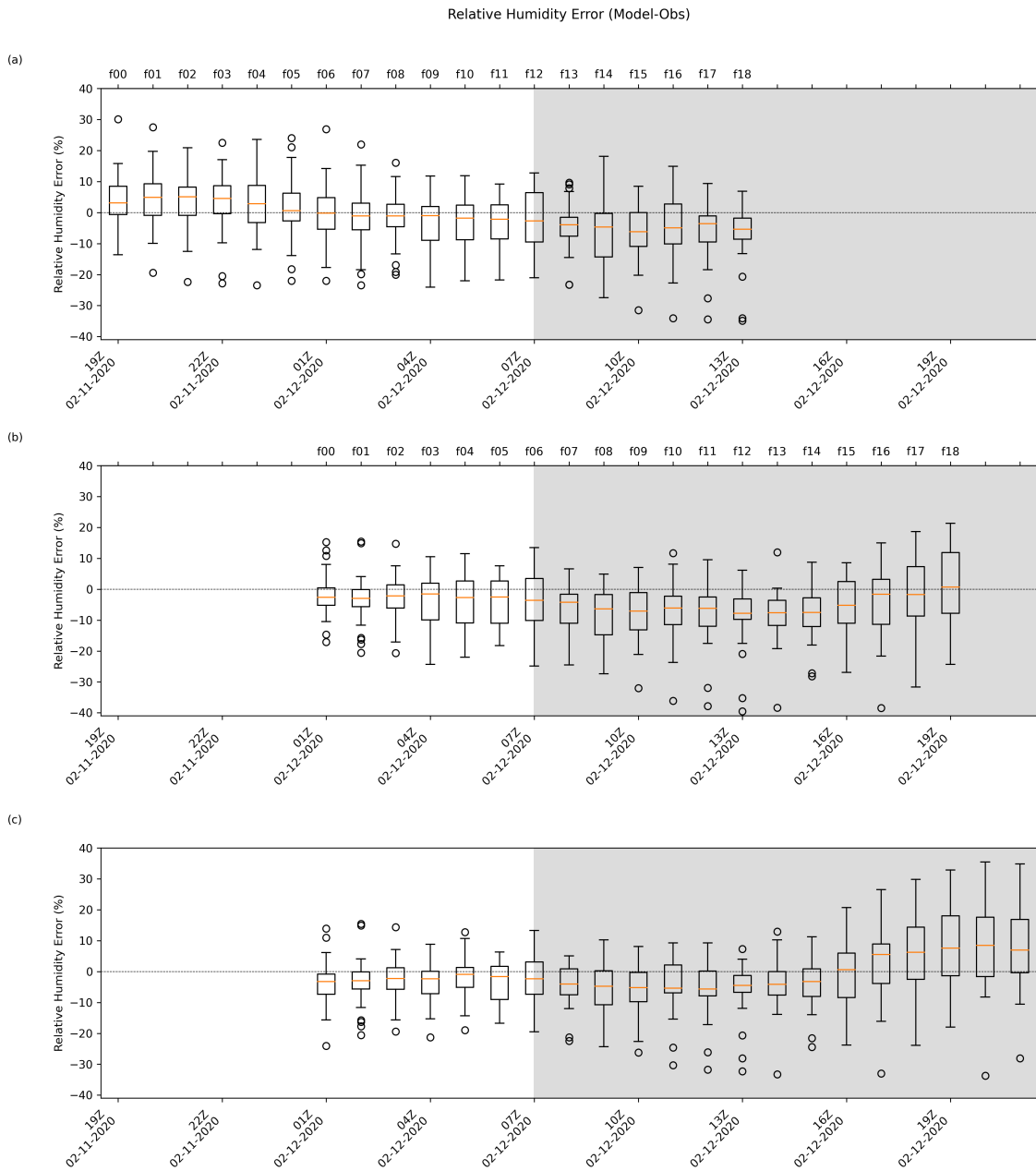
Figure 42. Box plots of HRRR relative humidity (%) for (a) 12HR, (b) 6HR, and (c) F01 forecasts for the 12 February 2020 event.

Table 12. Mean and standard deviation of the medians for relative humidity (%) bias.

Mean and Standard Deviation

of Relative Humidity Bias (%)

Forecast	Before	During	All
12HR	1.1 ± 2.7	-4.5 ± 1.1	-0.9 ± 3.5
6HR	-2.4 ± 0.5	-5 ± 2.6	-4.2 ± 2.5
F01	-2.2 ± 0.8	-0.3 ± 5.3	-0.8 ± 4.6
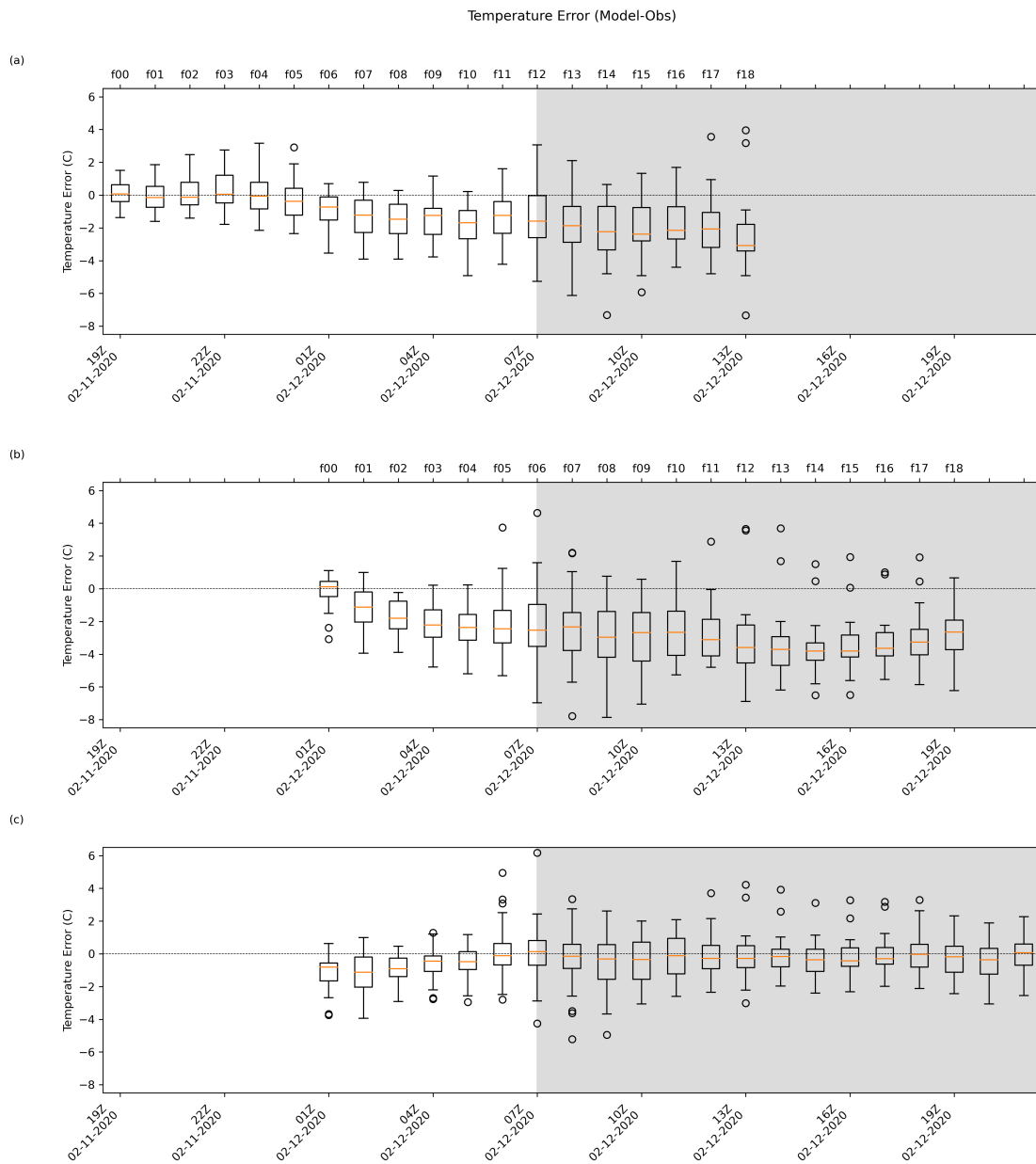
Figure 43. Box plots of HRRR temperature (ºC) for (a) 12HR, (b) 6HR, and (c) F01 forecasts for the 12 February 2020 event.

101

Table 13. Mean and standard deviation of the medians for temperature (°C) bias.

Mean and Standard Deviation

of Temperature Bias (°C)

Forecast	Before	During	All
12hr	-0.7 ± 0.6	-2.2 ± 0.4	-1.2 ± 0.9
6hr	-1.6 ± 0.9	-3.1 ± 0.5	-2.7 ± 1
F01	-0.6 ± 0.3	-0.2 ± 0.2	-0.3 ± 0.3

4.3 14 March 2019- Colorado Low

A strong Colorado low made its way through the Northern and Central Plains from 13-14 March 2019. This storm brough rain, heavy snow, and blizzard conditions to the FGF CWA from the evening on the 13th to the night of the 14th. The combination of strong winds with heavy snow created blizzard conditions across eastern ND and northwestern MN, while heavy rain and a wintry mix caused ponding of water and slippery roads in areas of northwest/west central Minnesota and the southern RRV (NWS 2019b). This storm system not only impacted the ND and MN area, but brought severe weather to New Mexico, extreme winds to Texas and Oklahoma, and blizzard conditions across Colorado, Wyoming, Nebraska, and South Dakota (NWS 2019b).

4.3.1 Environment

This system started as a strong upper-level low over the southwestern portion of the US. As the low moved over the Rocky Mountains, upper-level divergence and low-level convergence increased due to differential vorticity advection, lift from the exit region of the subtropical jet, and lee cyclogenesis (NWS 2019b). As a surface low in eastern Colorado intensified, winds near the surface increased cold and warm air advection around the cyclone. This increased the temperature gradient and in response the jet stream aloft was strengthened (NWS 2019b). The movement of air also helped to strengthen the upper-level wave. This in turn increased upper-level divergence, strengthening the surface low.

As the surface low began to move into the area, winds increased and advected warmer air into the southern RRV (Figure 44). Snow, rain, sleet, and freezing rain were all observed throughout the southern parts of the CWA. Areas north and west of the rain/snow line began to see snow during the evening hours on March 13th. During the overnight hours, heavy, wet snow

was observed as a mesoscale snow band set up over eastern ND and northwest MN. Later as the surface low began to move out of the area, high pressure behind the low increased the surface pressure gradient (NWS 2019b). This allowed for sustained winds near 30-40 mph (~26-35 kts) and wind gusts near 60 mph (~52 kts) throughout the RRV (NWS 2019b). With heavy snow and high winds, widespread blizzard conditions were seen across much of the CWA.

4.3.2 Impacts

Major impacts across the region occurred as heavy snow, damaging winds, ponding of water, and blizzard conditions created dangerous conditions. Many schools, community activities, and flights out of the Grand Forks International Airport and Hector International Airport were cancelled the evening of March 13th through most of the day on March 14th (NWS 2019b). Damage to houses and infrastructure also occurred due to the heavy, wet snow, icing, and strong winds, with power outages reported in many cities across ND (NWS 2019b). The greatest impact, however, was widespread road closures across ND and MN due to blowing snow creating low visibility and snow drifts large enough that snowplows were unable to get through them. Roads remained closed for most of the day on March 14th (Figure 45), with the main interstate between Fargo and Bismarck closed until March 15th due to 5 ft tall drifts and stranded cars blocking the road (NWS 2019b).

4.3.3 Qualitative Analysis

Meteograms for GFK, DVL, and FAR (Figure 46) demonstrate the sustained period of hazardous conditions. For this event, the start time, midpoint, and end time were identified as approximately 03Z, 12Z, and 21Z, respectively. Visibilities decreased < 1 mi in GFK and FAR

and sustained winds increased to 35 kts (~40 mph) starting during the evening hours on the 13th and continuing through the afternoon on the 14th. In FAR, visibilities varied greatly throughout the day, with most reported visibilities remaining above blizzard criteria. Note that while FAR had reduced visibility from 00Z to 03Z, this was determined to be due to precipitation vs. blowing snow.

Figure 47 provides a broader overview of observations for the entire CWA. Due to the timing of the event, near-infrared GOES-16 imagery was unavailable for much of the event. At 03Z, the system began to make its way towards the CWA, with decreased visibilities and increased wind speeds across the southwest portion of the CWA. At 12Z, widespread low visibilities and increased wind speeds were reported, with the combination of heavy snowfall and strong winds creating blizzard conditions across the area. By 21Z, thick cloud cover is still seen over the CWA, but visibilities had greatly improved, and winds speeds remained around 35 kts. Even if the event was better timed, cloud cover would have limited the detection of blowing snow from GOES-16.

Model data shows that at the start of the event the HRRR forecasted a large area of low visibility covering most of the CWA (Figure 48). HRRR surface wind gusts and relative humidity increased, and temperatures remained around -2- 2 ºC in these areas where HRRR had forecast snowfall (not shown). Note an area of 0 mi visibility, corresponding with high values of relative humidity, extends across southern MN. Observations from that region reported visibilities as low as 0.25 mi due to fog, with a mixture of rain and snow reported at some stations. These model visibilities of 0 mi could be an artifact of the HRRR trying to resolve this fog. At 12Z (Figure 49), the areas of low visibility thinned into a line covering most of the northern and western portions of the CWA and coincided with an increase in wind gusts (in DVL and GFK) while relative humidity remained between 85-100%. By 21Z (Figure 50), visibility improved to ≥10 mi for most

of the western portion of the CWA, while areas of reduced visibility remained just east of GFK and FAR. Surface wind gusts remained around 40 to 50 kts (46 to 57 mph) as relative humidity decreased and temperatures remained between -2 and 2 ℃ through most of the CWA.

Overall, the HRRR F01 forecasts adequately captured the evolution of the event. Low visibilities, higher relative humidity, and warm temperatures associated with heavy, wet snowfall and strong wind gusts from a strong pressure gradient were all evident. However, there were still some discrepancies in visibility between the model and observations. This is reflected in Figure 51 as model visibility improved towards mid-late hours of the event, while observations remained low. This is evidence that the end of the event was characterized by blowing vs. falling snow. There was good agreement between the model and observation in GFK and FAR for relative humidity (Figure 52). However, the model underestimated relative humidity over DVL for most of the event. There was overall good agreement between the F01 forecasts and observations of surface wind gusts and speeds (Figure 53-54), and temperature (Figure 55).

4.3.5 Quantitative Analysis

Like the Arctic front case, box plots of visibility show issues during times of blowing snow (Figure 56). In hours leading up to the event, medians remained around 0 mi, but there was much more spread in the data. During the event, both the 6HR and 12HR also show an overall negative bias from -0.5 to -0.9 mi (Table 14). Plots for the F01 forecast show a negative bias just after the start of the event and a positive bias towards the end of the event when blowing snow was observed.

Figure 57 shows that the wind gusts were consistently overestimated both before and during the event in all three forecasts. Over the entire event biases of 6.3 to 7.8 kts are shown, with

large spread in the data especially in the 12HR forecast (Table 15). Similarly, for wind speeds (Figure 58) an overall positive bias from 0.6 to 1.9 kts is shown in all three forecast runs (Table 16). F01 forecasts had the best agreement with a slight positive bias of 0.8 kts.

Figure 59 shows variability in relative humidity performance before the event; while the 12HR forecast had an overall positive bias of 2.4%, 6HR forecasts were drier than observations with a bias of -1.4%, and F01 forecasts showed good agreement between the model and observations (Table 17). As the event began, all forecasts showed a larger negative bias range from -1.8 to -2.2% for all three forecasts.

Analysis of temperatures (Figure 60) shows good agreement between the model and observations. The 6HR forecasts showed the best agreement with a bias of 0 ºC, with only a slight bias of 0.1-0.7 ºC for the 12HR and F01 forecasts (Table 18). During the event the bias does not change between the 12HR and F01 forecasts, however, the 6HR forecast shows a slight negative bias of -0.2 ºC. Overall, there is good agreement between model and observational temperatures with low spread in data throughout the event.

Using this analysis a few observations are made for this event. Similar to the Arctic Front case, during the event the HRRR forecasted higher visibilities and lower relative humidity than was reported in the observations during time periods of significant blowing snow. As discussed before, this is expected as the HRRR does not parameterize the process of blowing snow, and the lack of sublimation is consistent with the humidity bias. While wind gusts were forecasted consistently higher than observations, the F01 forecast of wind speeds and temperature showed good agreement between the model and observations.
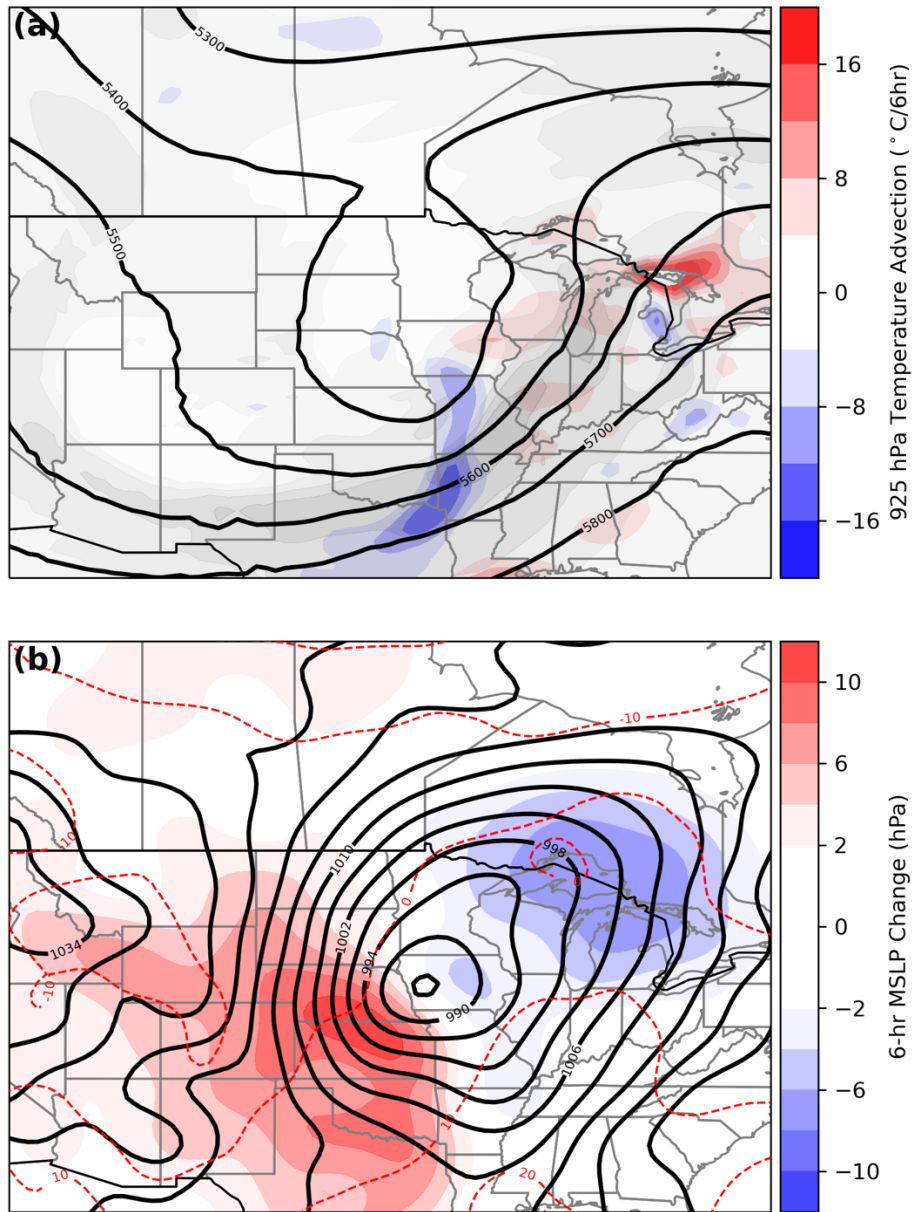
Figure 44. Meteorological fields from the GFS analysis valid at 0600 UTC 14 Mar 2019. (a) 500-hPa geopotential height (black contours), 500-hPa wind magnitude (semitransparent gray contours), and 925-hPa temperature advection (filled contours). (b) Mean sea level pressure (MSLP, black contours) and 6-h MSLP change (filled contours).
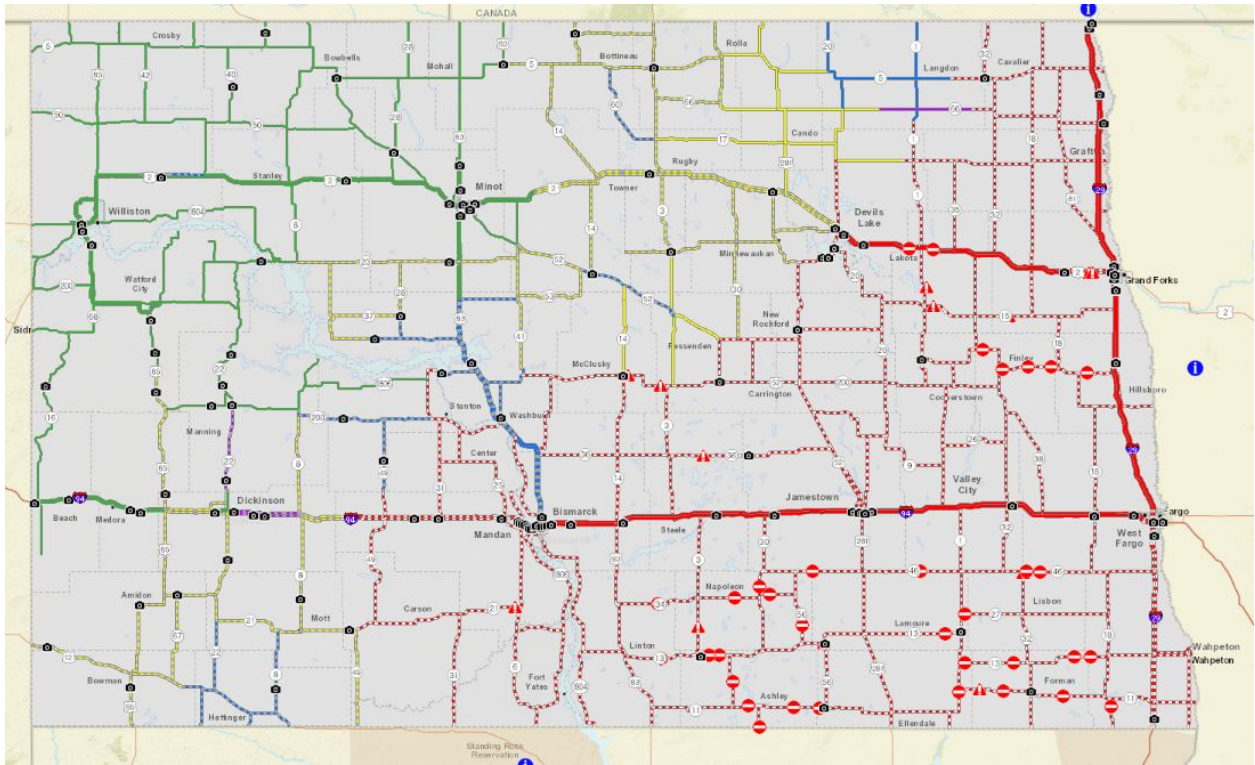
Figure 45. Road conditions as reported by the North Dakota Department of Transportation at 20Z on 20190314. Source: US Department of Commerce 2021
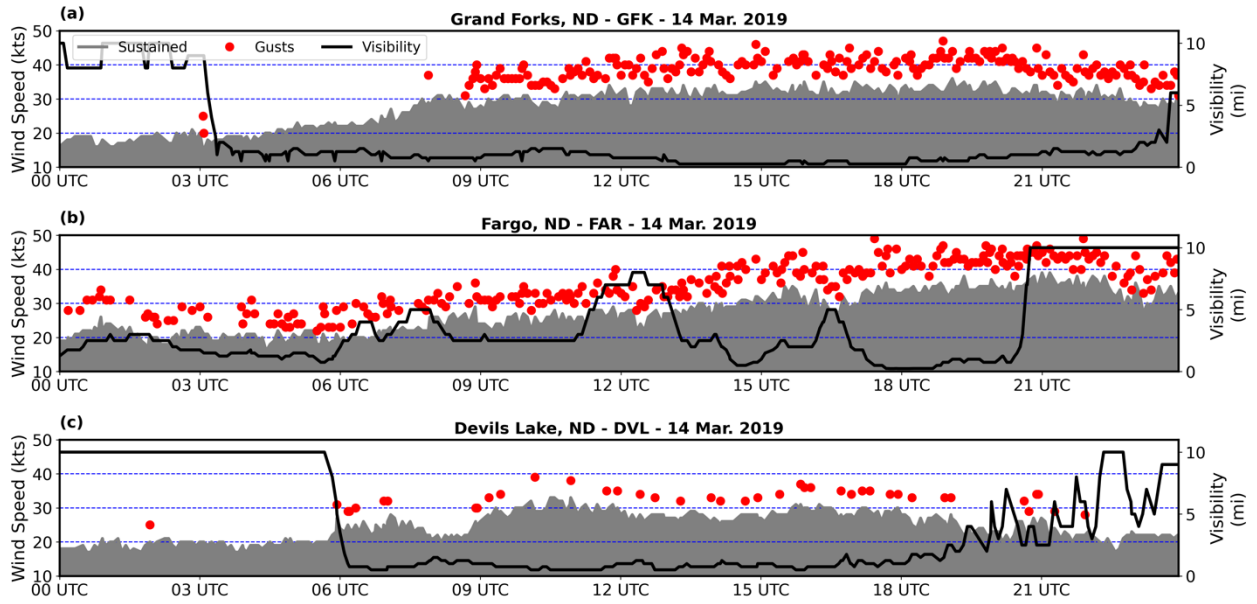
Figure 46. Meteograms of sustained winds (shaded grey), wind gusts (red dots), and visibility (black lines) for (a) GFK (Grand Forks, ND), (b) DVL (Devils Lake, ND), and (c) FAR (Fargo, ND) on 14 March 2019.
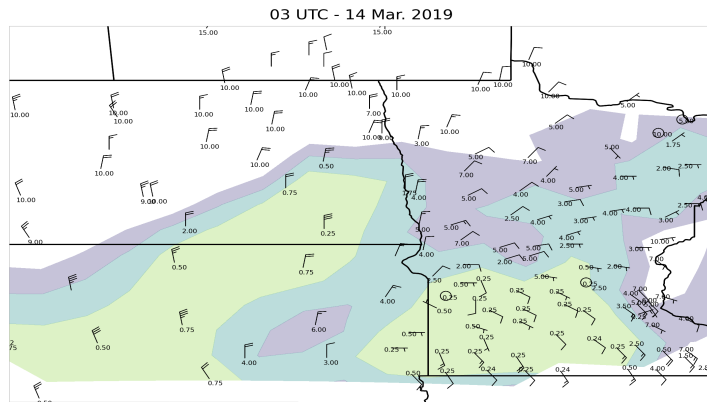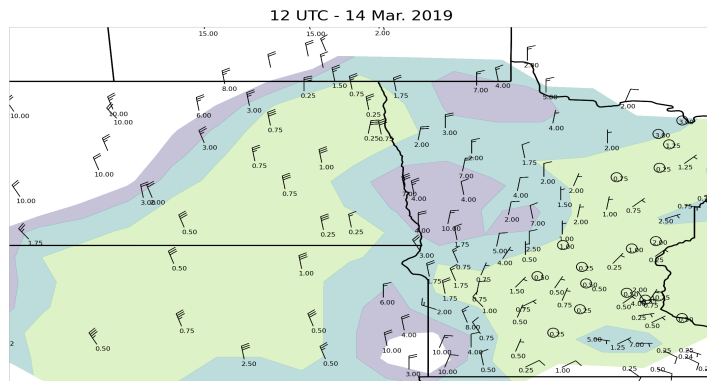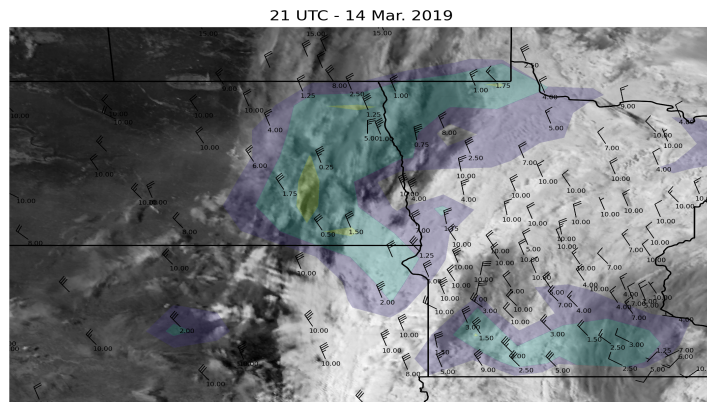
Figure 47. 1.6 μm GOES-16 reflectance overlaid with observations of visibility and wind speeds valid at (a) 03 UTC 03 March 2019, (b) 25 UTC 03 March 2019, and (c) 21 UTC 03 March 2019. Note that reflectance data is not available during the overnight hours in panel (a) and (b). Shaded areas represent regions of reduced visibility with warmer colors representing poorer conditions
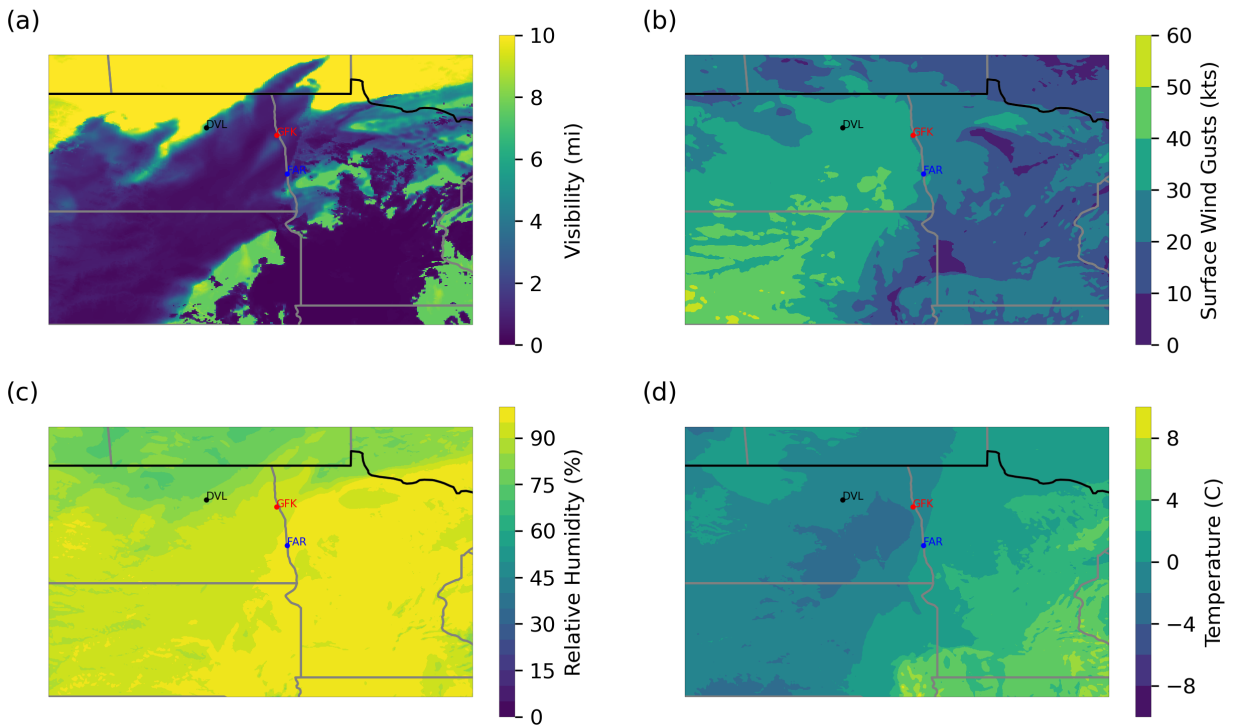
Figure 48. HRRR 14 March 2019 02 UTC F01 forecasts valid at 03 UTC 14 March 2019 for (a) visibility (mi), (b) wind gusts (kts), (c) relative humidity (%), and (d) temperature (ºC).
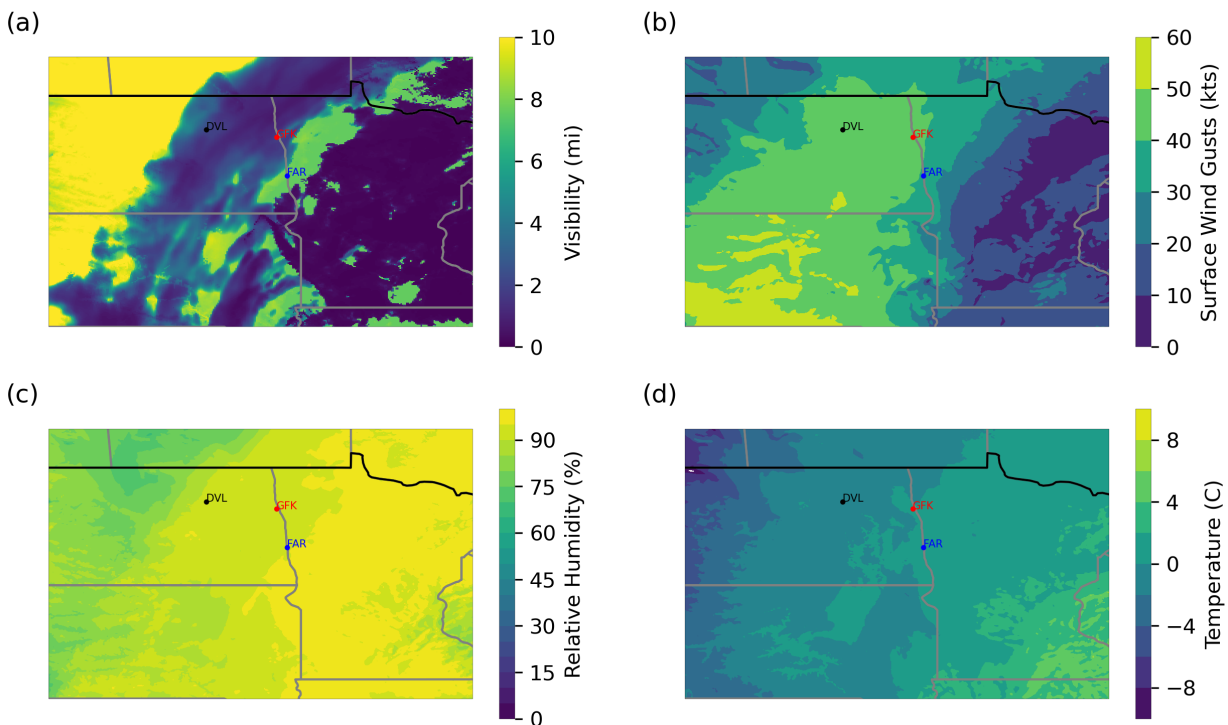
Figure 49. HRRR 14 March 2019 11 UTC F01 forecasts valid at 12 UTC 14 March 2019 for (a) visibility (mi), (b) wind gusts (kts), (c) relative humidity (%), and (d) temperature (ºC).
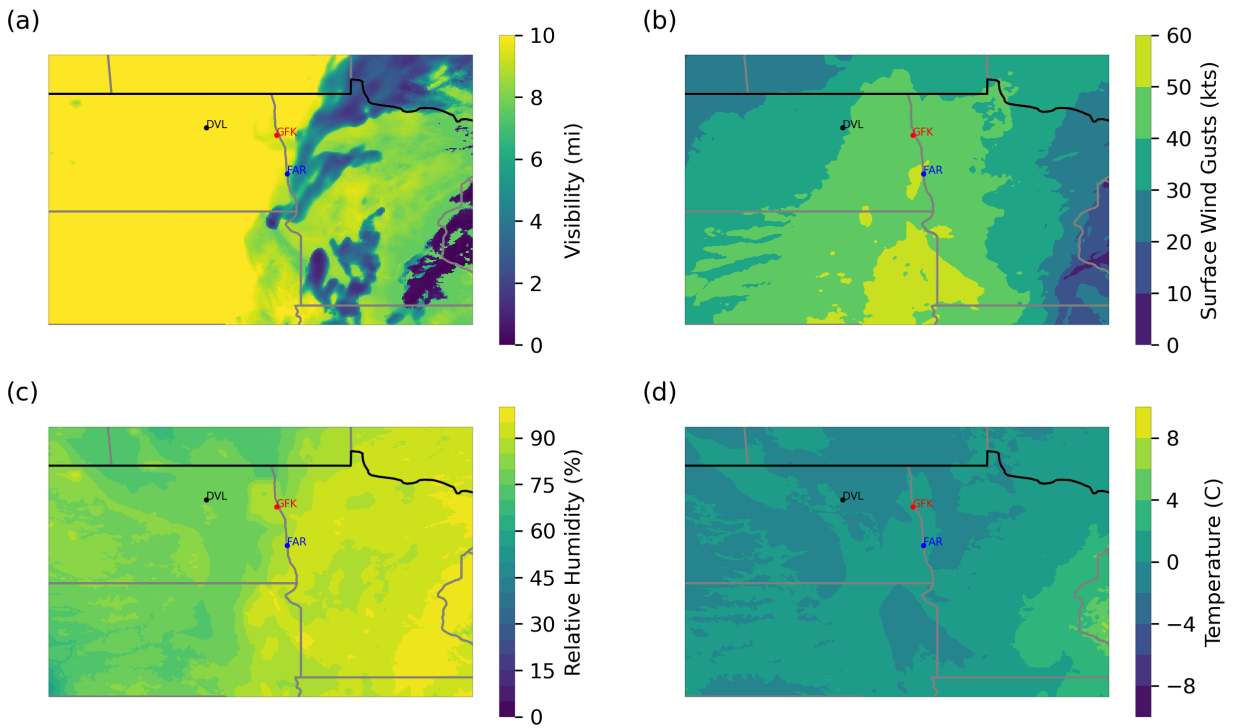
Figure 50. HRRR 14 March 2019 20 UTC F01 forecasts valid at 21 UTC 14 March 2019 for (a) visibility (mi), (b) wind gusts (kts), (c) relative humidity (%), and (d) temperature (ºC).
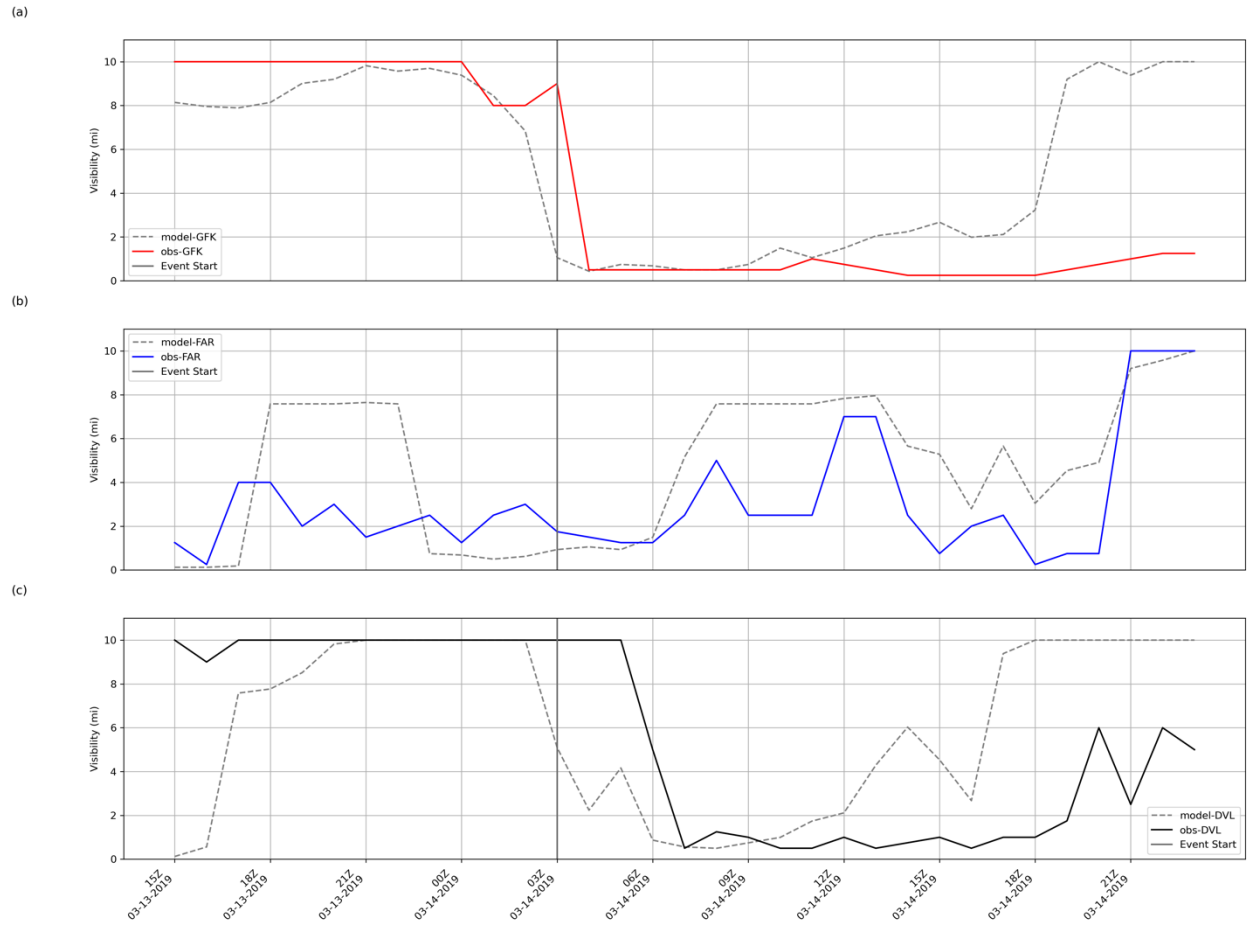
Figure 51. Time series of observed and HRRR 20190314 F01 forecasted visibility for (a) GFK, (b) DVL, and (c) FAR valid from 15Z 20190313 to 21Z 20190314.
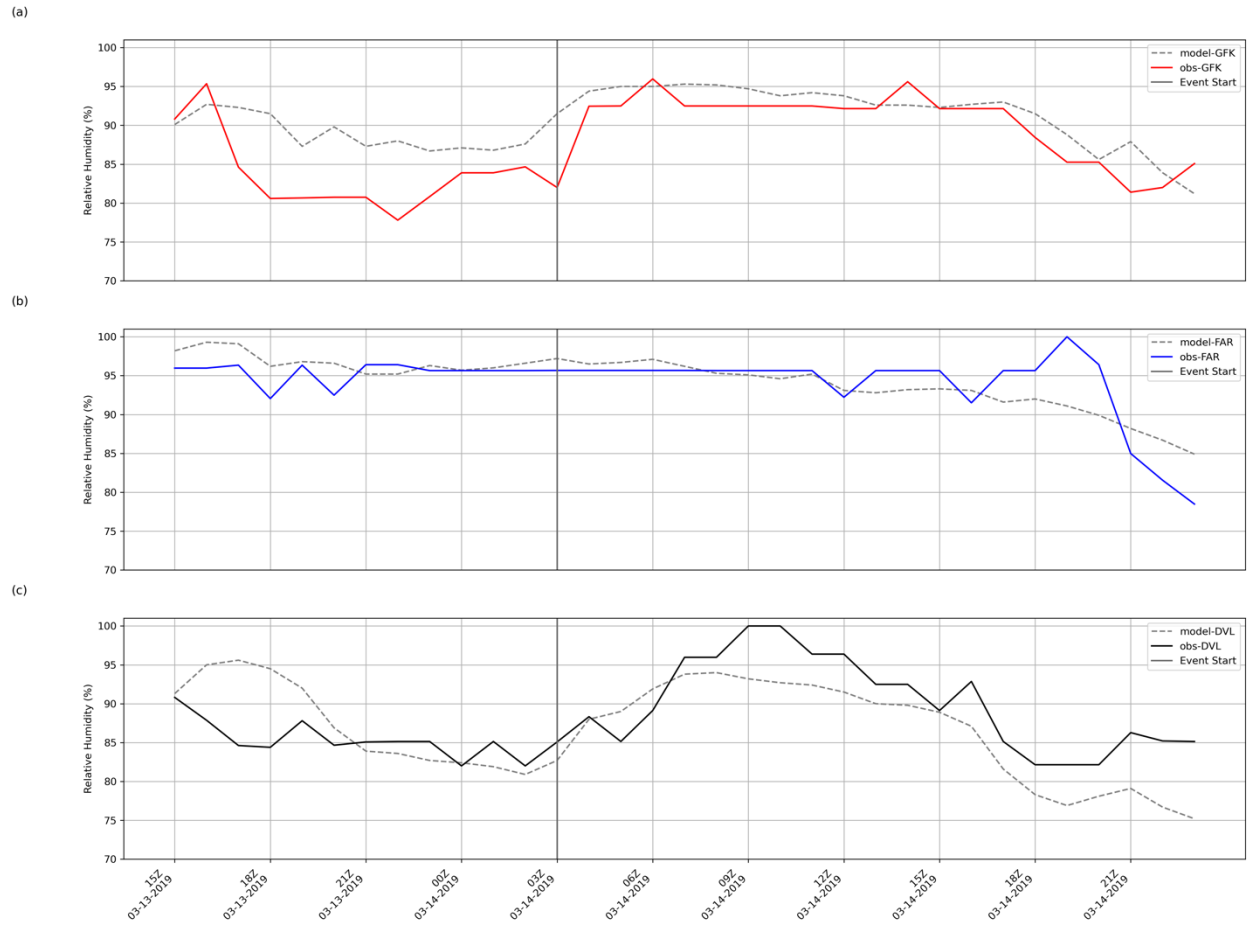
Figure 52. Time series of observed and HRRR 20190314 F01 forecasted relative humidity for (a) GFK, (b) DVL, and (c) FAR valid from 15Z 20190313 to 21Z 20190314
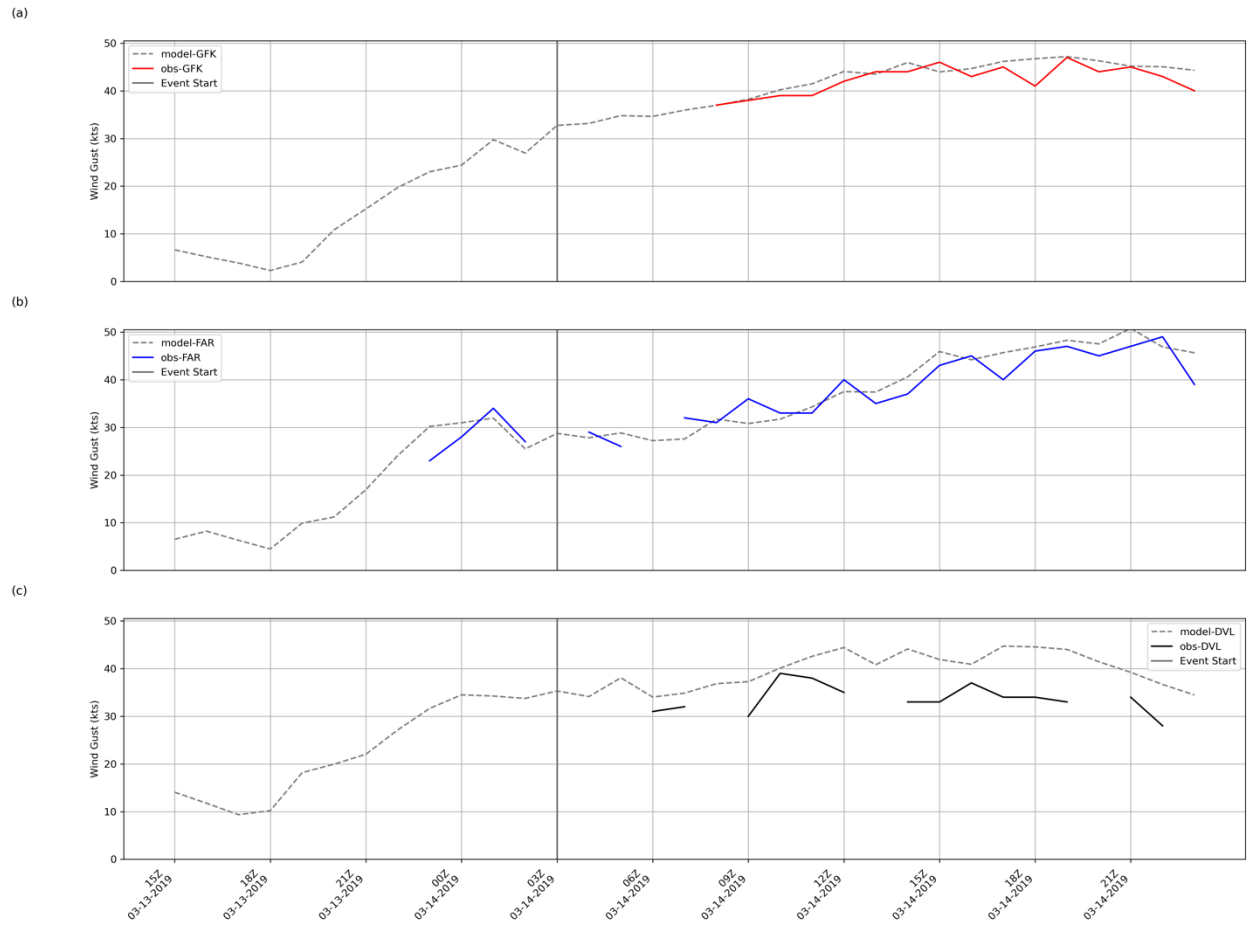
Figure 53. Time series of observed and HRRR 20190314 F01 forecasted wind gusts for (a) GFK, (b) DVL, and (c) FAR valid from 15Z 20190313 to 21Z 20190314.
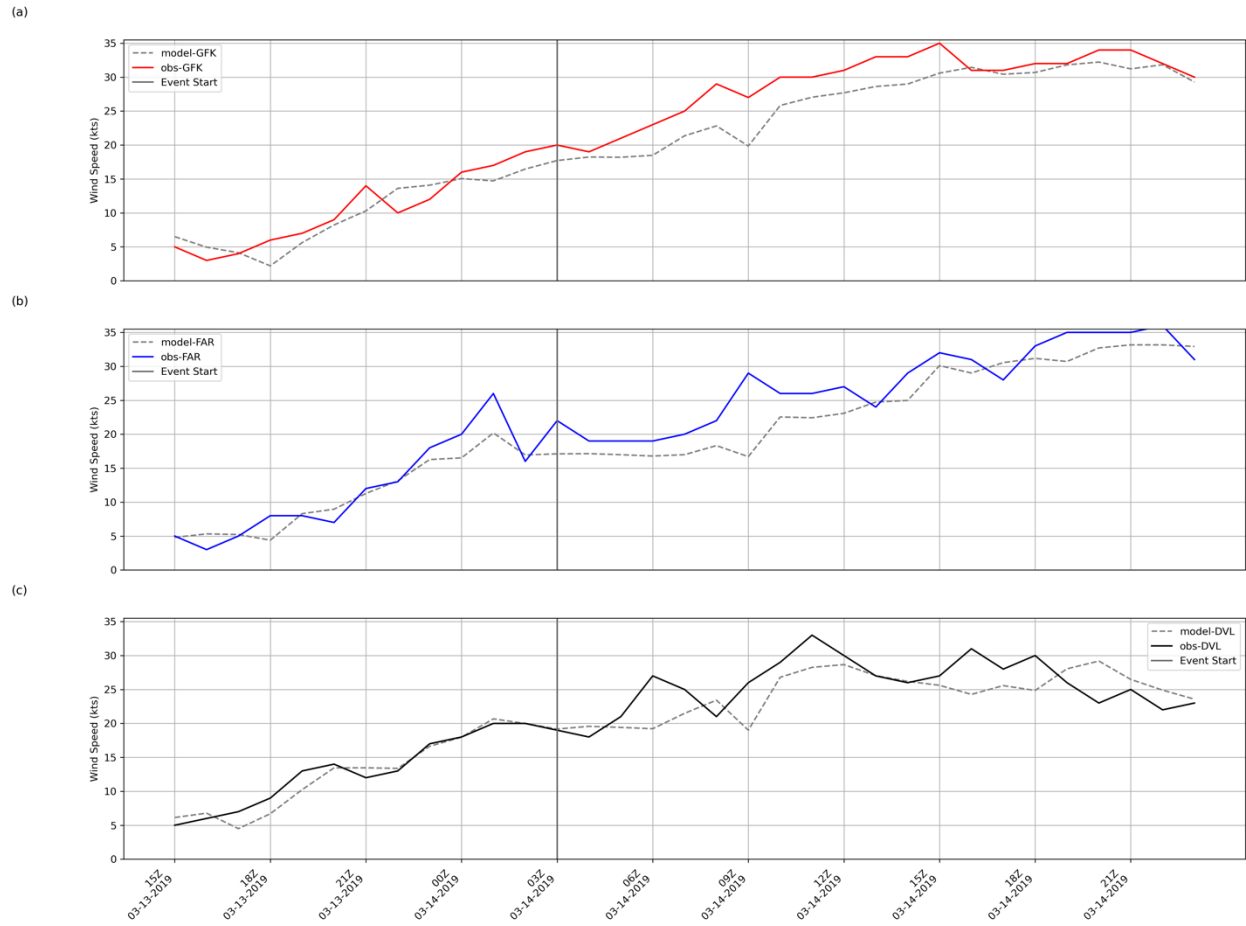
Figure 54. Time series of observed and HRRR 20190314 F01 forecasted wind speeds for (a) GFK, (b) DVL, and (c) FAR valid from 15Z 20190313 to 21Z 20190314.
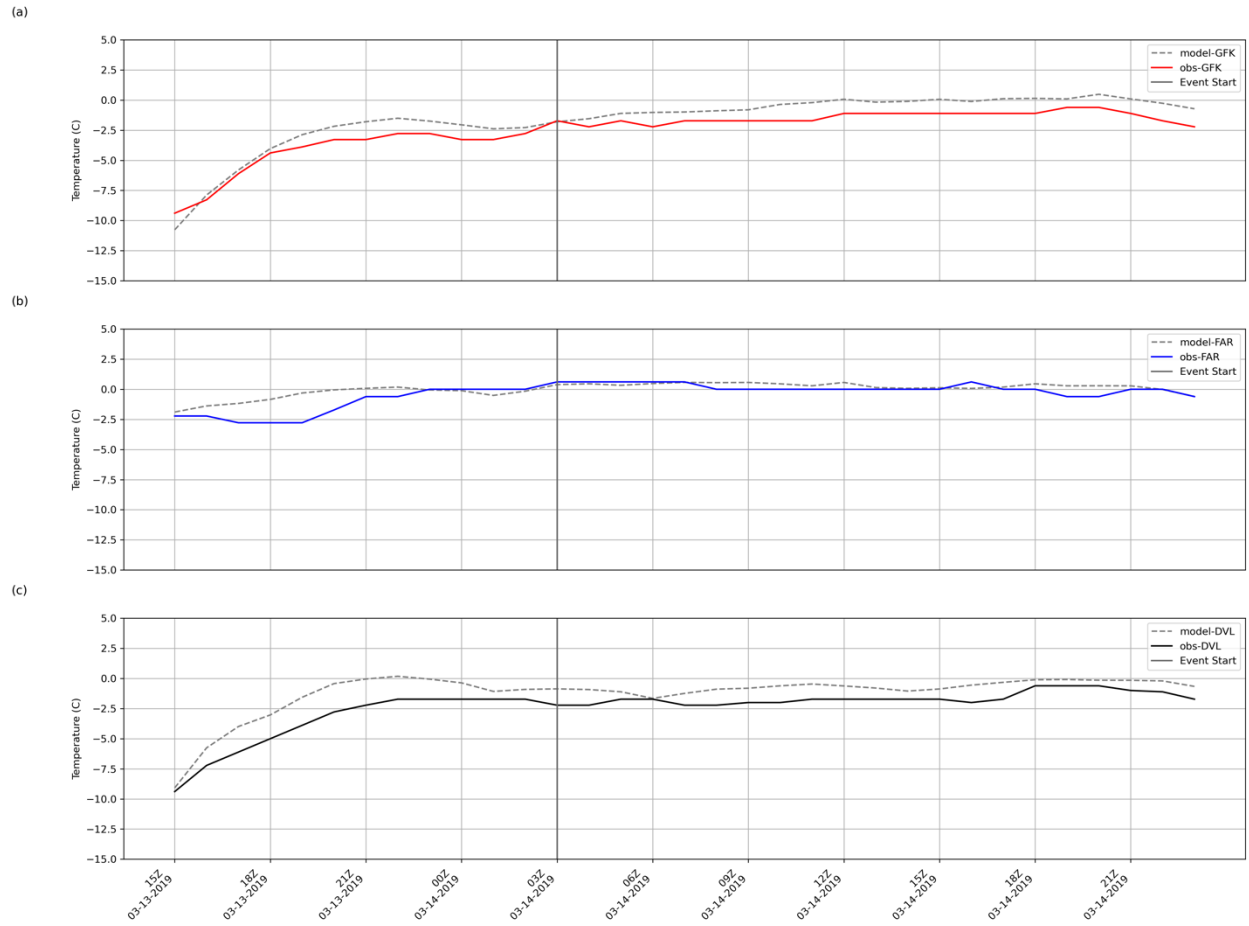
Figure 55. Time series of observed and HRRR 20190314 F01 forecasted temperature for (a) GFK, (b) DVL, and (c) FAR valid from 15Z 20190313 to 21Z 20190314.
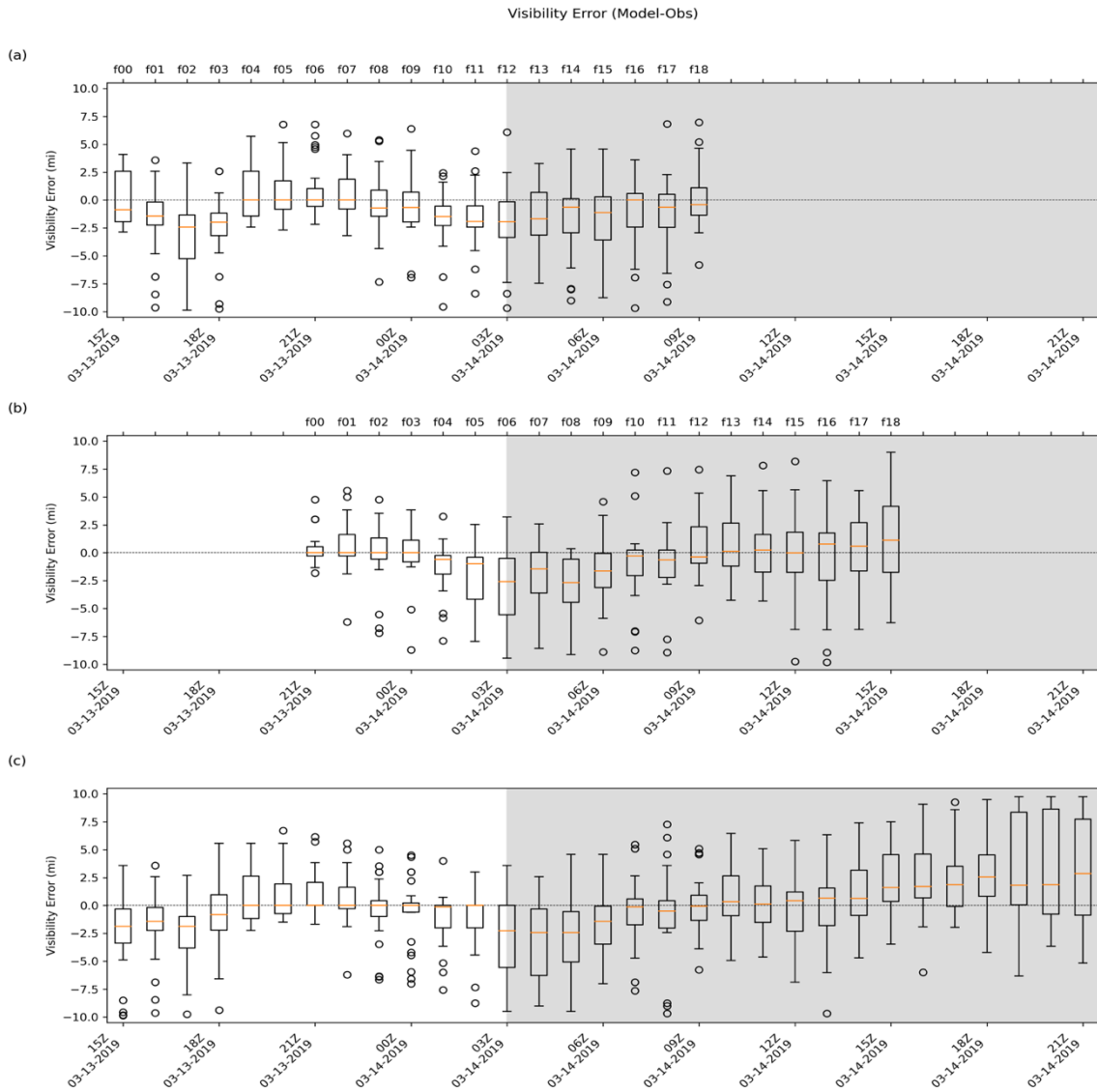
Figure 56. Box plots of HRRR visibility (mi) for (a) 12HR, (b) 6HR, and (c) F01 forecasts for the 14 March 2019 event.

Table 14. Mean and standard deviation of the medians for visibility(mi) bias.

Mean and Standard Deviation

of Visibility (mi)

Forecast	Before	During	All
12hr	-1 ± 0.8	-0.9 ± 0.6	-0.9 ± 0.8
6hr	-0.3 ± 0.4	-0.5 ± 1.2	-0.4± 1
F01	-0.5 ± 0.7	0.4 ± 1.6	0 ± 1.4

Wind Gust Error (Model-Obs)
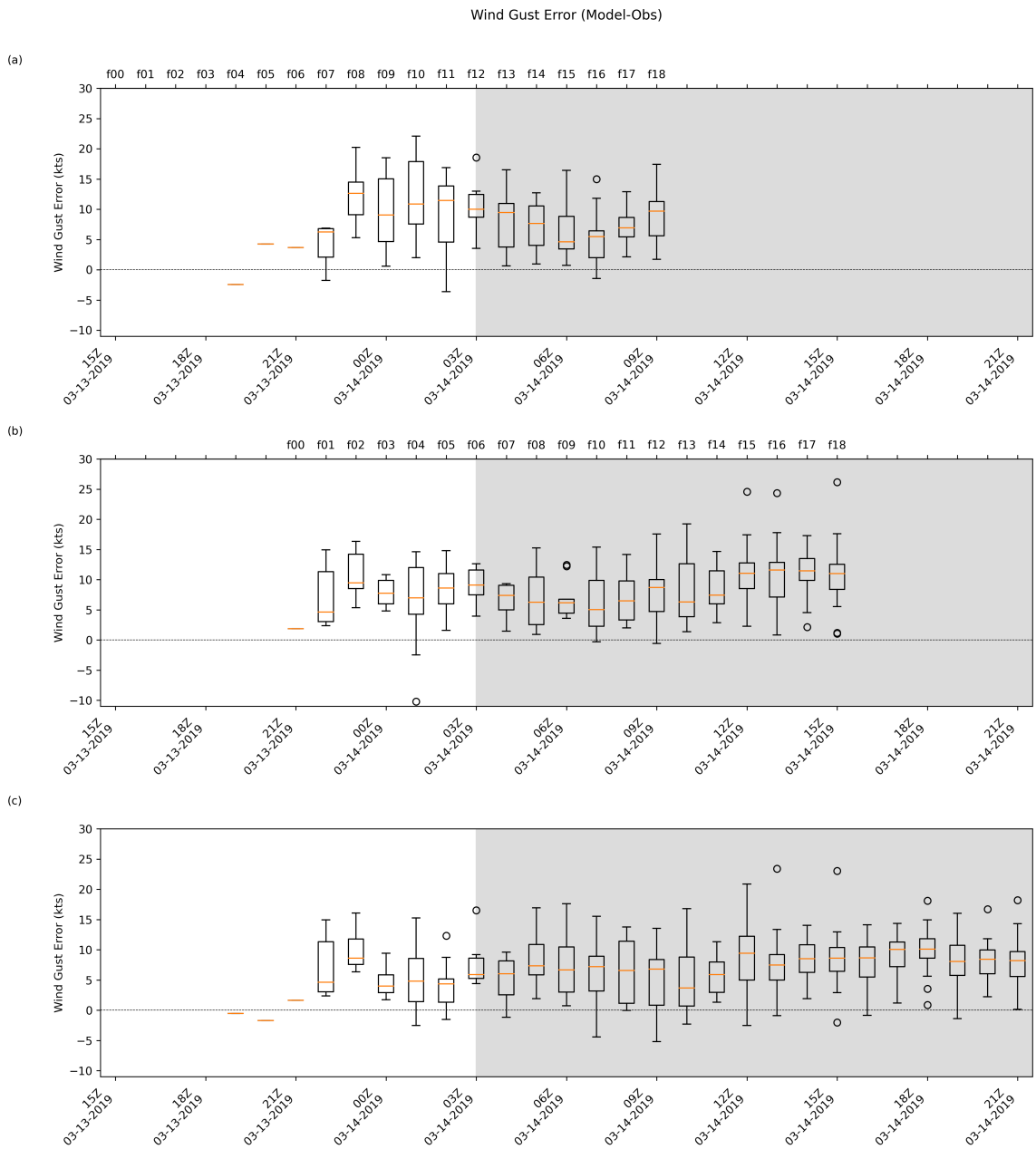
Figure 57. Box plots of HRRR wind gust (kts) for (a) 12HR, (b) 6HR, and (c) F01 forecasts for the 14 March 2019 event.

Table 15. Mean and standard deviation of the medians for wind gust (kts) bias.

Mean and Standard Deviation

of Wind Gust (kts)

Forecast	Before	During	All
12hr	7 ± 4.7	7.7 ± 2	7.3 ± 3.7
6hr	6.6 ± 2.6	8.3 ± 2.2	7.8 ± 2.5
F01	3.2 ± 3.1	7.6 ± 1.6	6.3 ± 2.9
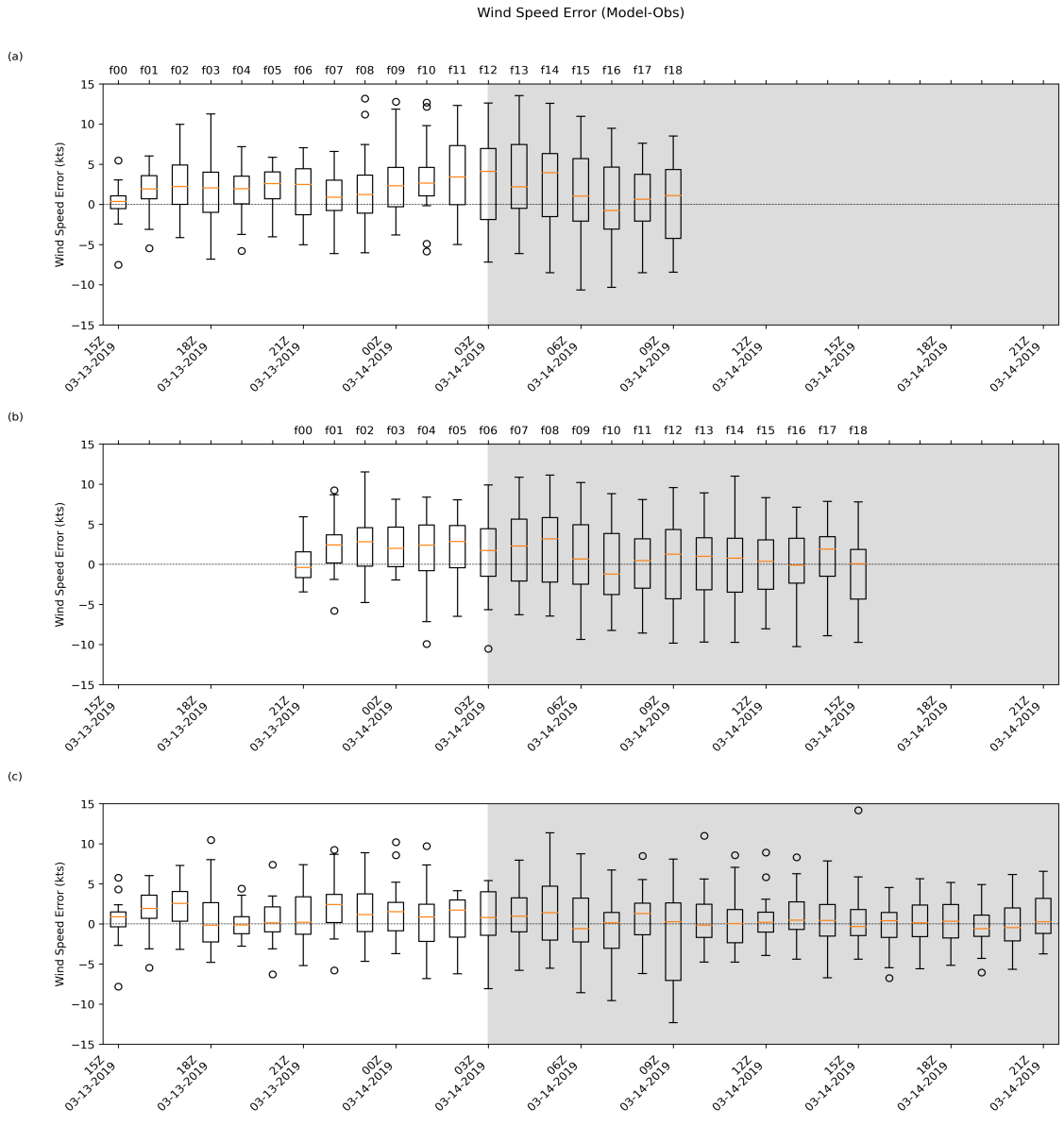
Figure 58. Box plots of HRRR wind speed (kts) for (a) 12HR, (b) 6HR, and (c) F01 forecasts for the 14 March 2019 event.

Table 16. Mean and standard deviation of the medians for wind speed (kts) bias.

Mean and Standard Deviation

of Wind Speed (kts)

Forecast	Before	After	All
12hr	2 ± 0.8	1.8 ± 1.7	1.9 ± 1.2
6hr	2 ± 1.1	1 ± 1.1	1.3± 1.2
F01	1.1 ± 0.9	0.3 ± 0.6	0.6 ± 0.8
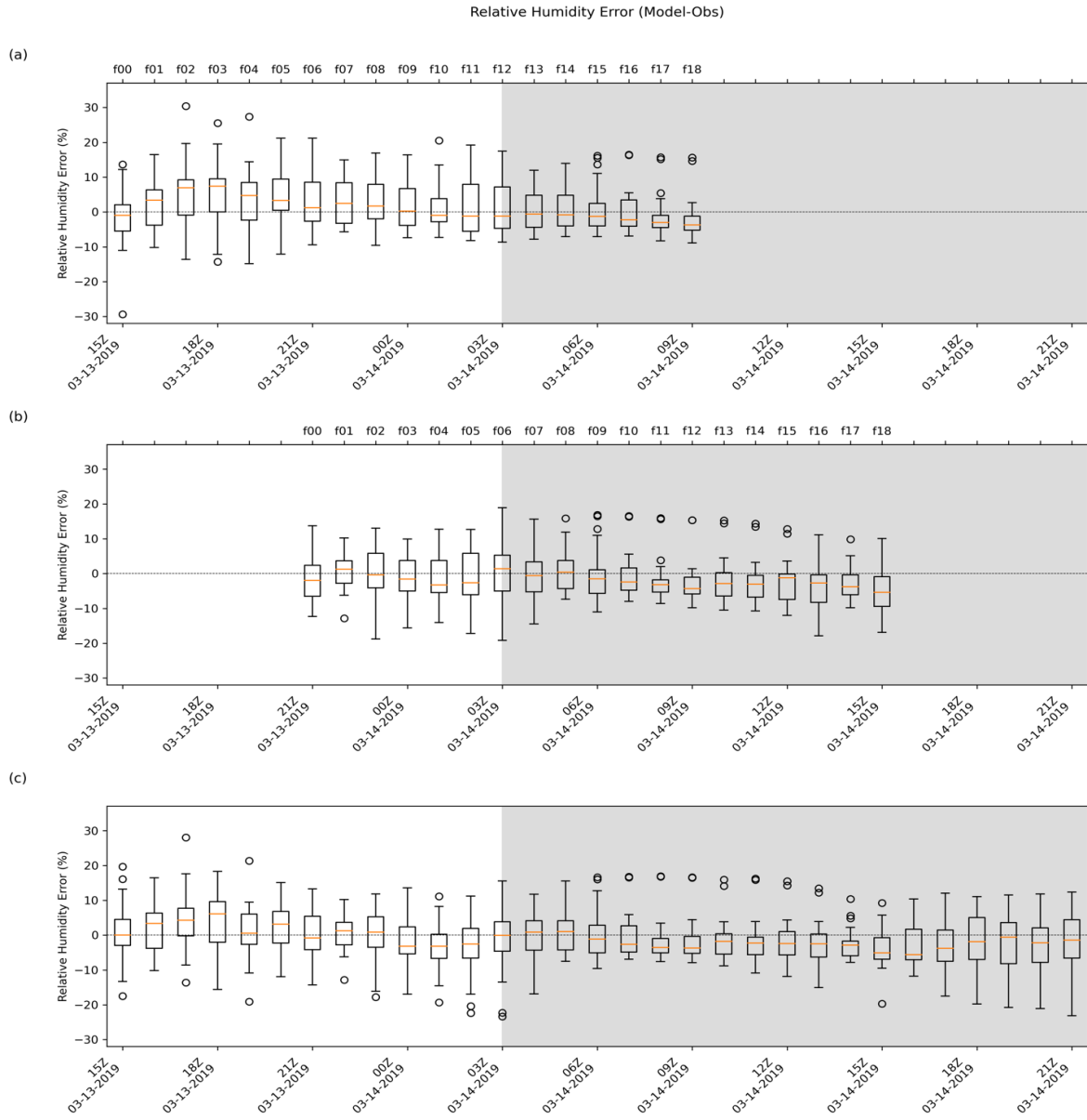
Figure 59. Box plots of HRRR relative humidity (%) for (a) 12HR, (b) 6HR, and (c) F01 forecasts for the 14 March 2019 event.

Table 17. Mean and standard deviation of the medians for relative humidity (%) bias.

Mean and Standard Deviation

of Relative Humidity Bias (%)

Forecast	Before	During	All
12hr	2.4 ± 2.8	-1.8 ± 1.1	0.8 ± 3.1
6hr	-1.4 ± 1.5	-2.2 ± 1.8	-2 ± 1.8
F01	0.8 ± 2.9	-2.2 ± 1.7	-1 ± 2.7
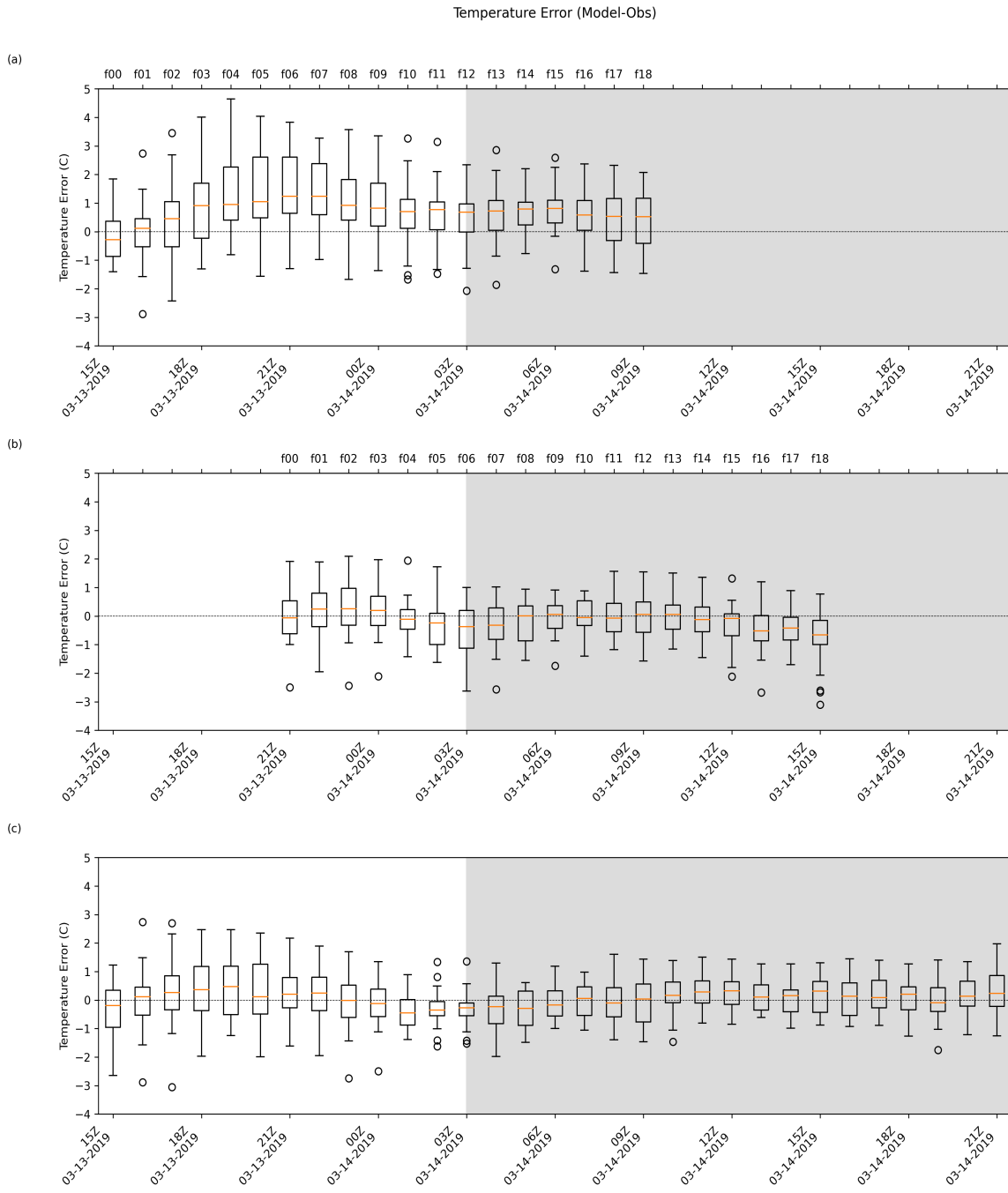
Figure 60. Box plots of HRRR temperature (ºC) for (a) 12HR, (b) 6HR, and (c) F01 forecasts for the 14 March 2019 event.

Table 18. Mean and standard deviation of the medians for temperature (ºC) bias.

Mean and Standard Deviation

of Temperature (ºC)

Forecast	Before	During	All
12hr	0.7 ± 0.4	0.7 ± 0.1	0.7 ± 0.4
6hr	0 ± 0.2	-0.2 ± 0.2	-0.1± 0.2
F01	0.1 ± 0.3	0.1 ± 0.2	0.1 ± 0.2

CHAPTER 5

RESULTS

This chapter expands on the methodology provided in Chapter 4 to provide an analysis for all events in the study. GOES-16 reflectance data were examined to determine the number of hours of available imagery and the fraction of these hours with visible blowing snow plumes. Model error statistics were then calculated for all cases. These analyses were also separated into categories for Arctic front, Colorado low, and Hybrid cases.

5.1 Arctic Front Events

Seven events were classified as Arctic front events (Table 3). Similar meteorological patterns were observed among each of the events as little snow fell but strong winds caused ground blizzards with an average duration of blizzard conditions lasting nearly 13 hours. Just over half of the events were confined to the RRV.

5.1.1 Utility of GOES-16

As demonstrated in the 12 February 2020 case study, GOES-16 imagery can be beneficial for operational forecasters during ground blizzard events. Similar to this case, analysis of GOES-16 data showed that blowing snow plumes could be seen in 6 out of 7 Arctic front events (Figure 61, Table 19). Timing played a large role as satellite imagery was limited to hours between 14-23Z when there was adequate sunlight for 1.6 μm reflectance data. This was nearly 63% of the hours for the events. While this is an encouraging result, this also demonstrates the continued need for in situ observations to monitor blizzard conditions especially during overnight hours.

5.1.2 Quantitative Analysis of HRRR

Box plots are consistent with the earlier presented case study; HRRR has significant issues in forecasting visibility both before and during the events (Figure 62). A large positive bias of 3.57- 4.08 mi during events is present regardless of forecast hour (Table 20). Large spread in data is also noted, especially just after the start of the events, likely due to timing of the fronts. The slightly higher positive bias 6-12 hours prior to events could potentially be due to pre-frontal snow. Finally, decreasing mean bias in F01 at the end of the events is likely due to visibility conditions improving.

Relative humidity shows a negative bias across all three forecast runs, with biases ranging from -1.70-1.77% across all hours (Figure 63, Table 21). Towards the ending hours, better agreement is shown between the model and observations as mean bias switches to being slightly positive. This generally occurs at approximately 8 hours after event start.

Similar to relative humidity, temperatures also exhibit a negative bias across all three forecast runs both before and during the events, with biases ranging from -0.18- -0.79 ºC (Figure 64, Table 22). Although a slight negative bias of -0.14 ºC is present during events, there appears to be good agreement between the model and observations for the F01 forecast. Earlier times (e.g., 9-12 hours before the event) suggest there may be some diurnal related bias due to the timing of most events occurring from 6-21 UTC. This corresponds to larger variability during the afternoon (~18 UTC).

Analysis of wind speeds indicate that earlier forecasts had more difficulty throughout the events (Figure 65). A negative bias for both the 6HR and 12HR forecasts ranging from -1.73- -2.51 kts is present, with significant spread in forecasts (Table 23). On the other hand, the F01 forecast shows better agreement between the model and throughout the events with mean bias of

131

< 1 kt. A positive increase in medians exists from 6-16 hours after the start of each event which is of similar magnitude of values 10-12 hours prior. This may be further evidence of diurnal variations in HRRR forecasts.

5.2 Colorado Low Events

Six events were classified as Colorado low events (Table 3). Each of these events brought heavy snow and strong winds typical of a Colorado low, creating blizzard conditions lasting an average of 18.5 hours across each event. Impacts across all events included low visibilities and large snow drifts from blowing snow, which created dangerous travel conditions in both rural and urban areas across large regions of the FGF NWSFO CWA.

5.2.1 Utility of GOES-16

Unlike Arctic cold fronts, GOES-16 imagery has minimal utility for Colorado low events. While satellite imagery was available for portions of many events, most cases extended into the overnight hours (Table 24). Even during the daytime hours, detection of blowing snow plumes was limited for all but one event due to the widespread cloud cover associated with Colorado low events (Figure 66). Only one of the Colorado low events, the 28 December 2018 case, had blowing snow plumes visible in GOES-16 imagery at the very end of the event (Figure 67). During these Colorado low events, in situ observations are likely to be the most beneficial tool for forecasters in determining impacts from blowing snow.

5.2.2 Quantitative Analysis of HRRR

Colorado lows also have a positive bias of HRRR forecasted visibility for events, but the magnitude of error is lower than Arctic front cases (Figure 68). In the hours leading up to each event, there is good agreement between the model and observations as medians remained < 1 mi, for all forecasts (Table 25). During the event, biases increase to 0.88-1.05 mi for the forecasts. Spread in forecasts is less than the Arctic front case, with an increase at the end likely due to the limited number of cases going into statistics. Overall, these findings are consistent with major reductions in visibility being caused by falling snow observed and forecasted in the model. The slight positive bias suggests blowing snow further reduces visibilities over that caused by snowfall.

Analysis of relative humidity (Figure 69) shows that in the hours before each event there is good agreement between the model and observations for all three forecasts with mean bias < 1% (Table 26). As events progressed, bias became slightly negative with time, with mean values < -1.8%. Overall, no consistent trend with forecast time is seen.

Larger forecast challenges are observed for temperature forecasts (Figure 70). Earlier forecasts (12HR and 6HR) have more difficulty with temperature, with a positive bias of 0.95-1.01 ºC that increases as the start of the event approaches (Table 27). While there is a slight positive bias of 0.22 ºC for the F01 forecasts, there is much better agreement between the model and observations.

Consistent with the case studies, there is good agreement between the model and observations of wind speeds for the F01 run (Figure 71). The 12HR and 6HR runs, however, both have a slight negative bias ranging between -0.26 - -0.44 kts (Table 28) both before and during the events. Spread is also large with the largest error being nearly 8 kts. This large variability suggests

133

that earlier forecasts may have differed in the placement of the low, resulting in a displaced pressure gradient.

5.3 Hybrid Events

Five events were identified as Hybrids (Table 3). Each event brought bands of heavy snowfall combined with strong winds that produced blizzard conditions for an average of 18 hours across each event. Coverage of these events varied, with blowing snow conditions observed in either open country or within or just outside of the RRV.

5.3.1 Utility of GOES-16

Analysis of GOES-16 imagery for the Hybrid events (Table 29) showed results between the Arctic front and Colorado low events. Timing was an important factor as a large portion of each of the events happened during the overnight hours. Although blowing snow plumes could be seen in ~49% of the available hours, some of the plumes were barely visible underneath clouds or were located just outside of the FGF CWA boundaries. (Figure 72). This information can still be helpful to forecasters in confirming areas of blowing snow.

5.3.2 Quantitative Analysis of HRRR

Consistent with previous sections, HRRR had difficulty with forecasts of visibility (Figure 73). An overall positive bias from 0.37- 1.78 mi was shown in the hours before event start in all three forecasts (Table 30). During the event, this bias increases to 2.06 – 2.75 mi. This bias along with the spread in data lies between that seen in the Arctic front and Colorado low events. These findings are consistent with reductions of snowfall caused by falling snow, with larger spread than

what is seen in Colorado Low events likely due to the coverage and amount of heaviest snowfall. The positive bias suggests that blowing snow further reduces visibilities.

Plots of relative humidity (Figure 74) show a negative bias ranging from -0.31 to -0.86% across all three forecasts before the start of the events (Table 31). During the events the bias improves to -0.55% for the 12HR forecast, while a positive bias of 0.63% is present in the 6HR forecast. The F01 forecast, however, has a negative bias of -1.11% during the events.

As with the Colorado low events, larger temperature (Figure 75) biases ranging from 1.29-1.40 ºC in the 12HR and 6HR forecasts are observed (Table 32). There is good agreement for the F01 forecast, with an overall positive bias of only 0.16 ºC during the events.

Results for wind speeds (Figure 76) display an overall negative bias across both the 6HR and 12HR forecasts closer to that observed in the Arctic front events (Table 33). The F01 forecast has good agreement between the model and observations with an overall bias of only 0.04 kts across all hours of the events. Large spread in data suggests that earlier forecasts may have variability in the placement of the low, resulting in a change in location of the pressure gradient similar to the results for Colorado low events.

5.4 All Events

A similar analysis can be done to look at the statistical summary of error across all events. Figure 77 demonstrates good agreement between the model and observations of visibility in the hours before the start of the events. As expected from the results of the different classifications, during the events the model overestimated visibility with positive biases ranging from 0.69-0.77 mi (Table 34). Although there is large spread in the data, this is likely due to the different variables discussed above for each event. A negative bias for forecasts of relative humidity (Figure 78)

135

ranging from -1.50 – -1.73% is seen across all three forecasts for all hours of the events (Table 35). This is consistent with the strong negative biases seen in each of the different events above.

Results for temperatures (Figure 79) show much better agreement between the model and observations for the hours leading up to the events. Although there is better agreement, a slight negative bias of -0.07 ºC for the 12HR and F01 forecasts and a slight positive bias of 0.05 ºC for the 6HR forecast are shown (Table 36). During the events, a larger positive bias ranging from 0.62-0.79 ºC is shown in the 6HR and 12HR forecasts consistent with the biases shown for the Colorado low and Hybrid events. However, the F01 forecast still shows good agreement between the model and observations with the spread in data decreasing as the events go on.

HRRR had more difficulty with wind speeds (Figure 80) for the 6HR and 12HR forecasts with a negative bias ranging from -1.24 - -1.55 kts during the events (Table 37). The F01 forecast showed much better agreement between the model and observations with only a slight positive bias of 0.21 kts during the events. This is consistent with the results for wind speeds in each classification above. In the previous analyses, box plots of wind gust were not shown. This is because wind gusts were consistently over forecast. This is reflected in the statistics of all of the events (Figure 81). A positive bias of 3.36-4.73 kts exists across all hours (Table 38).

18 UTC - 12 Feb. 2020

18 UTC - 24 Jan. 2019
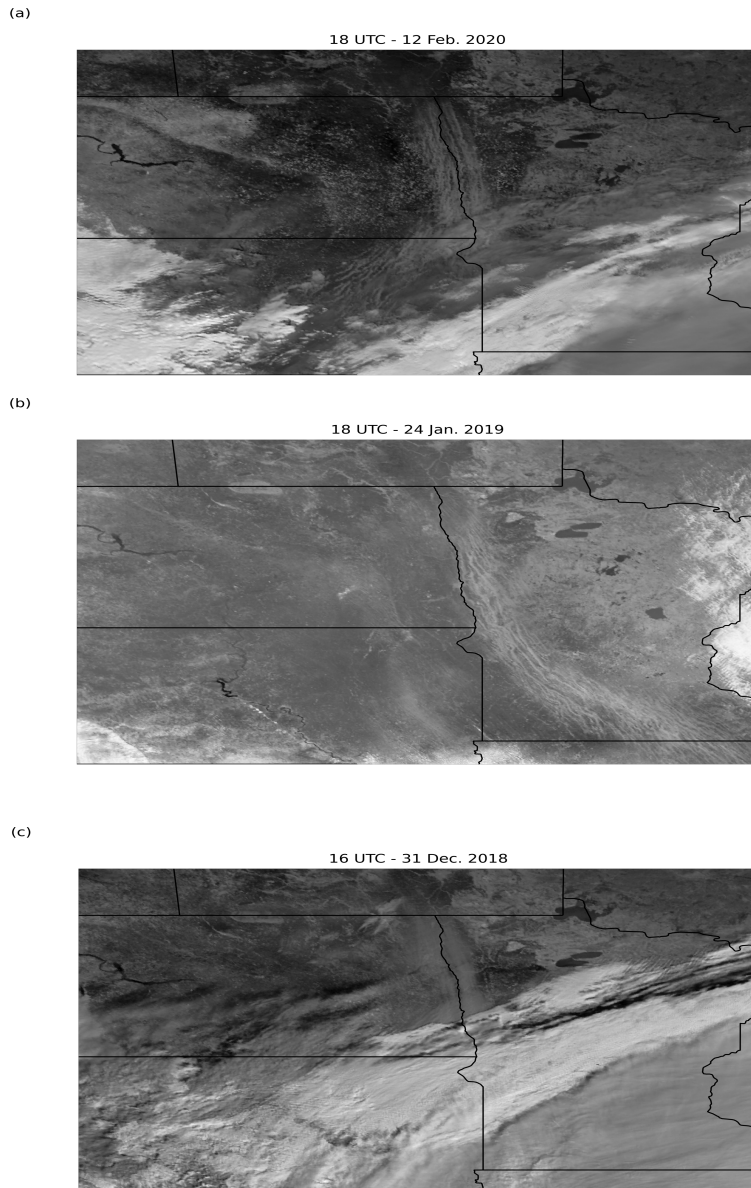
16 UTC - 31 Dec. 2018

Figure 61. 1.6 μm GOES-16 reflectance imagery over the RRV valid for 18 UTC (a) 12 Feb. 2020, (b) 24 Jan. 2019, and 16 UTC (c) 21 UTC 31 Dec. 2018.

Table 19. Hours of available satellite imagery for each Arctic front event. Blue boxes represent the length of the event, black hatching shows the hours GOES-16 imagery was available, and red hatching shows hours in which blowing snow could be seen within GOES-16 imagery.

Hours of Available Satellite Imagery

	00Z	03Z	06Z	09Z	12Z	15Z	18Z	21Z	00Z	03Z	06Z	09Z	12Z	15Z	18Z	21Z
31-Dec-18																
8-Jan-19																
29-Jan-19																
24-Feb-19																
19-Mar-20																
12-Feb-20																

138

Figure 62. Box plots of HRRR visibility error (mi) for (a) 12HR, (b) 6HR, and (c) F01 forecasts for Arctic front events.

Table 20. Mean and standard deviation of mean visibility (mi) bias.

Mean and Standard Deviation

of Visibility (mi)

Forecast	Before	During	All
12hr	1.21 ± 0.70	3.57 ± 0.48	2.08 ± 1.30
6hr	1.09 ± 0.75	4.08 ± 0.97	3.14 ± 1.66
F01	0.89 ± 0.39	3.65 ± 1.25	2.51 ± 1.68
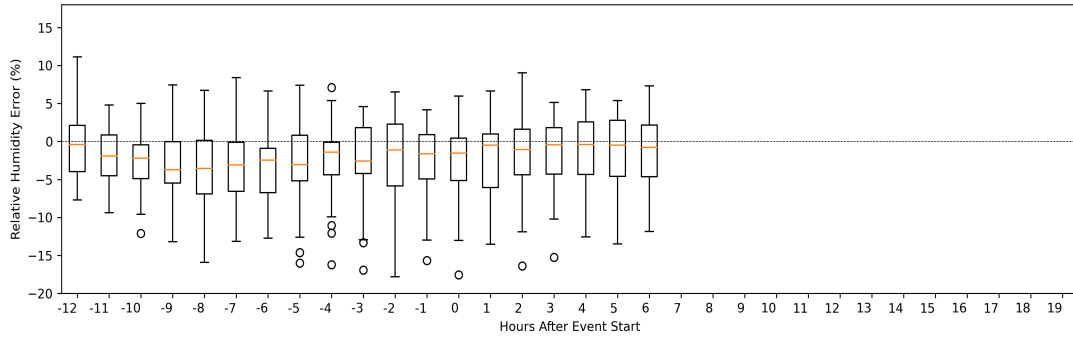
Figure 63. Box plots of HRRR relative humidity error (%) for (a) 12HR, (b) 6HR, and (c) F01 forecasts for Arctic front events.

Table 21. Mean and standard deviation of mean relative humidity (%) bias

Mean and Standard Deviation

of Relative Humidity (%)

Forecast	Before	During	All
12hr	-2.26 ± 0.97	-0.74 ± 0.39	-1.7 ± 1.09
6hr	-2.59 ± 1.07	-1.39 ± 0.82	-1.77 ± 1.06
F01	-3.5 ± 1.66	-0.48 ± 1.95	-1.73 ± 2.37

Figure 64. Box plots of HRRR temperature error (ºC) for (a) 12HR, (b) 6HR, and (c) F01 forecasts for Arctic front events.

Table 22. Mean and standard deviation of mean temperature (ºC) bias

Mean and Standard Deviation

of Temperature (ºC)

Forecast	Before	During	All
12hr	-0.27 ± 0.47	-0.45 ± 0.14	-0.33 ± 0.39
6hr	-0.72 ± 0.31	-0.83 ± 0.16	-0.79 ± 0.23
F01	-0.23 ± 0.22	-0.14 ± 0.13	-0.18 ± 0.18

Figure 65. Box plots of HRRR wind speed error (kts) for (a) 12HR, (b) 6HR, and (c) F01 forecasts for Arctic front events.

Table 23. Mean and standard deviation of mean wind speed (kts) bias

Mean and Standard Deviation

of Wind Speed (kts)

Forecast	Before	During	All
12hr	-0.67 ± 0.96	-2.51 ± 0.50	-1.35 ± 1.21
6hr	-1.27 ± 0.71	-1.73 ± 0.86	-1.59 ± 0.84
F01	0.12 ± 0.49	0.47 ± 0.65	0.33 ± 0.61
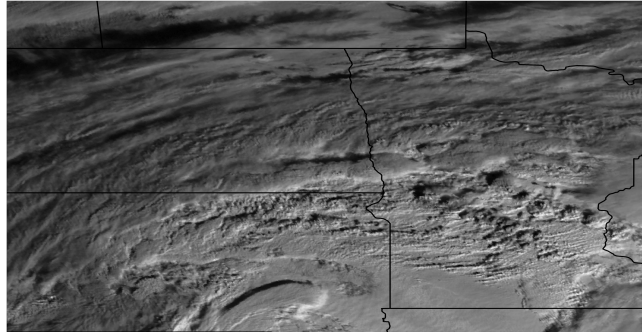
15 UTC - 30 Nov. 2019
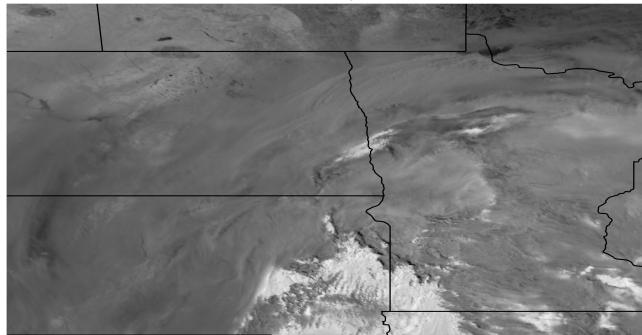
15 UTC - 11 Apr. 2019
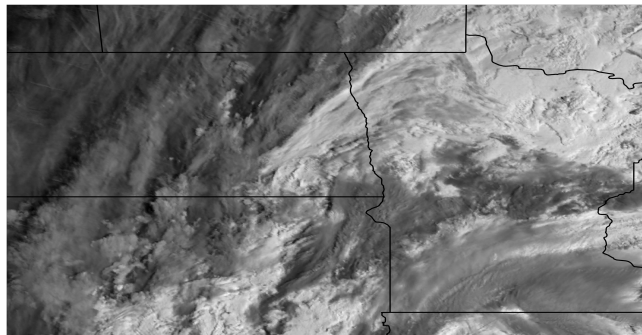
15 UTC - 14 Mar. 2019

Figure 66. 1.6 μm GOES-16 reflectance imagery of cloud cover over the CWA valid for 15 UTC (a) 30 Nov. 2019, (b) 11 Apr. 2019, and (c) 14 Mar. 2019.

147
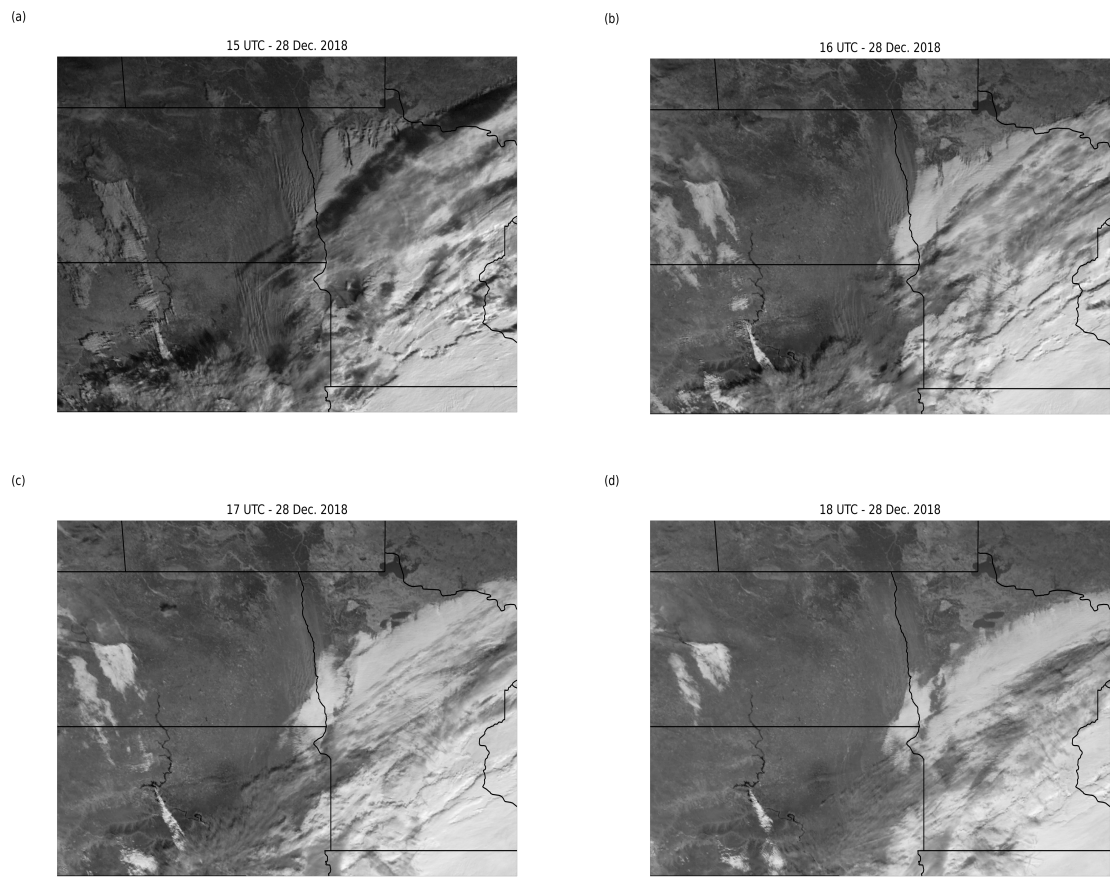
Figure 67. 1.6 μm GOES-16 reflectance imagery of blowing snow plumes over the RRV valid for (a) 15 UTC, (b) 16 UTC, (c) 17 UTC, (d) 18 UTC on 28 Dec. 2018.

Table 24. Hours of available satellite imagery for each Colorado low event. Blue boxes represent the length of the event, black hatching shows the hours GOES-16 imagery was available, and red hatching shows hours in which blowing snow could be seen within GOES-16 imagery.

Hours of Available Satellite Imagery

	00Z	03Z	06Z	09Z	12Z	15Z	18Z	21Z	00Z	03Z	06Z	09Z	12Z	15Z	18Z	21Z
28-Dec-18																
14-Mar-19																
11-Apr-19																
11-Oct-19																
30-Nov-19																
29-Dec-19																

Figure 68. Box plots of HRRR visibility error (mi) for (a) 12HR, (b) 6HR, and (c) F01 forecasts for Colorado Low events.

Table 25. Mean and standard deviation of mean visibility (mi) bias.

Mean and Standard Deviation

of Visibility (mi)

Forecast	Before	During	All
12hr	0.05 ± 0.25	0.88 ± 0.38	0.35 ± 0.50
6hr	0.48 ± 0.37	1.05 ± 0.42	0.87 ± 0.48
F01	0.09 ± 0.40	1.04 ± 0.55	0.67 ± 0.68
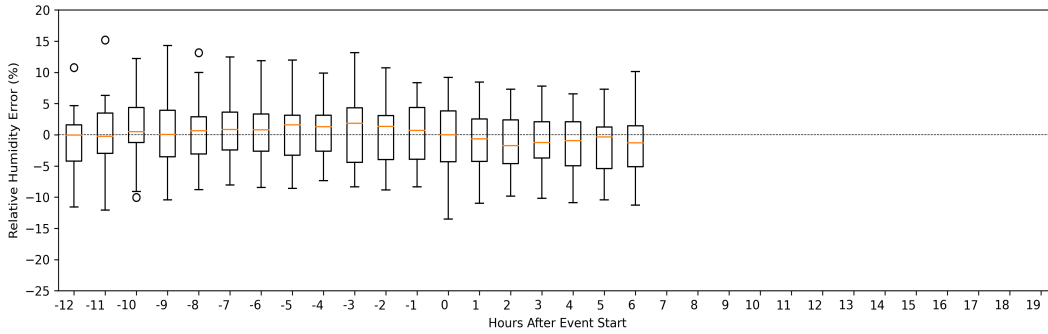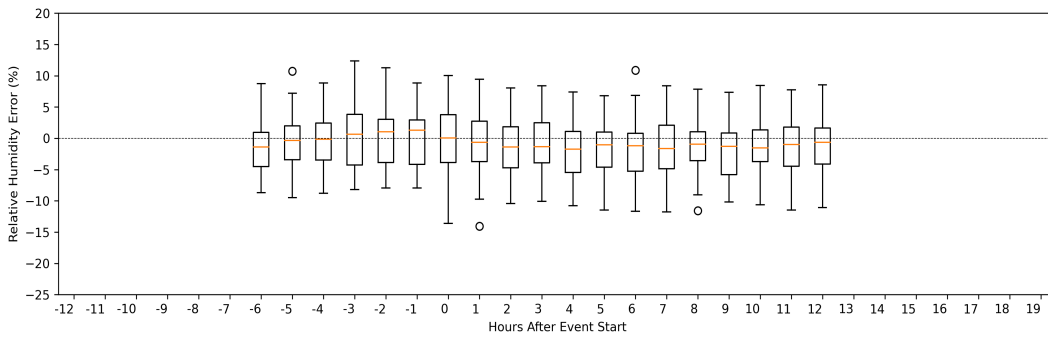
Figure 69. Box plots of HRRR relative humidity error (%) for (a) 12HR, (b) 6HR, and (c) F01 forecasts for Colorado Low events.

Table 26. Mean and standard deviation of mean relative humidity (%) bias.

Mean and Standard Deviation

of Relative Humidity (%)

Forecast	Before	During	All
12hr	0.76 ± 0.63	-0.90 ± 0.56	0.15 ± 1.00
6hr	0.17 ± 0.92	-1.11 ± 0.48	-0.71 ± 0.88
F01	0.43 ± 1.02	-1.80 ± 0.72	-0.94 ± 1.38
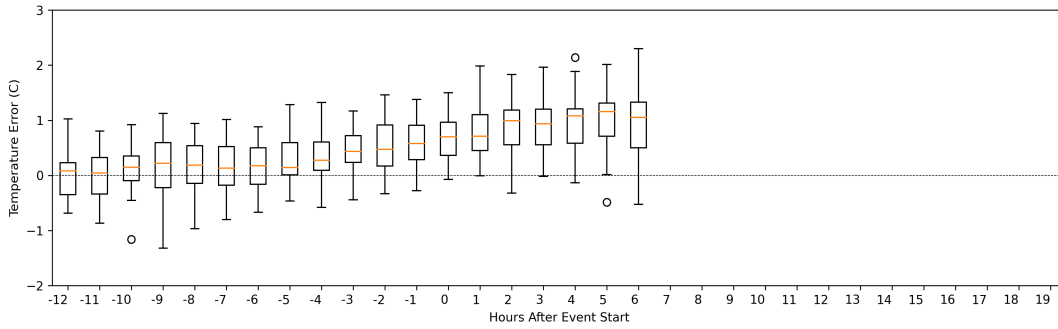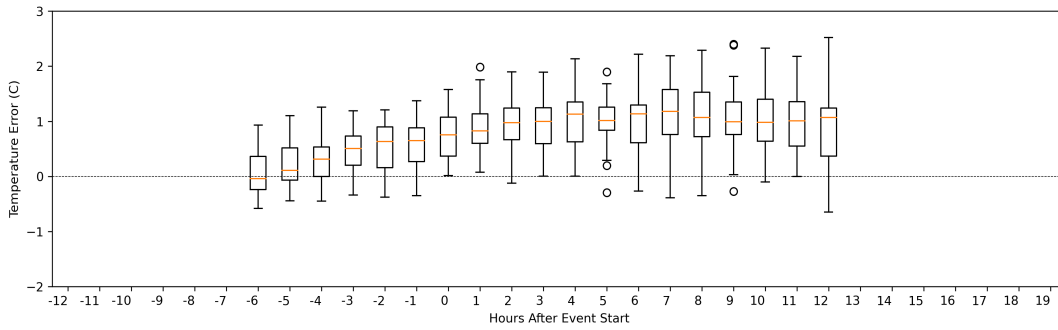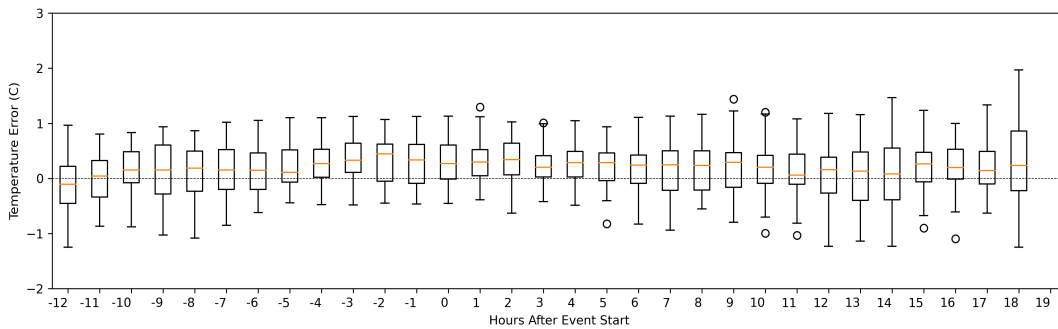
Figure 70. Box plots of HRRR temperature error (ºC) for (a) 12HR, (b) 6HR, and (c) F01 forecasts for Colorado Low events.

Table 27. Mean and standard deviation of mean temperature (ºC) bias.

Mean and Standard Deviation

of Temperature (ºC)

Forecast	Before	During	All
12hr	0.24 ± 0.16	0.95 ± 0.17	0.50 ± 0.38
6hr	0.36 ± 0.26	1.01 ± 0.11	0.81 ± 0.35
F01	0.19 ± 0.14	0.22 ± 0.07	0.21 ± 0.11
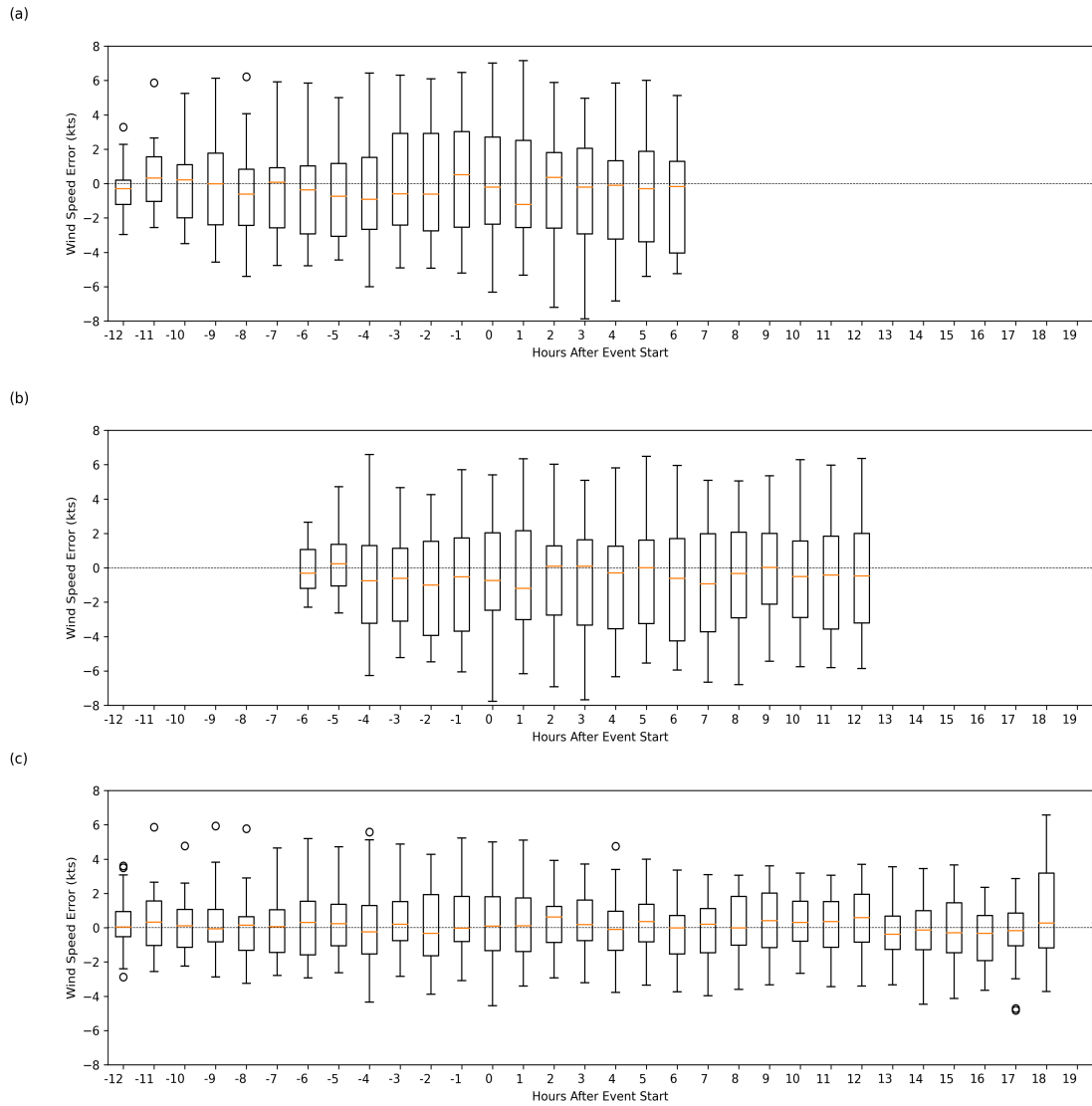
Figure 71. Box plots of HRRR wind speed error (kts) for (a) 12HR, (b) 6HR, and (c) F01 forecasts for Colorado Low events.

Table 28. Mean and standard deviation of mean wind speed (kts) bias.

Mean and Standard Deviation

of Wind Speed (kts)

Forecast	Before	During	All
12hr	-0.25 ± 0.45	-0.26 ± 0.44	-0.26 ± 0.44
6hr	-0.50 ± 0.39	-0.41 ± 0.39	-0.44 ± 0.39
F01	0.06 ± 0.19	0.11 ± 0.29	0.09 ± 0.26

Table 29. Hours of available satellite imagery for each Hybrid event. Blue boxes represent the length of the event, black hatching shows the hours GOES-16 imagery was available, and red hatching shows hours in which blowing snow could be seen within GOES-16 imagery.

Hours of Available Satellite Imagery

	00Z	03Z	06Z	09Z	12Z	15Z	18Z	21Z	00Z	03Z	06Z	09Z	12Z	15Z	18Z	21Z	00Z	03Z	06Z
4-Feb-19																			
7-Feb-19																			
14-Feb-19																			
14-Dec-19																			
18-Jan-20																			
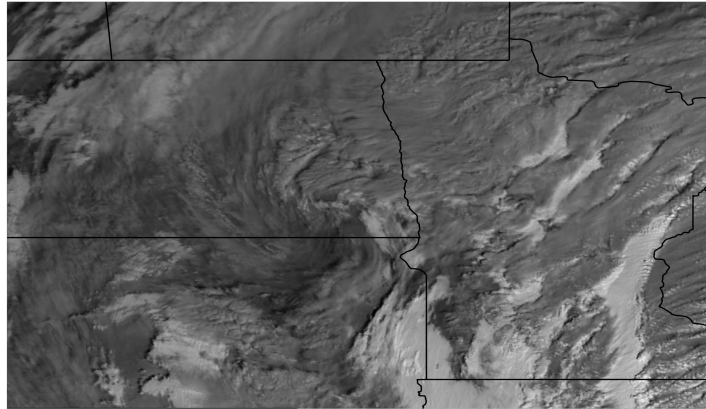
16 UTC - 07 Feb. 2019
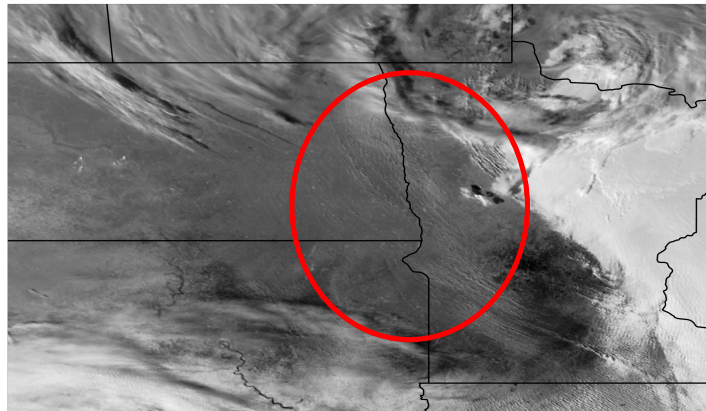
21 UTC - 04 Feb. 2019

Figure 72. 1.6 μm GOES-16 reflectance imagery of (a) cloud cover over the CWA valid for 16 UTC on 30 Nov. 2019 and (b) blowing snow plumes valid for 21 UTC on 4 Feb. 2019. The red circle denotes the area of blowing snow.
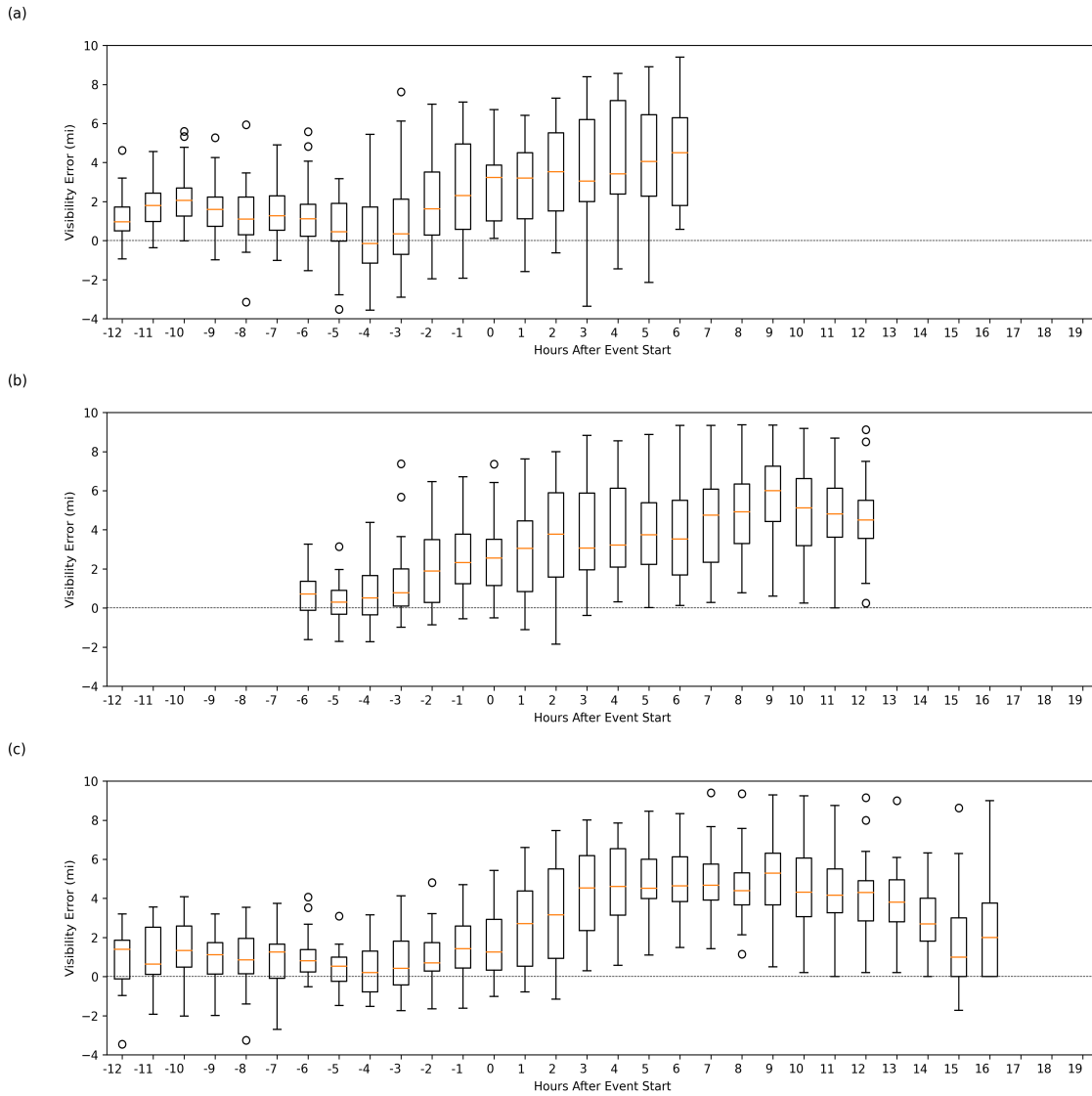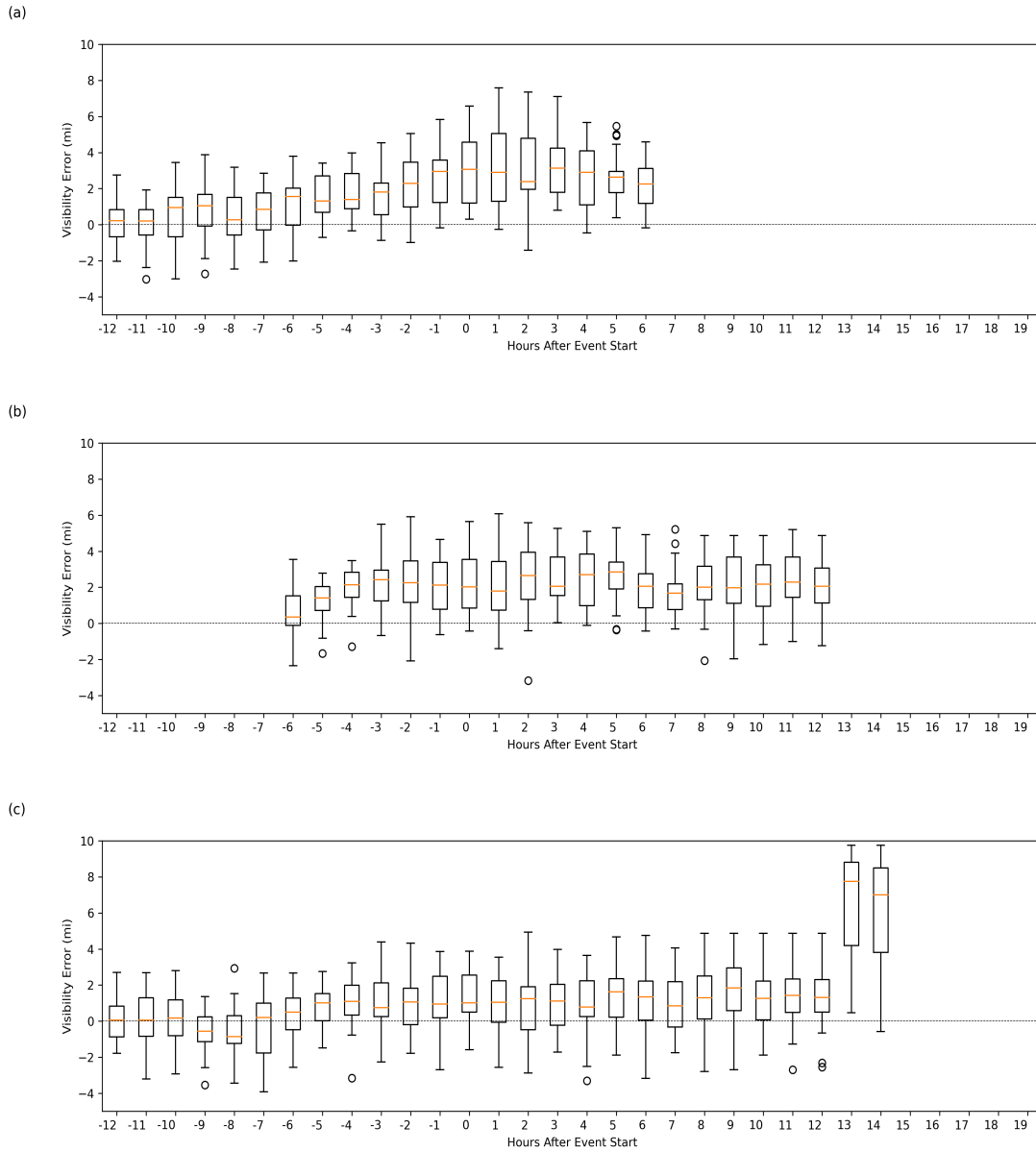
Figure 73. Box plots of HRRR visibility error (mi) for (a) 12HR, (b) 6HR, and (c) F01 forecasts for Hybrid events.

Table 30. Mean and standard deviation of mean visibility (mi) bias.
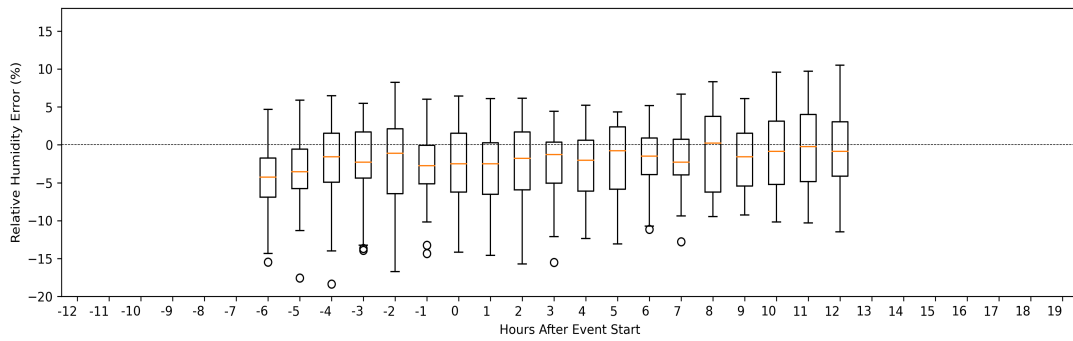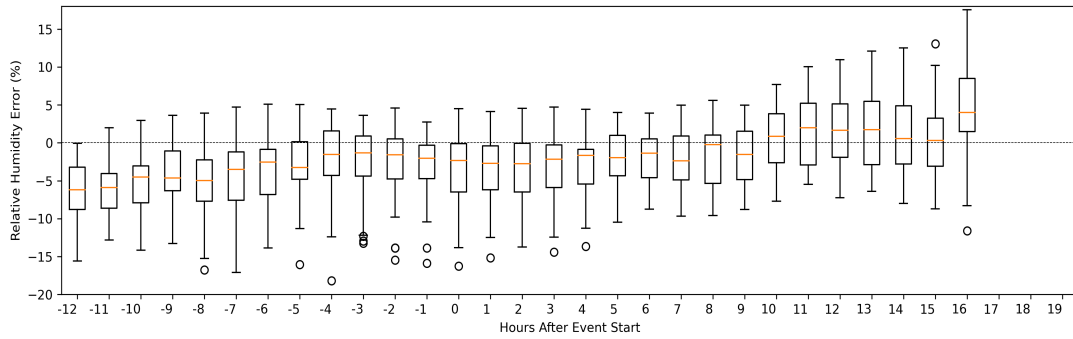
Mean and Standard Deviation

of Visibility (mi)

Forecast	Before	During	All
12hr	1.24 ± 0.81	2.75 ± 0.31	1.80 ± 0.99
6hr	1.78 ± 0.71	2.18 ± 0.34	2.05 ± 0.52
F01	0.37 ± 0.62	2.06 ± 2.11	1.31 ± 1.83

(a)
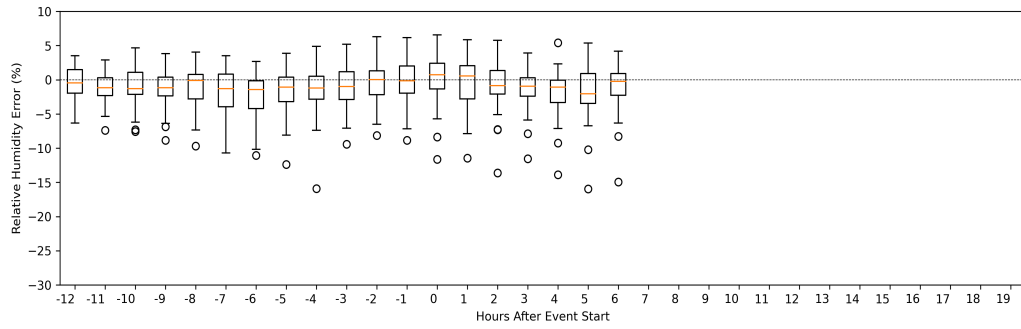
(b)

(c)

Figure 74. Box plots of HRRR relative humidity error (%) for (a) 12HR, (b) 6HR, and (c) F01 forecasts for Hybrid events.

Table 31. Mean and standard deviation of mean relative humidity (%) bias.

Mean and Standard Deviation

of Relative Humidity (%)

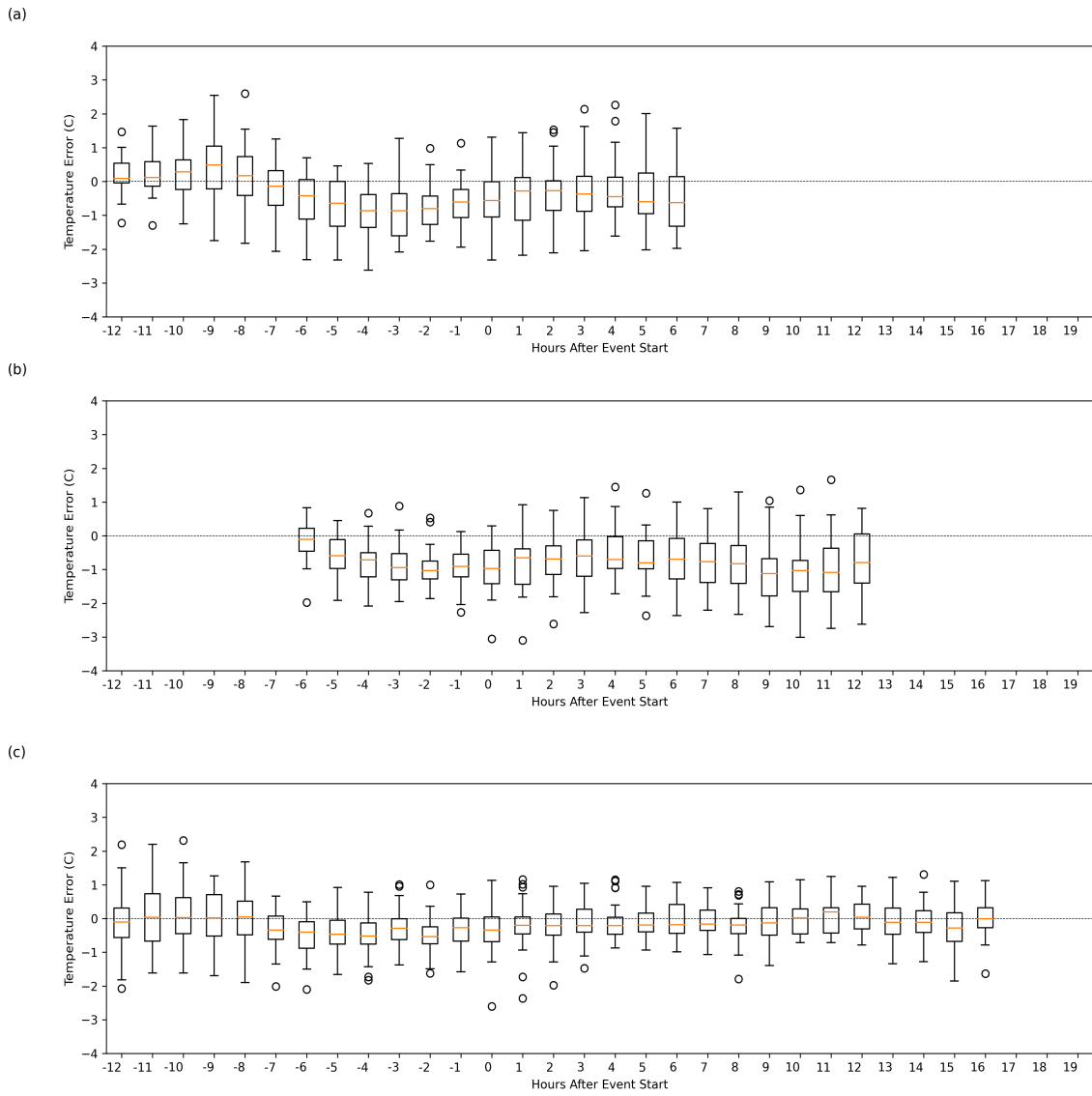| Forecast	Before	During	All
12hr	-0.86 ± 0.50	-0.55 ± 0.90	-0.74 ± 0.70
6hr	-0.31 ± 0.65	0.63 ± 1.12	0.33 ± 1.09
F01	-0.80 ± 0.74	-1.11 ± 1.27	-0.97 ± 1.08
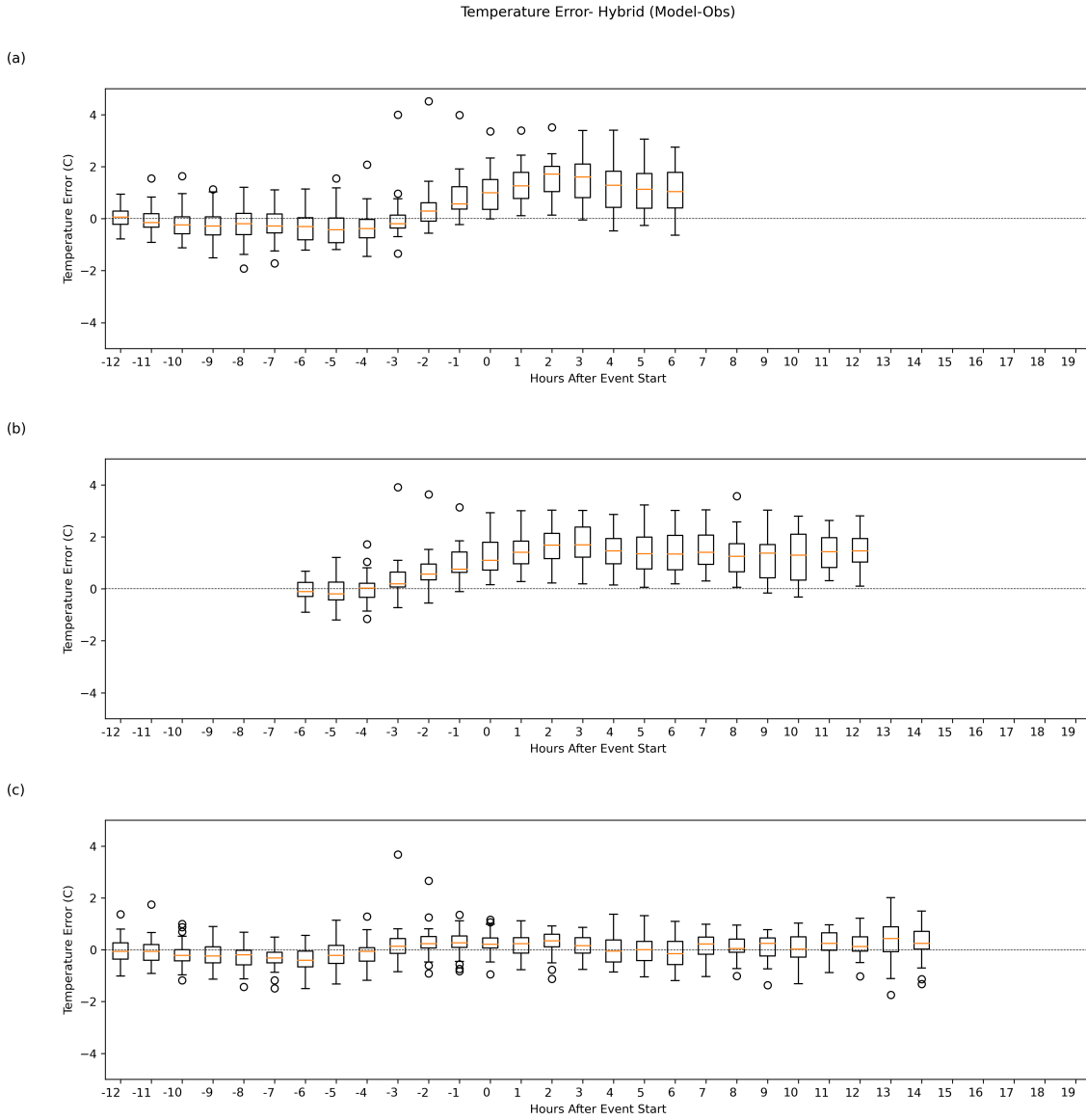
Figure 75. Box plots of HRRR temperature error (ºC) for (a) 12HR, (b) 6HR, and (c) F01 forecasts for Hybrid events.
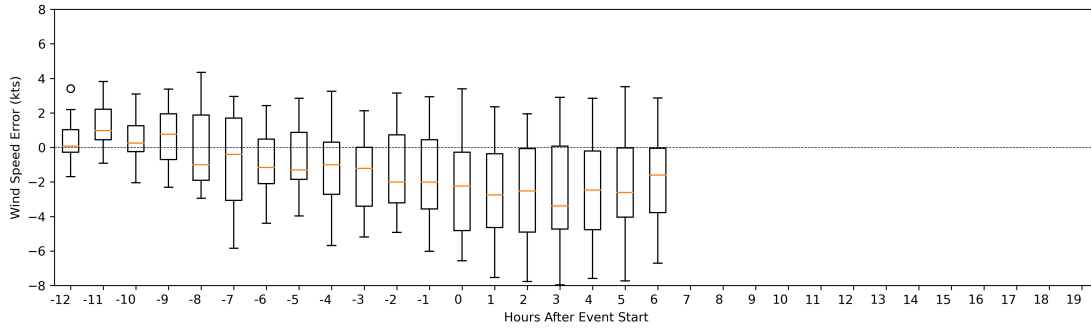
Table 32. Mean and standard deviation of mean for temperature (ºC) bias.

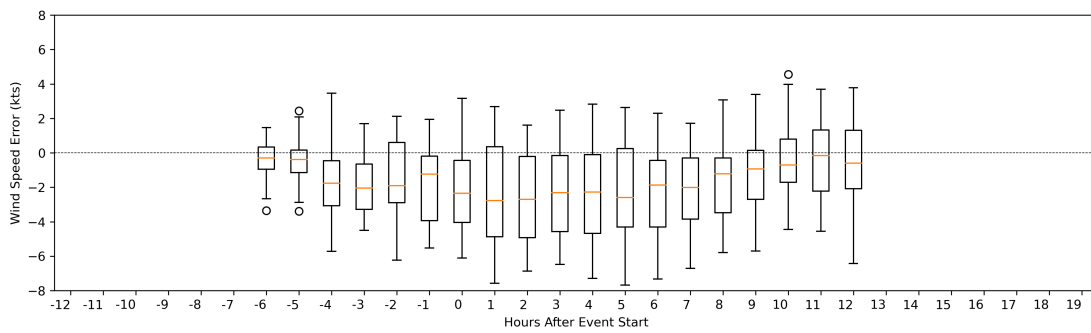**Mean and Standard Deviation**

of Temperature (ºC)

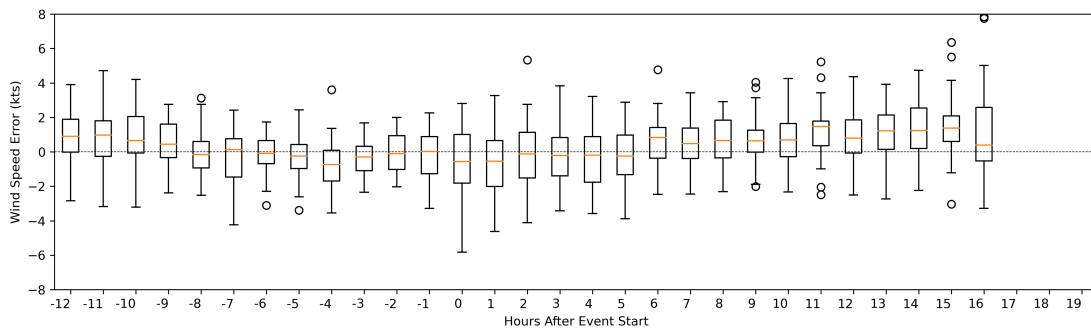| Forecast	Before	During	All
12hr	-0.13 ± 0.28	1.29 ± 0.25	0.39 ± 0.74
6hr	0.20 ± 0.35	1.40 ± 0.15	1.02 ± 0.60
F01	-0.10 ± 0.20	0.16 ± 0.15	0.04 ± 0.22

Wind Speed Error- Hybrid (Model-Obs)

(a)
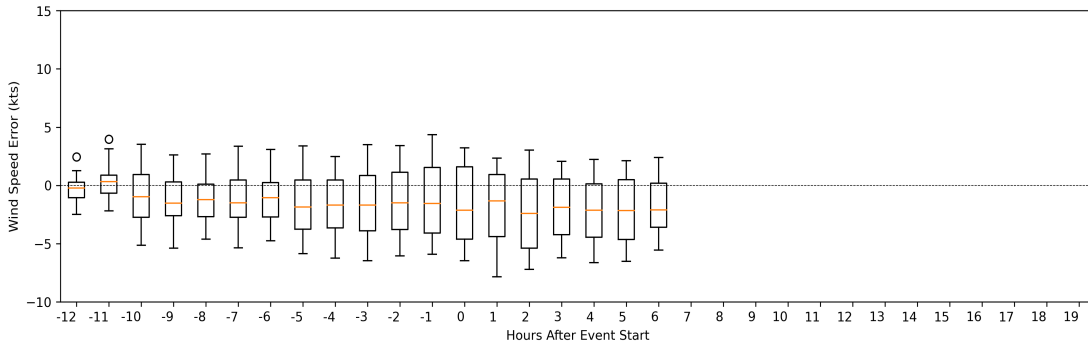
(b)
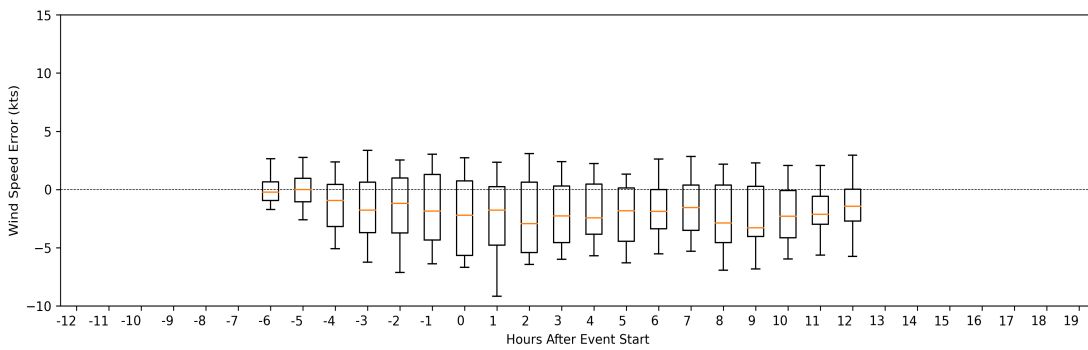
(c)
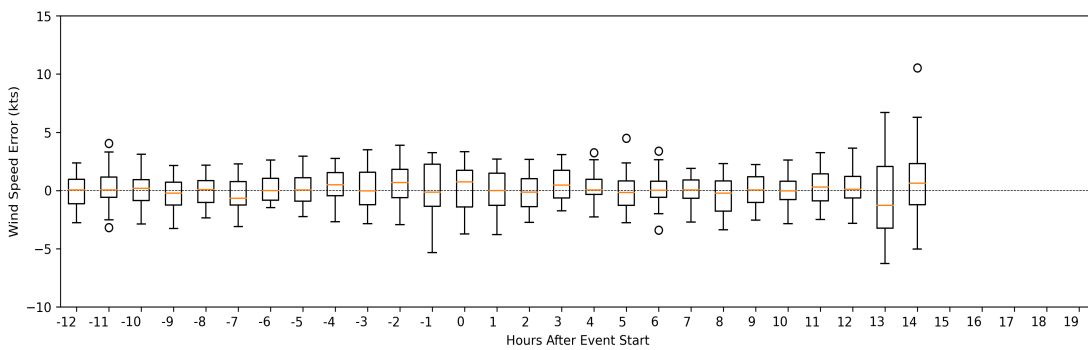
Figure 76. Box plots of HRRR wind speed error (kts) for (a) 12HR, (b) 6HR, and (c) F01 forecasts for Hybrid events.

Table 33. Mean and standard deviation of mean wind speed (kts) bias.

Mean and Standard Deviation

of Wind Speed (kts)

Forecast	Before	During	All
12hr	-1.20± 0.62	-2.02 ± 0.31	-1.50 ± 0.66
6hr	-1.00 ± 0.70	-2.23 ± 0.53	-1.84 ± 0.82
F01	0.04 ± 0.32	0.03 ± 0.45	0.04 ± 0.40
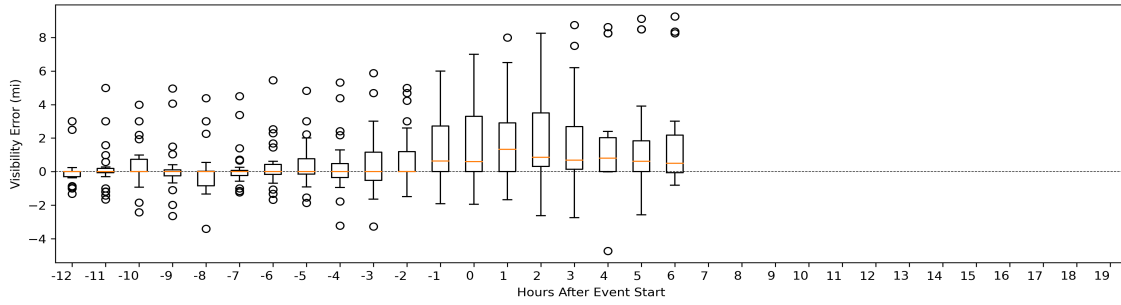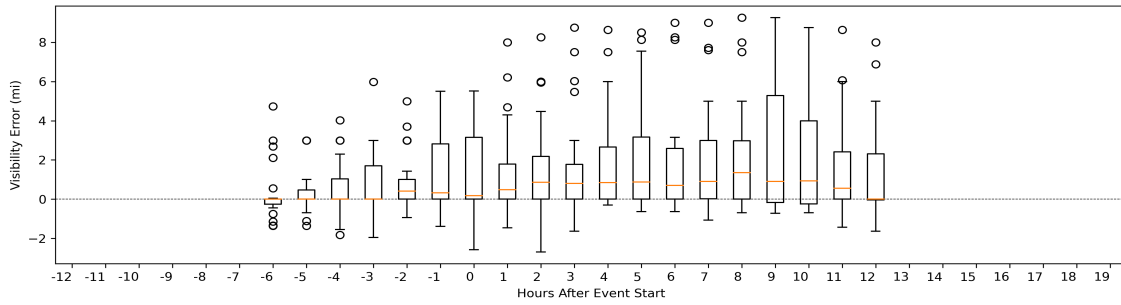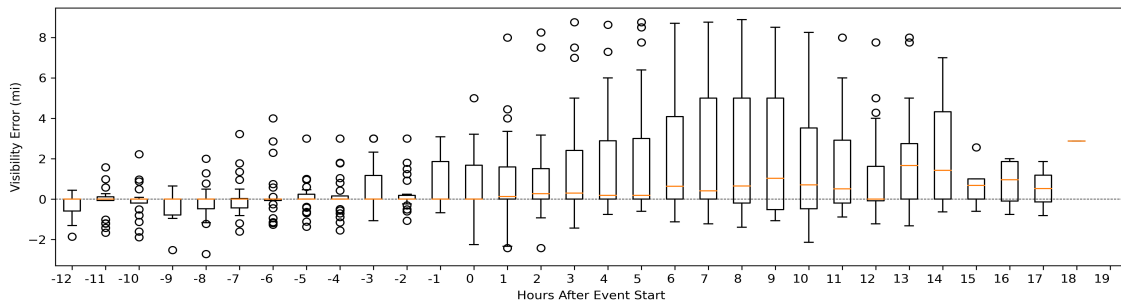
Figure 77. Box plots of HRRR visibility error (mi) for (a) 12HR, (b) 6HR, and (c) F01 forecasts for all events.

Table 34. Mean and standard deviation of median visibility (mi) bias.

Mean and Standard Deviation

of Visibility (mi)

Forecast	Before	During	All
12hr	0.05 ± 0.17	0.77 ± 0.25	0.32 ± 0.40
6hr	0.12 ± 0.17	0.72 ± 0.34	0.53 ± 0.41
F01	0 ± 0	0.69 ± 0.67	0.42 ± 0.63

(a)
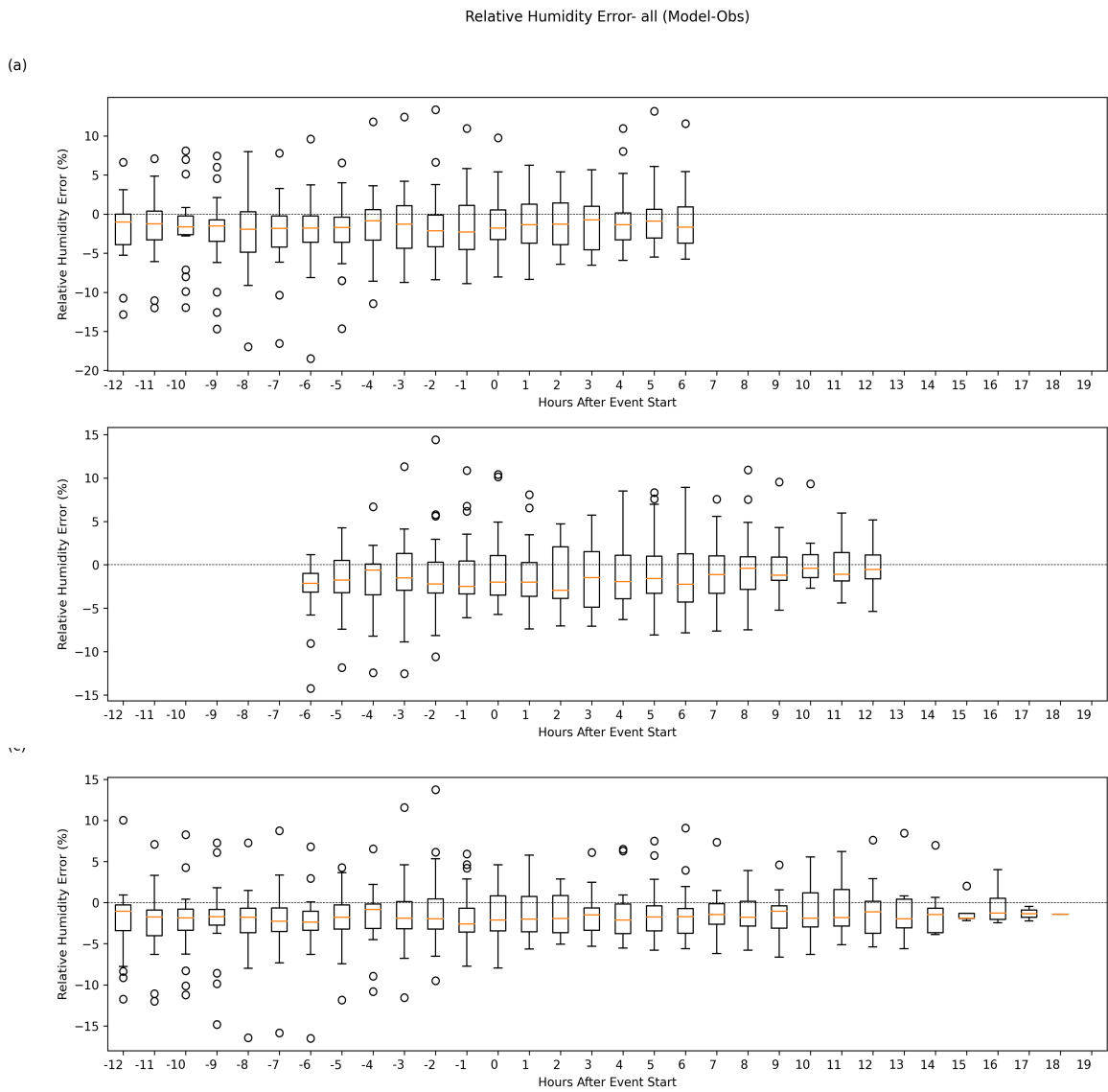
Figure 78. Box plots of HRRR relative humidity error (%) for (a) 12HR, (b) 6HR, and (c) F01 forecasts for all events.

Table 35. Mean and standard deviation of median relative humidity (%) bias.

Mean and Standard Deviation

of Relative Humidity (%)

Forecast	Before	During	All
12hr	-1.61 ± 0.42	-1.30 ± 0.35	-1.50 ± 0.42
6hr	-1.79 ± 0.61	-1.46 ± 0.73	-1.56 ± 0.71
F01	-1.83 ± 0.48	-1.67 ± 0.32	-1.73 ± 0.40

Temperature Error- all (Model-Obs)

(a)

(b)

(c)
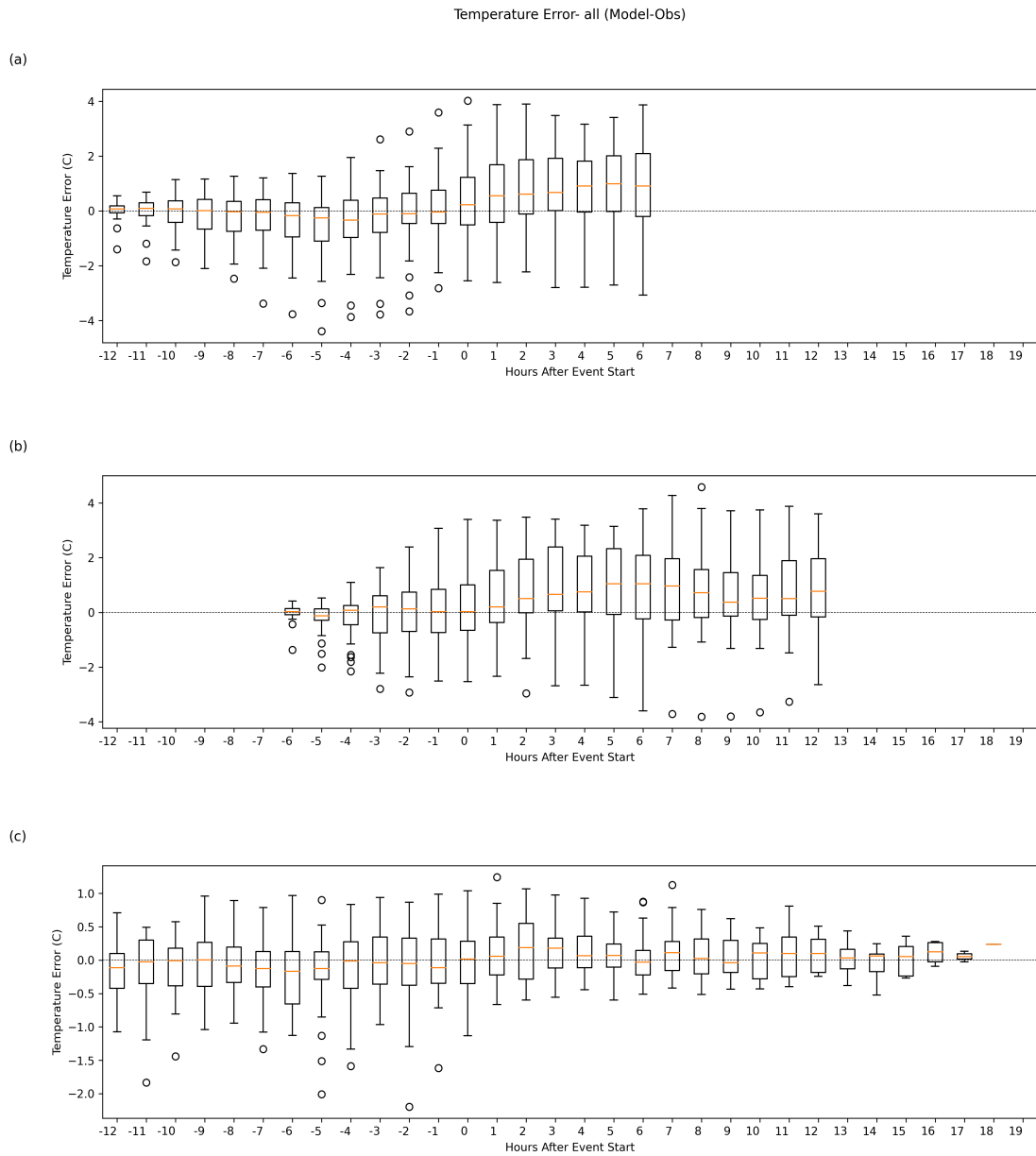
Figure 79. Box plots of HRRR temperature error (ºC) for (a) 12HR, (b) 6HR, and (c) F01 forecasts for all events.

Table 36. Mean and standard deviation of median temperature (ºC) bias.

Mean and Standard Deviation

of Temperature (ºC)

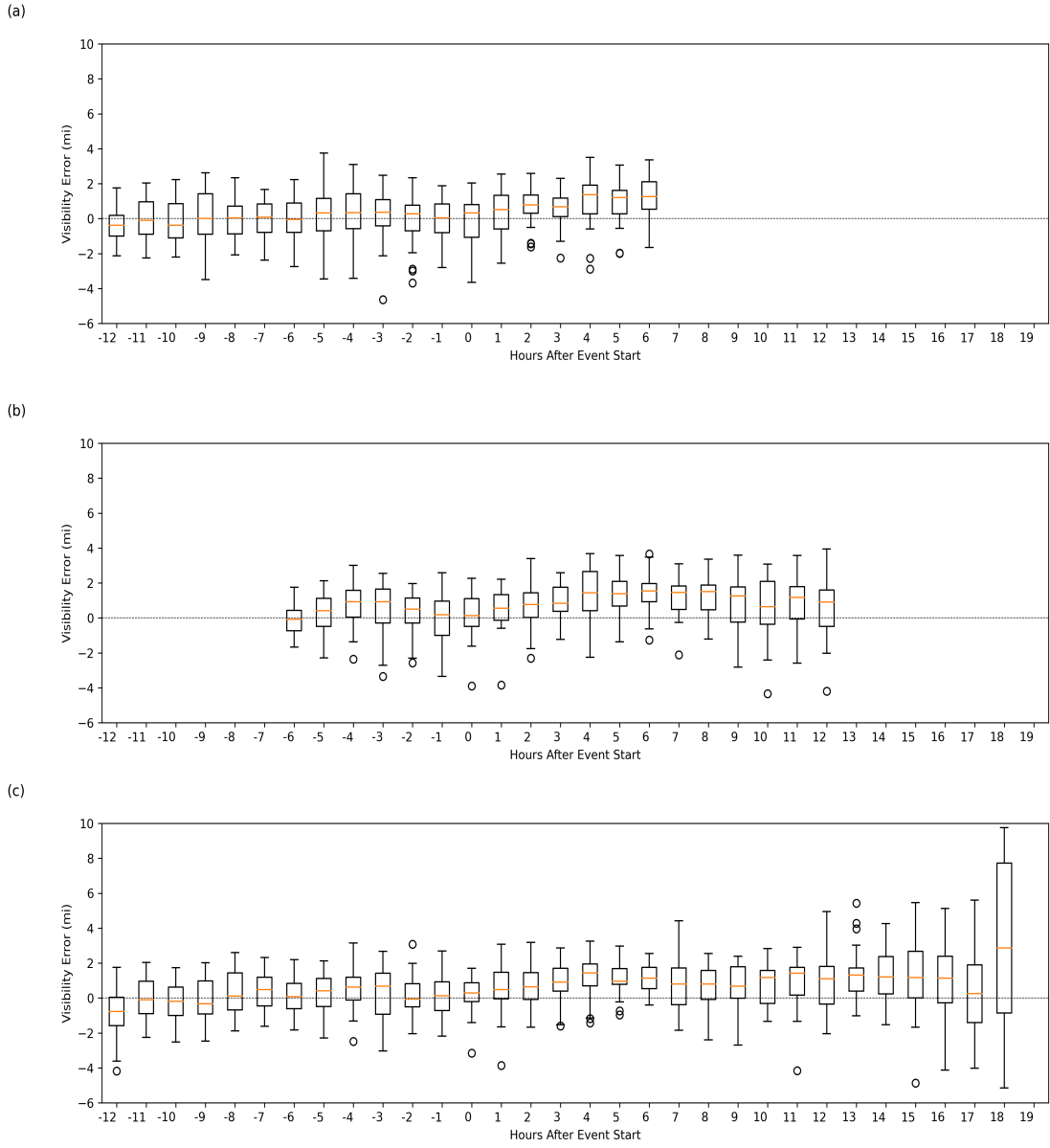| Forecast	Before	During	All
12hr	-0.07 ± 0.13	0.70 ± 0.25	0.21 ± 0.41
6hr	0.05 ± 0.10	0.62 ± 0.30	0.44 ± 0.36
F01	-0.07 ± 0.05	0.08 ± 0.07	0.02 ± 0.10
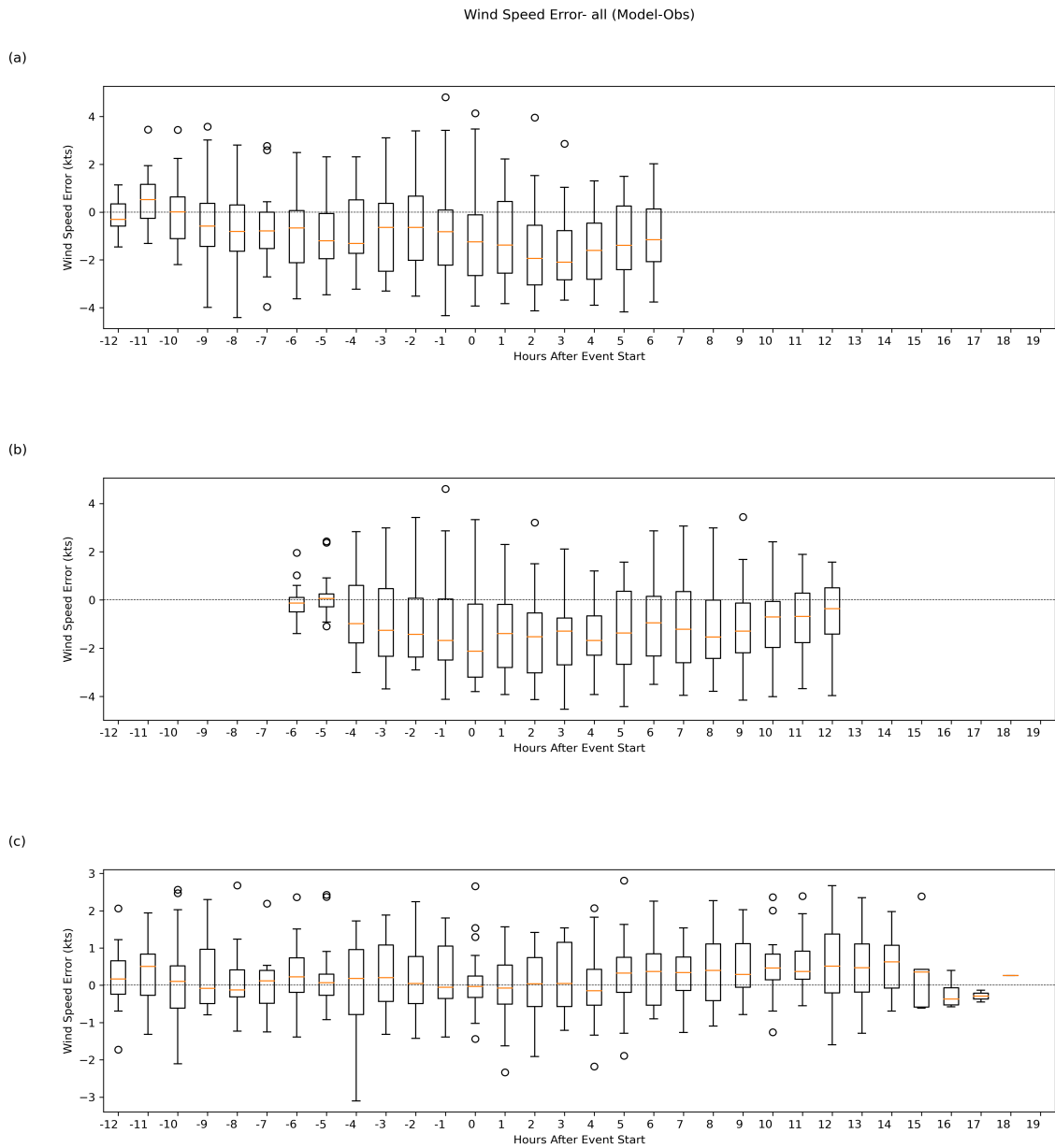
Figure 80. Box plots of HRRR wind speeds error (kts) for (a) 12HR, (b) 6HR, and (c) F01 forecasts for all events.

174

Table 37. Mean and standard deviation of median wind speed (kts) bias.

Mean and Standard Deviation

of Wind Speed (kts)

Forecast	Before	During	All
12hr	-0.61 ± 0.48	-1.55 ± 0.33	-0.95 ± 0.62
6hr	-0.9 ± 0.65	-1.24 ± 0.45	-1.13 ± 0.55
F01	0.11 ± 0.16	0.21 ± 0.28	0.17 ± 0.24
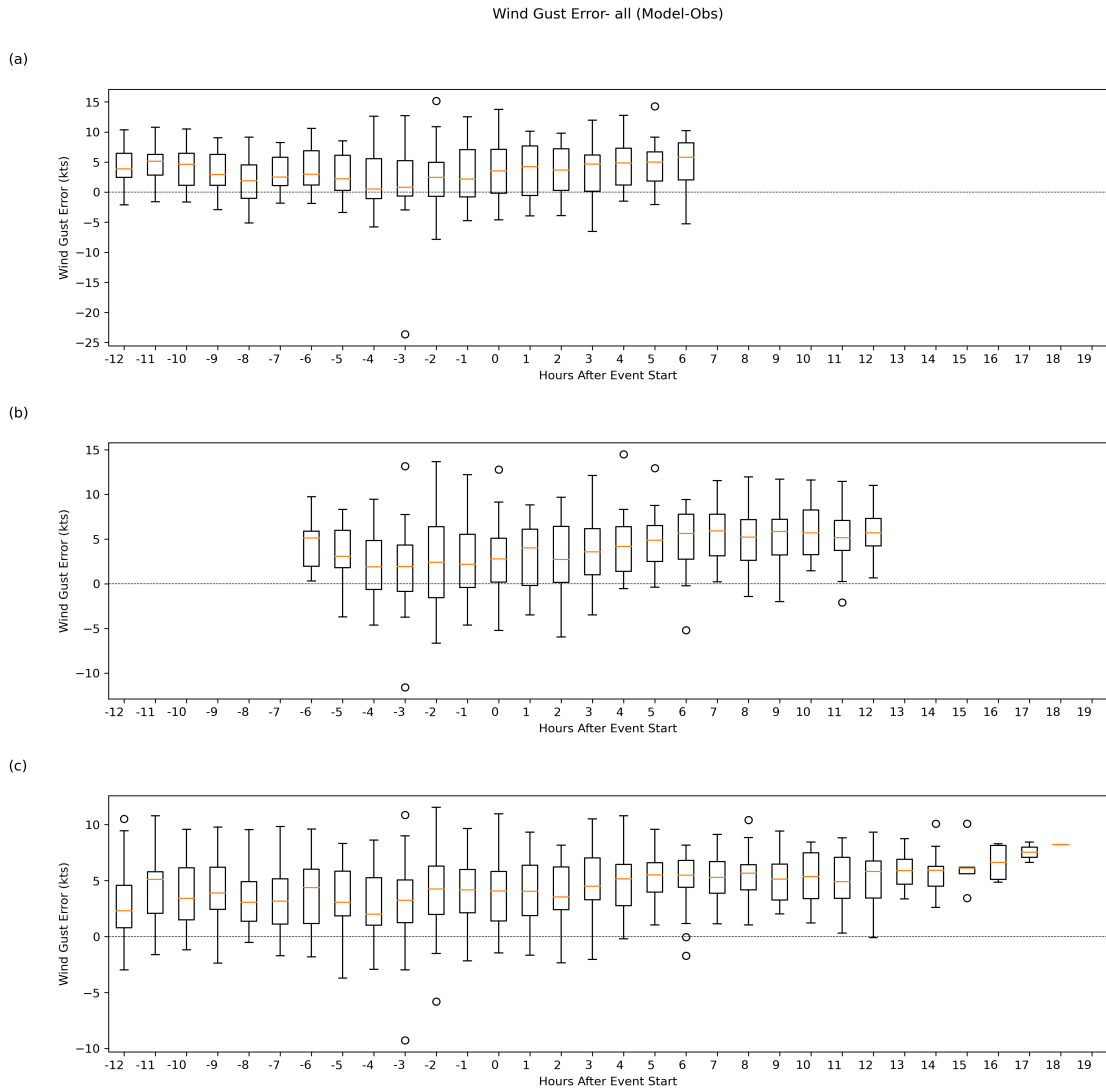
Figure 81. Box plots of HRRR wind gust error (kts) for (a) 12HR, (b) 6HR, and (c) F01 forecasts for all events.

Table 38. Mean and standard deviation of median wind gust (kts) bias.
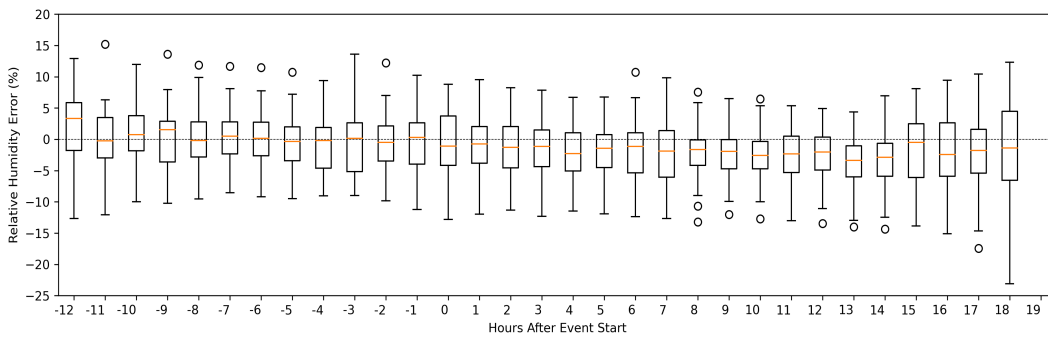
Mean and Standard Deviation

of Wind Gust (kts)

Forecast	Before	During	All
12hr	2.67 ± 1.32	4.53 ± 0.74	3.36 ± 1.45
6hr	2.76 ± 1.12	4.71 ± 1.1	4.09 ± 1.43
F01	3.5 ± 0.86	5.51 ± 1.11	4.73 ± 1.41

CHAPTER 6

DISCUSSION

6.1 Application to the Modeling of Blowing Snow

Performance of HRRR has relevance as fields could provide forcing for blowing snow parameterizations. Thus, results play an important role in understanding potential pitfalls for creating blowing snow guidance from the HRRR. Using the biases found in this study, wind speeds, temperature, and relative humidity from the model may be used to drive blowing snow schemes (Li and Pomeroy 1997b; Déry et al. 1998; Déry and Yau 1999, 2001b). Wind speed is arguably the most important factor as blowing snow models use a wind speed threshold (U10t in PIEKTUK) to initiate the process. This threshold wind speed is dependent on temperature, so if temperature forecasts are incorrect, then corrections may be needed to prevent incorrect wind speed thresholds. While relative humidity does not directly impact the initiation of blowing snow within the model, it can be important in computing the visibility. A higher (lower) relative humidity will mean less (more) sublimation and larger (smaller) particles.

Within this study, most wind speed errors were ≤ 4-6 kts across all event types for the 6HR and 12HR forecasts. With a slight negative bias, the threshold for blowing snow initiation may not be met. However, this can be dependent on the event; for example, winds during Arctic fronts tend to be very strong, meaning more error can be tolerated in meeting the wind threshold. As a result, problems may be limited to borderline cases where blizzard criteria are not met. Temperature errors remained ≤ 1-2 ºC which may only result in changes to the wind speed threshold of < 1/2 kts. In cases such as the Arctic fronts, a slight cold bias in the temperature and a slight negative bias in the winds may even offset the model biases. So, there is no clear evidence that the model would be biased one way or another. While a slight dry bias was noted for events, errors were

typically $\leq 5\%$. With a slight dry bias, more sublimation may be supported in the model. This would result in a quicker sublimation rate and smaller particles, so there would be a larger reduction in visibility.

Similar, and in many cases, smaller errors in F01 forecasts suggest that HRRR analyses or short term forecasts can be used to generate real-time maps of where blowing snow may be occurring. For IDSS purposes, this will be important in understanding possible societal impacts from reduced visibility. However, for forecasting purposes, this blowing snow may have downstream effects on future forecasts in the model. Model errors may be introduced if blowing snow is not currently included in the model. However, it is unclear how sensitive this process is and whether blowing snow would have a large enough impact to overcome other competing meteorological factors.

The development of blowing snow guidance is especially needed considering the poor performance of HRRR for forecasts of visibility. While performance is reasonable for events or periods with concurrent falling snow (e.g., Colorado lows), performance is extremely poor for ground blizzards. It is unknown how the lack of the blowing snow process ties into biases seen for other variables such as temperature, relative humidity, and wind speed. Current practices use blended models that develop empirical guidance, and often have their own biases (personal communication with forecasters). While improvements are continuously made with these blended models (e.g., improved bias correction), the HRRR may provide a better physical solution when a fully coupled blowing snow scheme is included vs. empirical output produced from blended data.

6.2 Further Operational use of the HRRR

Using both the qualitative and quantitative analysis and understanding the limitations of the model and biases in the model will help build confidence in forecasts for blowing snow events. The qualitative analysis demonstrated the HRRR did well with the overall environmental set up of each of the events. As a result, the HRRR can be helpful in identifying the potential and timing for blizzard conditions. It can also give a general idea of how long reduced visibility is expected for events such as Colorado lows, Alberta Clippers, and Hybrids, where the HRRR did better with visibility forecasts. It is important to note that the HRRR indicates lowered visibility over a larger area, whereas in reality, white out conditions may be more scattered. So, while HRRR forecasts may not exactly represent the precise patterns of blowing snow, forecasters can still use this information to determine the potential and duration of blowing snow in an area.

Locally, the biases from this study can be helpful for forecasters using the Sensitivity Webpage mentioned in section 1.4.4. Using the temperature, wind speeds, and snow age, the probability that a certain visibility threshold is met can be determined. This in turn allows forecasters to understand impact potential for these events. For example, if the HRRR shows a wind speed of 30 kts with little snowfall and around freezing temperatures, potential for visibility < ½ mi may be only 30%. However, if forecasters know that a bias exists they can adjust these values, leading to more accurate potential visibility reduction outcomes.

6.3 Strengths and Limitations of GOES-16

Analysis of GOES-16 imagery allowed for a better understanding of its utility for blowing snow events. As expected, the amount of time that satellite imagery was available for each event varied by month. Without considering event duration, 1.6 µm satellite imagery was available the

most hours per day in the month of April (~10 hrs), while the imagery was available for the fewest hours per day in late November, December, and early January (~7 hours). Overall, this meant that 1.6 μm satellite imagery was limited to hours between 13Z and 23Z, which covered nearly 47% of the hours for the events (Table 39). Further, of this available imagery, ~37% of the hours had visible blowing snow plumes, which is ~17.5% of the total event hours.

When segregating results by blizzard type, GOES-16 showed the most utility for ground blizzard events associated with Arctic fronts. These events often occur in clear sky conditions, so cloud obstruction was limited. Of the seven Arctic front events, blowing snow could be seen in 70.5% of the available hours (44% of total hours) (Table 40). GOES-16 also proved useful for Hybrid events as blowing snow plumes could be seen in 49% of the available hours (20% of total hours). Even though some of these plumes were barely visible underneath clouds or were located outside of the CWA boundaries, these results show that for Arctic front and Hybrid events, forecasters can use GOES-16 imagery to confirm blowing snow reports and visibility observations in real time and determine areas where blowing snow may be occurring underneath cloud cover. Minimal utility was observed for Colorado low, Alberta Clipper, and unclassified events. Detection of blowing snow was limited for all but one case due to widespread cloud cover over the region. However, in these cases, it can still be beneficial for forecasters to monitor satellite for blowing snow as clouds move out of the area. The HRRR also performed better for forecasts of visibility for these events and may be a useful tool in determining coverage and duration of reduced visibility.

Although it has been demonstrated that GOES-16 can be useful during clear sky events, limitations suggest a continued need for in situ observations to monitor for blowing snow conditions during overnight hours and events likely to have cloud cover (e.g., Colorado lows).

With this understanding, forecasters can use GOES-16 imagery alongside in situ observations for the detection of blowing snow, allowing forecasters to continue to refine warnings and messaging, leading to improved IDSS.

Table 39. Hours of available satellite imagery for all events grouped by month. Blue boxes represent the length of the event, black hatching shows the hours GOES-16 imagery was available, and red hatching shows hours in which blowing snow could be seen within GOES-16 imagery.

Hours of Available Satellite Imagery

	00Z	03Z	06Z	09Z	12Z	15Z	18Z	21Z	00Z	03Z	06Z	09Z	12Z	15Z	18Z	21Z	00Z	03Z	06Z
8-Jan-19																			
24-Jan-19																			
27-Jan-19																			
29-Jan-19																			
18-Jan-20																			
21-Jan-20																			
4-Feb-19																			
7-Feb-19																			
14-Feb-19																			
24-Feb-19																			
12-Feb-20																			
4-Mar-19																			
14-Mar-19																			
19-Mar-20																			
11-Apr-19																			
11-Oct-19																			
30-Nov-19																			
28-Dec-18																			
31-Dec-18																			
8-Dec-19																			
14-Dec-19																			
29-Dec-19																			

183

Table 40. Overview of total hours for each event, total hours of available satellite imagery, and total hours in which blowing snow could be seen in satellite imagery.

Blizzard Classification	Total Event Hours	Total Available Hours of Satellite	Total Available Hours of Visible Blowing Snow
Arctic front	81	51	36
Colorado low	119	49	3
Hybrid	119	49	24
Clipper	29	9	0
Unclassified	18	15	0

CHAPTER 7

CONCLUSIONS

The objective of this thesis was to identify how GOES-16 and HRRR data may improve IDSS during blowing snow events. The FGF NWSFO provided a list of 22 events over the winters of 2018-2019 and 2019-2020. A case study approach was then taken to understand model biases by comparing HRRR forecasts to surface observations across the FGF CWA for each event. Further, 1.6 μm GOES-16 imagery was examined to determine how often and how long imagery was useful during the blowing snow events. Results of this thesis are summarized below.

7.1 Evaluation of HRRR Model Guidance

While models such as the HRRR do not parameterize the process of blowing snow, high-resolution model fields such as temperature, humidity, and wind can be used as input for physical blowing snow models to determine blowing snow risk. Results from this study show that the HRRR may be a useful tool in driving blowing snow models for forecasting blowing snow events ahead of time (e.g., 12HR and 6HR), as well as in real time (e.g., F01).

Overall, general patterns could be seen among each of the events in this study. As expected, F01 forecasts performed well compared to the 12HR and 6HR forecasts which had more difficulty, specifically with forecasts of temperature and wind speed. Model visibility was consistently higher than observations for Arctic fronts, Colorado lows, and Hybrid events regardless of forecast hour. Colorado lows and Hybrids showed a much lower positive bias and smaller spread than was observed in Arctic front cases, suggesting that some reductions in visibility could be due to falling snow.

Forecasts of relative humidity showed a slight dry bias for each blizzard type and most forecast hours. Although, Arctic fronts showed the largest biases (~1.7%), median errors were still typically ≤ 5% for all blizzard types. While 12HR and 6HR forecasts showed difficulty for forecasts of temperature and wind speed, F01 forecasts showed good agreement between the model and observations for all three blizzard types. Even with these slight biases, most errors of temperature and wind speed remained ≤ 1-2 ºC and ≤ 4-6 kts, respectively.

As discussed in earlier sections, both the wind speed and temperature are important in initializing blowing snow models, whereas relative humidity can have an important downstream impact on variables such as visibility. With results from this study having demonstrated that overall median errors for these variables remain low, and in some cases could have possible offsetting impacts, the HRRR may prove to be an asset to operations compared to current practices. This is encouraging for future efforts in modeling of blowing snow, and for forecasters who can use this output to improve IDSS during blowing snow events.

7.2 Evaluation of GOES-16 Imagery

It has been demonstrated in previous work that GOES-16 imagery can be useful in the detection of blowing snow (Kennedy and Jones 2020, Jones 2020). With the availability of the "Day Snow-Fog" product, the GOES-16 near-IR 1.6-µm snow/ice band can be used to discriminate between snow, ice, and liquid/ice phase clouds, and thus can detect blowing snow plumes. Although GOES-16 can be helpful in detection of blowing snow, cloud cover and overnight timing of an event can limit the ability to see blowing snow.

Due to these limitations of cloud cover, GOES-16 imagery demonstrated the most utility for Arctic front and Hybrid events, where blowing snow could be seen in nearly 60% of the

available hours of satellite between both events. The least utility was demonstrated for Colorado low events where blowing snow could only be seen in 6% of the available hours of satellite. While the number of hours of available satellite imagery varied by month, hours of available satellite imagery ranged from 13Z and 23Z, which covered only 50% of the total event hours in this study. However, when this imagery is available, it can be an important tool for forecasters in real time as they can see the areal extent of the blowing snow and confirm observation reports. This will allow them to continually monitor conditions as well as refine warnings and messaging for blowing snow impacts.

Future Work

While results of this study are encouraging, continued work will provide further guidance and accessibility of products, improving forecaster confidence and IDSS during blizzard events. While the blowing snow event dataset used in this study included many Arctic front, Colorado low, and Hybrid events, limited cases were available for Alberta Clipper and unclassified events during the time period of study. With these events also causing large impacts due to blowing snow, it is important to have a better understanding of their associated biases. Inclusion of more years could allow for a more robust dataset, yielding results for all four different blizzard types.

Further, future studies to calculate the WSSI and CBSM output from HRRR surface fields would further the work presented here. Biases found in this study could be used to modify different meteorological fields (e.g., wind speed) as necessary. Guidance produced from the HRRR could then be compared to archived products from the NDFD. Quality feedback from forecasters would provide helpful information in making sure products are ready for operational use. Due to the number of data sources used in this work, an efficient visualization strategy will be needed for

operational forecasting settings. Allowing forecasters to sample a variety of real-time displays for blowing snow could provide useful feedback. With successful feedback at the local level, incorporation into products such as the Multi-Radar Multi-Sensor and/or AWIPS-II would allow for national use of such displays.

APPENDIX A: Qualitative Assessment Table Example

Table A1. Qualitative assessment of HRRR visibility, wind gusts, and ASOS observations for 24 January 2019.

4Panel_01242019:

FRONT

January 24, 2019

	HRRR Visibility	HRRR Winds Gust	ASOS Visibility/Winds	Notes
00Z	DVL: 10-20 GFK: 0-5 FAR: 10-15	DVL: 16-20kts GFK: 8-12kts FAR: 4-12kts	DVL: 4, 15kts GFK: 10, 0kts FAR: 6, 5kts	Widespread drop in vis for northern portion of ND. Slight match with HRRR.
01Z	DVL: 15-20 GFK: 0-5 FAR: 10-15	DVL: 16-24kts GFK: 12-20kts FAR: 8-12kts	DVL: 2.5, 25kts GFK: 3.5, 5kts FAR: 6, 0kts	Widespread drop in vis for northern portion of ND. Slight match with HRRR with HRRR more out in front of obs location wise. Winds in obs and HRRR vis increased in areas of low vis in obs.
02Z	DVL: 15-20 GFK: 0-10 FAR: 5-15	DVL: 12-20kts GFK: 12-20kts FAR: 12-20kts	DVL: 1.75, 5kts GFK: 1, 15kts FAR: 7, 10kts	Winds continue to increase. More widespread increase in HRRR winds. Widespread drop in obs vis across ND. Slight match with HRRR, but biggest drop in HRRR vis in MN not ND.
03Z	DVL: 15-20 GFK: 5-15 FAR: 10-20	DVL: 12-20kts GFK: 12-20kts FAR: 12-20kts	DVL: 2.50, 20kts GFK: 1.75, 25kts FAR: 2, 20kts	Winds increasing in obs. Highest wind in HRRR matched with largest vis drop in obs…no HRRR vis match in that spot. HRRR vis drop not lining up well with obs vis drop.
04Z	DVL: 15-20 GFK: 15-20 FAR: 10-20	DVL: 12-20kts GFK: 16-24kts FAR: 12-20kts	DVL: 1, 30kts GFK: 0.5, 30kts FAR: 1, 25kts	Visibility in GFK greatly reduced. Wind speeds in obs picked up… with HRRR increase in winds

				around GFK. HRRR vis drop beginning to break off and continue away from obs drops. Highest drop in vis in obs around GFK.
05Z	DVL: 20 GFK: 20 FAR: 15-20	DVL: 8-16kts GFK: 16-24kts FAR: 16-24kts	DVL: 3.5, 20kts GFK: 0.25, 30kts FAR: 0.75, 25-30kts	Winds continue to pick up and vis in obs continues to drop. Lowest vis in GFK area, with no match to vis drop in HRRR. At peak drop in vis at GFK.
06Z	DVL: 20 GFK: 20 FAR: 15-20	DVL: 8-16kts GFK: 16-24kts FAR: 16-24kts	DVL: 7, 15kts GFK: 0.5, 30kts FAR: 0.25, 25-30kts	Winds stay stronger and vis in obs continues to drop. Lowest vis b/w GFK and FAR, with little to no match to vis drop in HRRR. At peak drop in vis at FAR. NE MN still large drop in HRRR vis with drop in obs vis.
07Z	DVL: 20 GFK: 20 FAR: 20	DVL: 8-16kts GFK: 12-20kts FAR: 12-20kts	DVL: 9, 15kts GFK: 0.75, 25kts FAR: 0.25, 25kts	Widespread drop in vis in obs from top of ND/MN to bottom. Lowest vis b/w GFK and FAR. Winds have dropped slightly but remain high. No match to HRRR vis.
08Z	DVL: 20 GFK: 20 FAR: 20	DVL: 8-16kts GFK: 12-20kts FAR: 12-20kts	DVL: 10, 15kts GFK: 1.5, 25kts FAR: 0.5 25kts	Lowest vis now in FAR. With far E vis drops following drops in vis in HRRR. Vis increases in GFK and back to full vis in DVL. Winds remain higher in areas of lowest vis around GFK and FAR and are low in areas of low vis matching with HRRR drops in vis.
09Z	DVL: 20 GFK: 20 FAR: 20	DVL: 8-16kts GFK: 12-20kts FAR: 12-20kts	DVL: 8, 15kts GFK: 3, 20kts FAR: 0.5, 25kts	Widespread vis drop in obs continue. Low vis in far MN matched with HRRR. No match in the valley. Winds remain. Possible area of localized vis drop.

10Z	DVL: 20 GFK: 20 FAR: 20	DVL: 8-16kts GFK: 12-20kts FAR: 12-20kts	DVL: 8, 15kts GFK: 1, 25kts FAR: 0.5, 25kts	Widespread vis drop in valley into MN. Vis in HRRR at nearly 20mi. Winds vary in obs and remain in HRRR. Far E MN last of HRRR vis drop.
11Z	DVL: 20 GFK: 20 FAR: 20	DVL: 4-12kts GFK: 12-20kts FAR: 12-20kts	DVL: 10, 15kts GFK: 2.5, 20kts FAR: 1, 20kts	Widespread vis drop in valley into MN. Vis in HRRR at nearly 20mi. Winds vary in obs and start to drop in HRRR. Localized areas of low vis in HRRR.. could match to localized areas in obs.
12Z	DVL: In between drop in vis. GFK: 20 FAR: 20	DVL: 4-12kts GFK: 12-20kts FAR: 12-20kts	DVL: 9, 15kts GFK: 1, 20kts FAR: 1.25, 20kts	Drop in vis in obs not as widespread. Most moved out of CWA. Large area covering FAR and GFK and W of FAR still low obs. Couple localized areas possibly matched with HRRR… most obs vis not matched with HRRR.
13Z	DVL: 0-10 GFK: 20 FAR: 20	DVL: 4-12 kts GFK: 8-16 kts FAR: 8-16 kts	DVL: 10, 15kts GFK: 5, 15kts FAR: 1.75, 20kts	Drop in vis in obs not as widespread. Most moved out of CWA. Large area covering FAR and GFK and W of FAR still low obs. Couple localized areas possibly matched with HRRR… most obs vis not matched with HRRR.
14Z	DVL: 0-10 GFK: 20 FAR: 20	DVL: 4-12 kts GFK: 8-16 kts FAR: 8-16 kts	DVL: 10, 5kts GFK: 6, 15kts FAR: 3.5, 20kts	Drop in vis obs along the valley. Vis begins to increase a bit in some areas. Winds beginning to die down… winds match with general trend in HRRR.
15Z	DVL: 20 GFK: 20 FAR: 20	DVL: 4-12 kts GFK: 8-16 kts FAR: 8-16 kts	DVL: 10, 10kts GFK: 6, 20kts FAR: 10, 15kts	Drop in vis obs along the valley. Vis begins to increase a bit in some areas. Area of low vis in HRRR same area as in obs… localized area of low vis remains in one area W of FAR S of DVL.

16Z	DVL: 20 GFK: 20 FAR: 20	DVL: 8-16 kts GFK: 8-16 kts FAR: 8-16 kts	DVL: 10, 10kts GFK: 10, 15kts FAR: 3 20kts	Drop in obs begins to move E of FAR. Winds in HRRR stay in general kts. Area of low vis in HRRR same area as in obs… localized area of low vis remains in one area W of FAR S of DVL.
17Z	DVL: 20 GFK: 20 FAR: 20	DVL: 4-12 kts GFK: 8-16kts FAR: 8-16kts	DVL: 10, 15kts GFK: 10, 20kts FAR: 3, 20kts	Drop in obs vis remains in same area. Localized drop remains. GFK back to full vis. HRRR drop in vis breaking up a bit… general location that drop in vis is located, but not as widespread.
18Z	DVL: 20 GFK: 20 FAR: 20	DVL: 4-12 kts GFK: 8-16kts FAR: 8-16kts	DVL: 10, 15kts GFK: 10, 15kts FAR: 7 20kts	Drop in obs vis remains in same area. Localized drop remains. GFK back to full vis. HRRR drop in vis much smaller, but remains in same area… general location that drop in vis is located, but not as widespread as obs.
19Z	DVL: 20 GFK: 20 FAR: 20	DVL: 4-12 kts GFK: 8-16kts FAR: 8-16kts	DVL: 10, 10kts GFK: 10, 15kts FAR: 10, 15kts	Vis back to 10mi in all three cities. Small areas of reduced vis E and S of FAR… no match in drop in vis in HRRR.
20Z	DVL: 20 GFK: 20 FAR: 20	DVL: 8-12 kts GFK: 8-12kts FAR: 8-12kts	DVL: 10, 15kts GFK: 10, 10kts FAR: 10, 15kts	Few ASOS individual locations with vis reduced slightly. For most part vis back to 10mi. Winds remain, Drop in winds for HRRR. Localized drops in vis no match to HRRR vis.
21Z	DVL: 20 GFK: 20 FAR: 20	DVL: 8-12 kts GFK: 8-12kts FAR: 8-12kts	DVL: 10, 15kts GFK: 10, 10kts FAR: 10, 15kts	Few ASOS individual locations with vis reduced slightly. For most part vis back to 10mi. Localized drops in vis no match to HRRR vis.
22Z	DVL: 20 GFK: 20 FAR: 20	DVL: 8-12kts GFK: 4-8kts FAR: 4-8kts	DVL: 10, 15kts GFK: 9, 15kts FAR: 2.5, 10kts	Localized drop in vis around FAR. No match in HRRR. Winds in HRRR decreased… winds in FAR lighter than reported earlier.

23Z	DVL: 20	DVL: 4-12kts	DVL: 10, 10kts	Winds have decreased in valley.
	GFK: 20	GFK: 4-8kts	GFK: 10, 5kts	Most area returned to 10mi vis. No
	FAR: 20	FAR: 4-8kts	FAR: 9, 5kts	drop in vis in HRRR.

APPENDIX B: Blizzard Tables Example

Table B1. Timing of products issued by the NWS as well as maximum, minimum, and average visibility, maximum gusts, and coverage of blizzard conditions for each hour on 12 February 2020.

Feb. 12, 2020	2/12/20							
	00Z	03Z	06Z	09Z	12Z	15Z	18Z	21Z
Blizzard Warning				███	███	███	███	
Winter Storm Watch			███	███	███	███	███	
Winter Weather Advisory			███	███	███	███		

Feb. 12 2020

	00Z	01Z	02Z	03Z	04Z	05Z	06Z	07Z	08Z	09Z	10Z	11Z	12Z	13Z	14Z	15Z	16Z	17Z	18Z	19Z	20Z	21Z	22Z	23Z
Max Vis	10	10	10	10	10	10	10	10	10	10	10	10	10	10	10	10	10	10	10	10	10	10	10	10
Min Vis	9	10	10	10	1	0.5	0.25	0.25	0.24	0.24	0.24	0.25	0.25	0.25	0.24	0.24	0.24	0.24	0.24	0.25	0.5	0.75	0.75	1.25
Avg Vis	9.98	10	10	10	9.05	7.81	5.66	5.4	4.51	3.37	3.16	2.92	3.8	4.31	4.19	4.35	4.47	5.5	6.59	6.94	7.36	8.34	9	9.53
Max Gust	25	24	27	25	23	37	37	42	49	52	50	44	47	45	46	40	42	45	38	35	35	35	32	32
Coverage	Isolated	Isolated	Isolated	Isolated	Isolated	Isolated	Isolated	Isolated	Isolated	Isolated	Isolated	Isolated	Isolated	Isolated	Isolated	Isolated	Scattered	Isolated	Isolated	Isolated	Isolated	Isolated	Isolated	Isolated

REFERENCES

American Meteorological Society, 2012a: Blowing snow - Glossary of Meteorology. https://glossary.ametsoc.org/wiki/Blowing_snow (Accessed September 5, 2021).

——, 2012b: Visibility - Glossary of Meteorology. https://glossary.ametsoc.org/wiki/Visibility (Accessed September 2, 2021).

ASOS Users Guide, 1998: Automated Surface Observing System (ASOS) Users Guide.

Baggaley, D. G., and J. M. Hanesiak, 2005: An Empirical Blowing Snow Forecast Technique for the Canadian Arctic and the Prairie Provinces. *Weather and Forecasting*, **20**, 51–62, https://doi.org/10.1175/WAF-833.1.

Blaylock, B. K., J. D. Horel, and S. T. Liston, 2017: Cloud archiving and data mining of High-Resolution Rapid Refresh forecast model output. *Computers & Geosciences*, **109**, 43–50, https://doi.org/10.1016/j.cageo.2017.08.005.

Bodner, M., S. Perfater, and A. Benjamin, 2017: The 2017 HMT-WPC Winter Weather Experiment.

Burrows, W. R., and C. J. Mooney, 2021: Blizzard Conditions in the Canadian Arctic: Observations and Automated Products for Forecasting. *Weather and Forecasting*, **36**, 1113–1129, https://doi.org/10.1175/WAF-D-20-0077.1.

Burrows, W. R., R. A. Treidl, and R. G. Lawford, 1979: The Southern Ontario Blizzard of January 26 and 27, 1978. *Atmosphere-Ocean*, **17**, 306–320, https://doi.org/10.1080/07055900.1979.9649068.

Christopherson, J., S. N. Ramaseri Chandra, and J. Q. Quanbeck, 2019: *2019 Joint Agency Commercial Imagery Evaluation—Land remote sensing satellite compendium*. U.S. Geological Survey,.

Clark, A. J., and Coauthors, 2012: An Overview of the 2010 Hazardous Weather Testbed Experimental Forecast Program Spring Experiment. *Bulletin of the American Meteorological Society*, **93**, 55–74, https://doi.org/10.1175/BAMS-D-11-00040.1.

——, and Coauthors, 2018: The Community Leveraged Unified Ensemble (CLUE) in the 2016 NOAA/Hazardous Weather Testbed Spring Forecasting Experiment. *Bulletin of the American Meteorological Society*, **99**, 1433–1448, https://doi.org/10.1175/BAMS-D-16-0309.1.

Coleman, J. S. M., and R. M. Schwartz, 2017: An Updated Blizzard Climatology of the Contiguous United States (1959–2014): An Examination of Spatiotemporal Trends. *Journal of Applied Meteorology and Climatology*, **56**, 173–187, https://doi.org/10.1175/JAMC-D-15-0350.1.

Déry, S., P. Taylor, and J. Xiao, 1998: The Thermodynamic Effects of Sublimating, Blowing Snow in the Atmospheric Boundary Layer. *Boundary-Layer Meteorology*, **89**, 251–283, https://doi.org/10.1023/A:1001712111718.

Déry, S. J., and M. K. Yau, 1999: A Bulk Blowing Snow Model. *Boundary-Layer Meteorology*, **93**, 237–251, https://doi.org/10.1023/A:1002065615856.

——, and ——, 2001a: Simulation of an Arctic Ground Blizzard Using a Coupled Blowing Snow–Atmosphere Model. *Journal of Hydrometeorology*, **2**, 579–598, https://doi.org/10.1175/1525-7541(2001)002<0579:SOAAGB>2.0.CO;2.

——, and ——, 2001b: Simulation Of Blowing Snow In The Canadian Arctic Using A Double-Moment Model. *Boundary-Layer Meteorology*, **99**, 297–316, https://doi.org/10.1023/A:1018965008049.

Duda, J. D., and D. D. Turner, 2021: Large-Sample Application of Radar Reflectivity Object-Based Verification to Evaluate HRRR Warm-Season Forecasts. *Weather and Forecasting*, **36**, 805–821, https://doi.org/10.1175/WAF-D-20-0203.1.

Grafenauer, T., 2021: *The Blizzard Warning Decision Process*.

Grand Forks Herald, 2017: April 4, 1997: Hard-hearted Hannah was the worst in a series of blizzards. *Grand Forks Herald*,. https://www.grandforksherald.com/news/4244903-april-4-1997-hard-hearted-hannah-was-worst-series-blizzards (Accessed September 13, 2021).

——, 2019: Herald names storm after UND's Adam Scheel. *Grand Forks Herald*,. https://www.grandforksherald.com/news/weather/4718039-Herald-names-storm-after-UNDs-Adam-Scheel (Accessed September 13, 2021).

Herzmann, D., 2021: IEM: Download ASOS/AWOS/METAR Data.

Horel, J., and B. Blaylock, 2015: Metadata for the High Resolution Rapid Refresh Model Archives. https://dx.doi.org/10.7278/S5JQ0Z5B (Accessed August 31, 2021).

Ikeda, K., M. Steiner, and G. Thompson, 2017: Examination of Mixed-Phase Precipitation Forecasts from the High-Resolution Rapid Refresh Model Using Surface Observations and Sounding Data. *Weather and Forecasting*, **32**, 949–967, https://doi.org/10.1175/WAF-D-16-0171.1.

Jones, C., 2020: Arctic Cold Front – Blizzard: Feb 12, 2020. *Satellite Liaison Blog*,. https://satelliteliaisonblog.com/2020/02/13/arctic-cold-front-blizzard-feb-12-2020/ (Accessed October 15, 2021).

Kennedy, A., and C. Jones, 2020: GOES-16 Observations of Blowing Snow in Horizontal Convective Rolls on 24 February 2019. *Monthly Weather Review*, **148**, 1737–1750, https://doi.org/10.1175/MWR-D-19-0354.1.

——, A. Trellinger, T. Grafenauer, and G. Gust, 2019: A Climatology of Atmospheric Patterns Associated with Red River Valley Blizzards. *Climate*, **7**, 66, https://doi.org/10.3390/cli7050066.

——, A. Scott, N. Loeb, A. Sczepanski, K. Lucke, J. Marquis, and S. Waugh, 2021: Bringing Microphysics to the Masses: The Blowing Snow Observations at the University of North Dakota: Education through Research (BLOWN-UNDER) Campaign. *Bulletin of the American Meteorological Society*, **1**, 1–41, https://doi.org/10.1175/BAMS-D-20-0199.1.

King, M. M., Claire. L. Parkinson, and A. Ward, 2006: Earth Science Reference Handbook: A Guide to NASA's Earth Science Program and Earth Observing Satellite Missions.

Kyoko Ikeda, Matthias Steiner, James Pinto, and Curtis Alexander, 2013: Evaluation of Cold-Season Precipitation Forecasts Generated by the Hourly Updating High-Resolution Rapid Refresh Model in: Weather and Forecasting Volume 28 Issue 4 (2013). https://journals.ametsoc.org/view/journals/wefo/28/4/waf-d-12-00085_1.xml (Accessed August 16, 2021).

Lee, T. R., M. Buban, D. D. Turner, T. P. Meyers, and C. B. Baker, 2019: Evaluation of the High-Resolution Rapid Refresh (HRRR) Model Using Near-Surface Meteorological and Flux Observations from Northern Alabama. *Weather and Forecasting*, **34**, 635–663, https://doi.org/10.1175/WAF-D-18-0184.1.

Letcher, T. W., S. L. LeGrand, and C. Polashenski, 2021: Applying a Physically Based Blowing Snow Diagnostic Parameterization to Improve Wintertime Visibility Forecasts in the WRF Model. *Weather and Forecasting*, **36**, 615–626, https://doi.org/10.1175/WAF-D-20-0106.1.

Li, L., and J. Pomeroy, 1997b: Estimates of Threshold Wind Speeds for Snow Transport Using Meteorological Data. *Journal of Applied Meteorology - J APPL METEOROL*, **36**, 205–213, https://doi.org/10.1175/1520-0450(1997)036<0205:EOTWSF>2.0.CO;2.

——, and J. W. Pomeroy, 1997a: Probability of occurrence of blowing snow. *Journal of Geophysical Research: Atmospheres*, **102**, 21955–21964, https://doi.org/10.1029/97JD01522.

Luo, L., J. Zhang, R. Hock, and Y. Yao, 2021: Case Study of Blowing Snow Impacts on the Antarctic Peninsula Lower Atmosphere and Surface Simulated With a Snow/Ice Enhanced WRF Model. *Journal of Geophysical Research: Atmospheres*, **126**, e2020JD033936, https://doi.org/10.1029/2020JD033936.

Makowski, J. A., and T. J. Grafenauer, 2016: Verification of a Blowing Snow Model with Utility for Decision Support Services. *Central Region Technical Attachment*, **16–02**, 10.

Nakanishi, M., and H. Niino, 2009: Development of an Improved Turbulence Closure Model for the Atmospheric Boundary Layer. *Journal of the Meteorological Society of Japan. Ser. II*, **87**, 895–912, https://doi.org/10.2151/jmsj.87.895.

NASA, 2021: EOSDIS Worldview. https://worldview.earthdata.nasa.gov/ (Accessed September 5, 2021).

NWS, 2009: Glossary - NOAA's National Weather Service. https://w1.weather.gov/glossary/index.php?letter=b (Accessed September 5, 2021).

——, 2020: February 12, 2020 Blizzard. https://www.weather.gov/fgf/02122020_Blizzard (Accessed December 7, 2021).

——, 2019a: January 27, 2019, Blizzard Event Summary. https://www.weather.gov/fgf/2019_01_27_Blizzard (Accessed December 7, 2021).

——, 2019b: Review of March 14, 2019 Blizzard Event over eastern North Dakota and northwest Minnesota. https://www.weather.gov/fgf/2019_03_14_Blizzard (Accessed December 7, 2021).

Palm, S. P., Y. Yang, J. D. Spinhirne, and A. Marshak, 2011: Satellite remote sensing of blowing snow properties over Antarctica. *Journal of Geophysical Research: Atmospheres*, **116**, https://doi.org/10.1029/2011JD015828.

——, V. Kayetha, and Y. Yang, 2018: Toward a Satellite-Derived Climatology of Blowing Snow Over Antarctica. *Journal of Geophysical Research: Atmospheres*, **123**, 10,301-10,313, https://doi.org/10.1029/2018JD028632.

Pinto, J. O., J. A. Grim, and M. Steiner, 2015: Assessment of the High-Resolution Rapid Refresh Model's Ability to Predict Mesoscale Convective Systems Using Object-Based Evaluation. *Weather and Forecasting*, **30**, 892–913, https://doi.org/10.1175/WAF-D-14-00118.1.

Pomeroy, J. W., and D. H. Male, 1988: Optical Properties of Blowing Snow. *Journal of Glaciology*, **34**, 3–10, https://doi.org/10.3189/S0022143000008996.

Radford, J. T., G. M. Lackmann, and M. A. Baxter, 2019: An Evaluation of Snowband Predictability in the High-Resolution Rapid Refresh. *Weather and Forecasting*, **34**, 1477–1494, https://doi.org/10.1175/WAF-D-19-0089.1.

Rasmussen, R., J. Vivekanandan, J. Cole, B. Myers, and C. Masters, 1999: The Estimation of Snowfall Rate Using Visibility. *Journal of Applied Meteorology - J APPL METEOROL*, **38**, 1542–1563, https://doi.org/10.1175/1520-0450(1999)038<1542:TEOSRU>2.0.CO;2.

Scarchilli, C., M. Frezzotti, P. Grigioni, L. De Silvestri, L. Agnoletto, and S. Dolci, 2010: Extraordinary blowing snow transport events in East Antarctica. *Clim Dyn*, **34**, 1195–1206, https://doi.org/10.1007/s00382-009-0601-0.

Schmidt, R. A., 1980: Threshold Wind-Speeds and Elastic Impact in Snow Transport. *Journal of Glaciology*, **26**, 453–467, https://doi.org/10.3189/S0022143000010972.

Schwartz, R. M., and T. W. Schmidlin, 2002: Climatology of Blizzards in the Conterminous United States, 1959–2000. *Journal of Climate*, **15**, 1765–1772, https://doi.org/10.1175/1520-0442(2002)015<1765:COBITC>2.0.CO;2.

Service, N. N. W., Winter Storm Severity Index. https://www.wpc.ncep.noaa.gov/wwd/wssi/wssi.php (Accessed August 16, 2021).

Shirley |, H., 2020: Blizzard Aaliyah arrives as first winter storm of season in Greater Grand Forks region. *Grand Forks Herald*,. https://www.grandforksherald.com/news/weather/6814658-Blizzard-Aaliyah-arrives-as-first-winter-storm-of-season-in-Greater-Grand-Forks-region (Accessed September 13, 2021).

Thompson, G., and T. Eidhammer, 2014: A Study of Aerosol Impacts on Clouds and Precipitation Development in a Large Winter Cyclone. *Journal of the Atmospheric Sciences*, **71**, 3636–3658, https://doi.org/10.1175/JAS-D-13-0305.1.

Tuomaala, L., 2005: US National Weather Service Chooses Vaisala's Modified Version of the Vaisala WINDCAP® Ultrasonic Wind Sensor WS425 as Part of Its Nationwide Surface Observation System.

Turner, D. D., and Coauthors, 2020: A Verification Approach Used in Developing the Rapid Refresh and Other Numerical Weather Prediction Models. *J. Operational Meteor.*, 39–53, https://doi.org/10.15191/nwajom.2020.0803.

US Department of Commerce, 2021c: January 27, 2019, Blizzard. https://www.weather.gov/fgf/2019_01_27_Blizzard (Accessed October 15, 2021).

US Department of Commerce, N., 2018: Improved High-Resolution Models Support Accurate Forecast of a Very Rare Winter Storm. https://www.weather.gov/news/183101_winter-storm (Accessed August 16, 2021).

——, 2021a: The Historic Blizzard of March 2-5, 1966. https://www.weather.gov/fgf/blizzardof66 (Accessed September 21, 2021).

——, 2021b: Event Summaries. https://www.weather.gov/fgf/events (Accessed September 5, 2021).

——, What is a Ground Blizzard? https://www.weather.gov/safety/winter-ground-blizzard (Accessed August 16, 2021).

——, 2019a: What is a Ground Blizzard? https://www.weather.gov/safety/winter-ground-blizzard (Accessed September 5, 2021).

US Department of Transportation, F., 2017: Advisory Circular: Automated Weather Observing Systems (AWOS) for Non-Federal Applications.

Xiao, J., R. Bintanja, S. J. Déry, G. W. Mann, and P. A. Taylor, 2000: An Intercomparison Among Four Models Of Blowing Snow. *Boundary-Layer Meteorology*, **97**, 109–135, https://doi.org/10.1023/A:1002795531073.

Yang, J., M. K. Yau, X. Fang, and J. W. Pomeroy, 2010: A triple-moment blowing snow-atmospheric model and its application in computing the seasonal wintertime snow mass budget. *Hydrol. Earth Syst. Sci.*, **14**, 1063–1079, https://doi.org/10.5194/hess-14-1063-2010.

Section 4: Red River Valley | North Dakota Studies. https://www.ndstudies.gov/gr4/geology-geography-and-climate/part-2-geography/section-4-red-river-valley (Accessed August 18, 2021).